NOAA Technical Memorandum ERL ESG-7

PRELIMINARY RESULTS OF ASSOCIATING CLOUD-TO-GROUND LIGHTNING WITH SURFACE CONVERGENCE AND RADAR REFLECTIVITY AT KENNEDY SPACE CENTER IN 1983

Andrew I. Watson
Raúl E. López
Ronald L. Holle
John R. Daugherty

Environmental Sciences Group
Boulder, Colorado
July 1984

noaa NATIONAL OCEANIC AND ATMOSPHERIC ADMINISTRATION / Environmental Research Laboratories

NOAA Technical Memorandum ERL ESG-7

PRELIMINARY RESULTS OF ASSOCIATING CLOUD-TO-GROUND LIGHTNING WITH SURFACE CONVERGENCE AND RADAR REFLECTIVITY AT KENNEDY SPACE CENTER IN 1983

Andrew I. Watson
Raúl E. López
Ronald L. Holle
John R. Daugherty

Weather Research Program

Environmental Sciences Group
Boulder, Colorado
July 1984

UNITED STATES
DEPARTMENT OF COMMERCE

Malcolm Baldrige,
Secretary

NATIONAL OCEANIC AND
ATMOSPHERIC ADMINISTRATION

John V. Byrne,
Administrator

Environmental Research
Laboratories

Vernon E. Derr
Director

NOTICE

Mention of a commercial company or product does not constitute an endorsement by NOAA Environmental Research Laboratories. Use for publicity advertising purposes of information from this publication concerning proprietary products or the tests of such products is not authorized.

CONTENTS

PRELIMINARY RESULTS OF ASSOCIATING CLOUD-TO-GROUND LIGHTNING WITH SURFACE CONVERGENCE AND RADAR REFLECTIVITY AT KENNEDY SPACE CENTER IN 1983

Andrew I. Watson, Raul E. Lopez,
Ronald L. Holle, and John R. Daugherty

ABSTRACT. The association of cloud-to-ground lightning with prior surface convergence was studied at Kennedy Space Center (KSC) for several days during the summer of 1983. Earlier studies in south Florida using large data sets had showed that surface convergence was associated with radar-derived precipitation, and that radar reflectivity was associated with cloud-to-ground lightning. Therefore, it was expected that convergence could be used to anticipate lightning on short time scales. The cases in 1983 are presented to indicate that such relationships from south Florida also apply at KSC. When clouds build overhead at KSC, there is up to 45 minutes or more of lead time before lightning begins. When cloud systems move to KSC from outside the wind network, very little or no lead time is available from local winds; however, moving systems are usually tracked well by lightning and radar data available over areas larger than the network. For three cases, maps are shown on the synoptic and regional scales; then the detailed evolution of cloud systems over KSC is followed in time and space. Several other cases under different synoptic situations are briefly presented to show the evolution of convergence, radar echoes, and lightning in the small network area.

1. INTRODUCTION

The prospects for improved short-term forecasting of lightning at Kennedy Space Center (KSC) based on surface wind convergence were developed from several studies undertaken in south Florida. In that area, studies showed that (1) surface convergence had some predictive value in anticipating rainfall as measured by radar, (2) radar reflectivity was related in a particular way to cloud-to-ground lightning, and (3) daily lightning activity was related to synoptic-scale regimes. However, no simultaneous sets of surface winds, radar echoes and lightning had been collected and recorded prior to 1983 in a network where convection is predominantly forced by surface heating. For the summer of 1983 at KSC, arrangements were made to gather such information with full knowledge that the existing KSC wind network was too small to adequately describe the evolution of a typical lightning-producing storm in the area. Nevertheless, the case studies presented in this report have been prepared to illustrate that the relationships expected to apply at KSC indeed appear to hold true. Because of the limitation of the KSC network size, it is not possible to construct statistical relationships between convergence and either rainfall or lightning from the summer of 1983. A larger wind network must be installed to sample these cloud systems properly

before these relationships can be developed; it is hoped that such a network will be deployed in 1984.

2. BACKGROUND

A. Convergence-Rainfall Relation

The relation between surface wind convergence and rainfall was developed with data from the Florida Area Cumulus Experiment (FACE) in south Florida, using mesonetworks deployed in 1973 and 1975. An additional, similar project was undertaken as part of the University of Virginia-Illinois State Water Survey-NOAA program (VIN) in Illinois in 1979. In these projects, surface wind networks were deployed on a temporary basis and precipitation was related to the convergence in a variety of ways.

Watson and Blanchard (1984) have presented the analyses and results of convergence-rainfall relations in the FACE 1975 network, which covered 1440 km^2. They found that the change in total area divergence associated with a particular convergence event is related to the resulting radar-measured rainfall. For 121 convergence events during July and August 1975, the correlation was -.59 between the divergence change and the rainfall amount. It was also apparent that data should be partitioned according to stability, buoyancy, humidity, and wind represented by the local morning upper-air sounding, because the convergence relationships varied as conditions changed from day to day. The average time between defining a convergence event and initial rain was 18 minutes, with a rather high standard deviation. Once a given threshold was reached, stronger convergence values generally indicated stronger rainfall events. The technique was best suited to slow-moving convective systems that complete their life cycle within the network. At the end of the storm, the relation between the change in divergence and rainfall was better than the relation between the change in convergence and rainfall; that is, the ending of storms could be better nowcast than the beginning stage. Watson and Blanchard emphasized that total area divergence is only part of the entire forecasting process that helps focus a day's activity on specific times and locations. In addition, Ulanski and Garstang (1978) used FACE network data in a somewhat different way to relate convergence gradient data to maximum point rainfall. A case study from FACE 1975 using total area divergence as defined by Watson and Blanchard is described by Cunning et al. (1982).

Results from the Illinois VIN project (Watson and Holle, 1982) were generally less favorable than FACE in all aspects. The lead time was less and the convergence-rainfall relation correlated at -.50. The reasons for the differences, however, are quite apparent in that most cloud systems in the VIN network were mature and moved rapidly across the network, whereas in the FACE region they were slow-moving entities. From these considerations, it was considered appropriate to apply the FACE results to the KSC network.

B. Radar and Lightning Studies

The work in Florida and Illinois is strong evidence for the existence of a relationship between surface convergence and subsequent radar echoes. If a quantitative relationship can be determined between radar echoes of different reflectivities and the probability of having lightning associated with them, then the line of evidence can be completed.

During the 1978 field operation of FACE, lightning data were collected simultaneously with radar data, providing an opportunity to determine if such a quantitative relationship existed. The lightning information was obtained using a two-direction finder (DF) system manufactured by Lightning Location and Protection, Incorporated (LLP). Except for the number of DF's, it is identical in operation and accuracy to the medium gain system used at KSC. The radar data for FACE were obtained from an S-band WSR-57 radar operating at a low scanning angle (0.5^{o}). The lightning and radar data were related to each other and the results presented by Holle et al. (1984).

Basically, the Holle et al. study consisted of inspecting the radar reflectivity present at the time and location of each lightning stroke. Several days were analyzed in this way. A very sharp distinction appeared between the frequency distributions of reflectivities of echoes associated with lightning and echoes not associated with lightning. The flashless reflectivities were mostly low, with a frequency peak at around 20 dBz, and with less than 15% having reflectivities larger than 36 dBz. Echo reflectivities associated with flashes, on the other hand, had a frequency maximum near 46 dBz, and about 65% had values of 36 dBz or more. Only echoes having a reflectivity of 44 dBz or more had a probability of more than 5% of being associated with a lightning flash. Thus, it appears that in south Florida there is a distinct relationship between the reflectivity of the echo and the probability that lightning will be associated with it. The threshold for significant probability appears to be around 44 dBz, increasing very rapidly to about 48 dBz. Interestingly enough, the probability of having lightning associated with an echo drops as sharply when the reflectivity becomes more than 48 dBz, being less than 5% when it is equal to or greater than 50 dBz. The reason for this behavior remains unclear, although it could be related to the fact that low-level echoes with very high reflectivities are indicative of collapsing convective cells that are no longer dynamically active.

C. Synoptic Controls

An important consideration in studying the relationship between surface convergence and lightning is the possible influence exerted by the synoptic situation. It is conceivable that the same amount of low-level convergence might correspond to very different levels of lightning activity under conditions of suppression and stability and under conditions of overall convective destabilization and forcing.

In order to explore the relationship between lightning activity and synoptic situation, Lopez et al. (1984a) used the lightning data collected in FACE during 1978. All the available days for the summer were stratified and grouped in terms of the maximum flash rate over a fixed large area during the

day. The early morning soundings for each group were then inspected with regard to stability and wind direction and speed. These parameters correlate very well with different synoptic regimes (Lopez et al., 1984b).

It was found that days marked by overall convective destabilization, indicative of synoptic forcing, typically produced the weakest clouds in terms of lightning activity. Large amounts of rainfall were produced during those days but the number of flashes per cloud was very low. On the other hand, during days of slight or neutral stabilization, when the synoptic influence was not prevalent, and when the convective field developed only under the forcing of local heating and sea-breeze circulations, the clouds produced considerably more lightning. Finally, the most severe producers of lightning were the very suppressed days when the low-level winds were slow. Very few clouds developed under those conditions, but the ones that did develop were in general the most active of the entire summer.

These preliminary studies tend to indicate that it is possible to anticipate the subsequent degree of lightning activity from a measurement of prior low-level wind convergence. They also stress the need for considering not only the mesoscale situation, but the synoptic background in which the mesoscale convective processes are developing.

3. 1983 KSC DATA COLLECTION AND PROCESSING

A. Mesonetwork Data -- Collection and Analysis Methods

Surface meteorological conditions were continuously monitored by the Automatic Range Meteorological System (ARMS). For this study, 15 instrumented towers at Cape Canaveral Air Force Station (CCAFS) and Kennedy Space Center (KSC) were used. As seen in Fig. 1, these meteorological stations are concentrated around launch sites and not distributed equitably throughout the area. The primary purpose of the ARMS is to monitor low-level diffusion for toxic corridor calculations. Twelve sites provided information at 12 and 54 ft, two sites were instrumented to 204 ft, and one went to 500 ft. Tower data included wind direction and speed, temperature and dewpoint, and atmospheric pressure.

Through the Weather Information Network Display System (WINDS), the meteorological information is retained on tape and provided on a real-time basis to various users at the Cape and KSC. The data were kindly provided to NOAA by the United States Air Force via the Meteorological Data Reduction Section (MDRS).

For the purposes of this study, the main emphasis was placed on the tower wind data recorded at 54 ft. The surface divergence fields were calculated from 5-min averaged winds. A 6 x 12 grid of equally spaced (2.8 km) points was superimposed upon the original network (Fig. 1). Through the use of an objective analysis scheme (Cressman, 1959), the network winds were transformed into a uniform grid of u- and v-components. The values of the wind components at each grid point were then used to compute the divergence quantities using a centered finite-difference scheme.

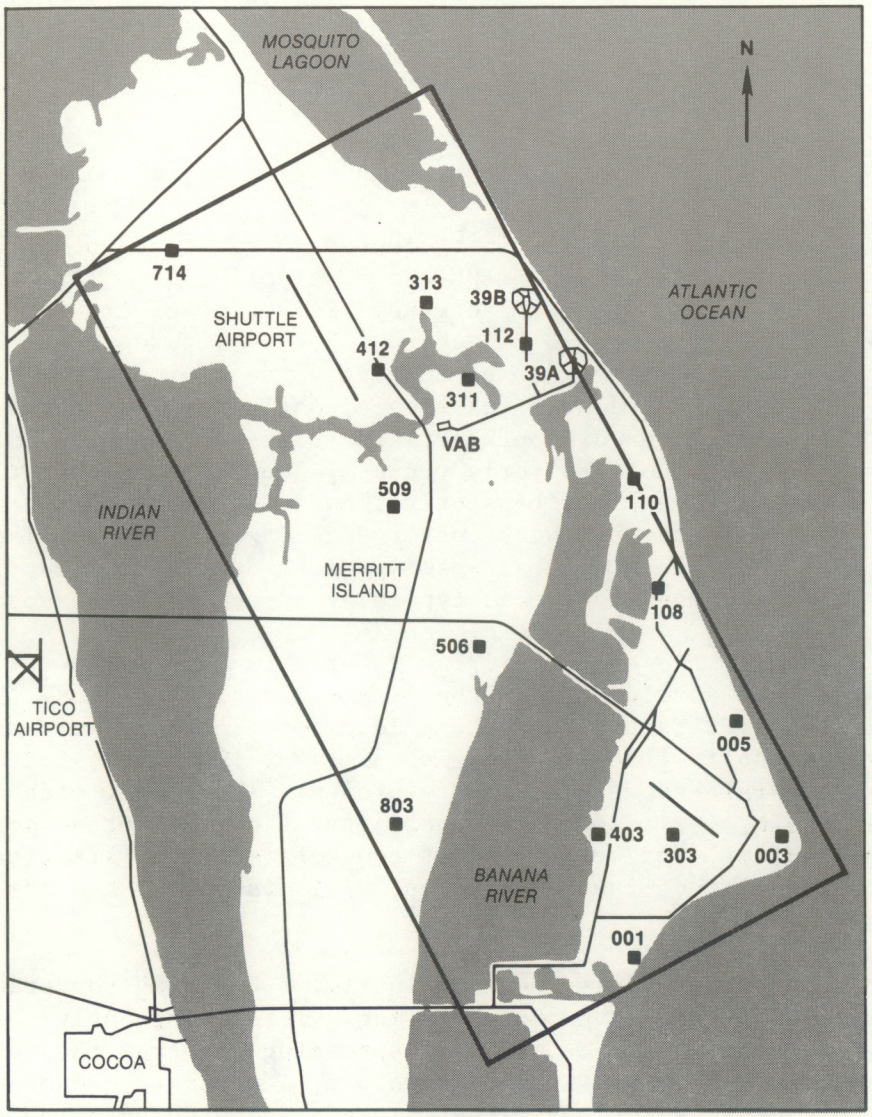

Figure 1. Kennedy Space Center (KSC) and Cape Canaveral Air Force Station (CCAFS) area. The rectangle marks the mesonetwork boundary. Solid squares indicate towers (meteorological stations).

B. Divergence Quantities

Divergence is defined as the expansion or spreading out of the wind velocity field. Divergence is taken to include convergence, i.e., negative divergence. In the discussion to follow divergence is defined as

$$\text{Divergence} = \nabla_h \bullet V = \frac{du}{dx} + \frac{dv}{dy} ,$$

where u and v are the x- and y-components of the velocity.

Through the use of a densely instrumented surface wind network, detailed information concerning the development and dissipation of a convective system can be inferred with the surface divergence field (Cooper et al., 1982; Cunning et al., 1982; Watson and Blanchard, 1984). Figures 2 and 3 present two examples from which the degree of convective development can be inferred. Figure 2a shows a weak sea-breeze confluence zone penetrating inland near the shuttle runway southeastward across the Cape on 16 September 1983 at 1655 GMT. Weak northeasterly winds are dominant northeast of the convergence line while weak southeasterly flow is recorded on the southwest side. Figure 2b indicates two weak convergence maxima (dashed lines) along the sea-breeze line indicating that weak vertical development may be occurring in these areas, since convergence is typically associated with upward motion.

Figure 3 details the events 1 1/2 h later. By this time (1845 GMT), a strong downdraft has developed over the Banana River. The winds (Fig. 3a) are spreading out in all directions from one location. A relatively strong divergence value (solid lines in Fig. 3b) of $1.4 \times 10^{-3} s^{-1}$ is indicative of moderate to heavy rain showers in that vicinity. Therefore, with a knowledge of the larger scale, i.e., moisture, stability, flow, and other possible triggering mechanisms, the meteorologist can determine the likelihood that convective cells will continue to develop, will dissipate, and where cells will move.

Another important feature is shown in Fig. 3. Strong convergence is found to the north of the divergence maximum. This is probably the gust front boundary dividing the cooler outflow air spreading out from the rain showers from the prevailing easterly winds. Therefore, a moderate convergence signal is shown in this zone as the gust front expands and undercuts the prevailing flow. This convergence zone is a prime area for continued convective development.

It has been found that several other divergence quantities are important indicators of convective development.

o Total Area Divergence. The first of these quantities is an area-averaged divergence. Cunning et al. (1982) have called that quantity "Total Area Divergence", DIV_T, and have defined it as

$$DIV_T = N_T^{-1} \sum_{i=1}^{N_T} (\nabla_h \bullet V)_i$$

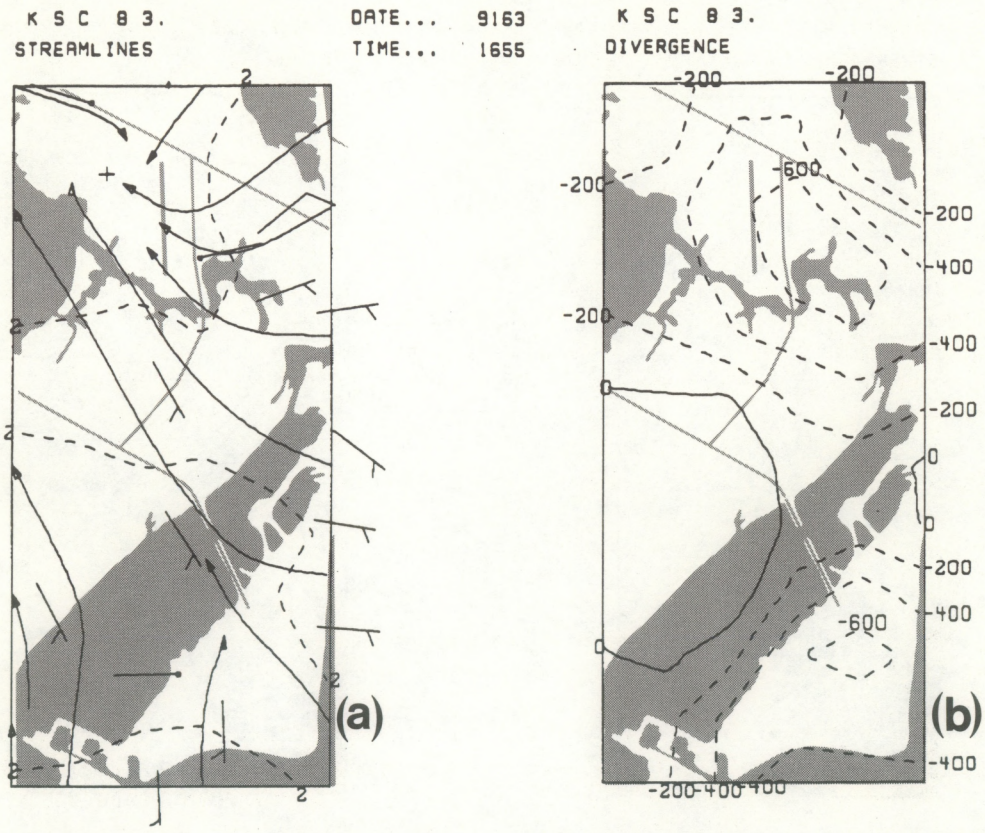

Figure 2. Wind and divergence patterns in KSC mesonetwork on 16 September 1983 at 1655 GMT. (a) Streamline, isotachs (in m s^{-1}), and station winds (full barb is 5 m s^{-1}); (b) divergence in 2 x $10^{-4}s^{-1}$ increments.

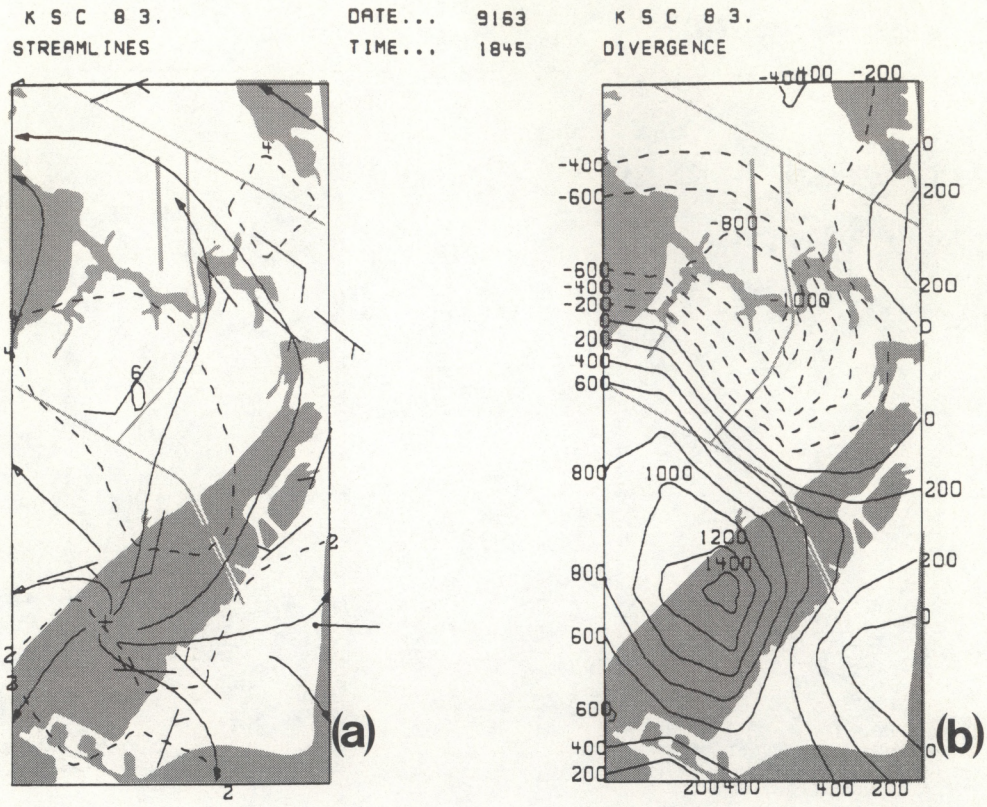

Figure 3. Wind and divergence patterns in KSC mesonetwork on 16 September 1983 at 1845 GMT. (a) Streamline and isotach patterns; (b) divergence in 2 x $10^{-4}s^{-1}$ increments.

for each 5-min period, where N_T is the total number of grid points in the network and $\nabla_h \cdot V$ is the magnitude of the horizontal divergence at each grid point. DIV_T is the same as the line integral of the normal component of the wind around the network boundary divided by the area of the network. Two other quantities that can be related to development and dissipation of deep convection are weighted convergence and weighted divergence.

o Weighted Convergence. It is the summation of only convergence values at grid points divided by the total number of grid points for each 5-min period.

o Weighted divergence. The opposite of weighted convergence, this relies on only grid points with positive divergence values.

The sum of weighted convergence and weighted divergence is total area divergence. Weighted convergence filters out positive divergence whereas the inverse is true for weighted divergence. Weighted convergence and divergence require an inner grid where positive and negative divergence quantities are calculated, but total area divergence can be calculated by the line integral method around the network boundary.

Figure 4 shows sample profiles of total area divergence, weighted convergence, and weighted divergence for 16 September 1983 at KSC. The sinusoidal pattern depicted by the total area divergence (Fig. 4a) beginning at 1345 GMT, has been observed to be coupled with rainfall events elsewhere (Watson et al., 1981). The convergence stage is related to inflow and the development of the storm. This is the period when there is, more or less, a monotonic drop in divergence. This stage ends at peak convergence and the first detection of precipitation on the ground. The divergence stage is associated with downdrafts and outflow at the surface. In FACE and VIN, a maximum in precipitation was observed to be followed by a maximum in divergence, and eventual dissipation of the system within the mesonetwork.

Only network convergence is portrayed in the weighted convergence profile in Fig. 4b. Strong peaks in the convergence profile have usually been found to be associated with developing convection. On this particular day, convergence was quite prevalent due to the fact that the sea-breeze convergence zone remained quasi-stationary over the Cape and KSC area for a considerable amount of time prior to the occurrence of precipitation. Thunder was first heard by the weather observer at the Shuttle Airport runway at 1830 GMT in a convective cell south of that position. Precipitation was not detected at the Shuttle runway until 1936 GMT. However, the 5-min wind and divergence analyses (see Fig. 3) indicate precipitation at the ground south of the Shuttle landing strip at approximately 1815 GMT.

Figure 4c vividly describes the influence of the downdraft and precipitation on the weighted divergence profile. Promptly at 1815 GMT, there was a sharp increase in weighted divergence which peaked at 1900 GMT. Again, the weighted divergence time series indicate the effects of precipitation and downdrafts hitting the ground and spreading the air horizontally.

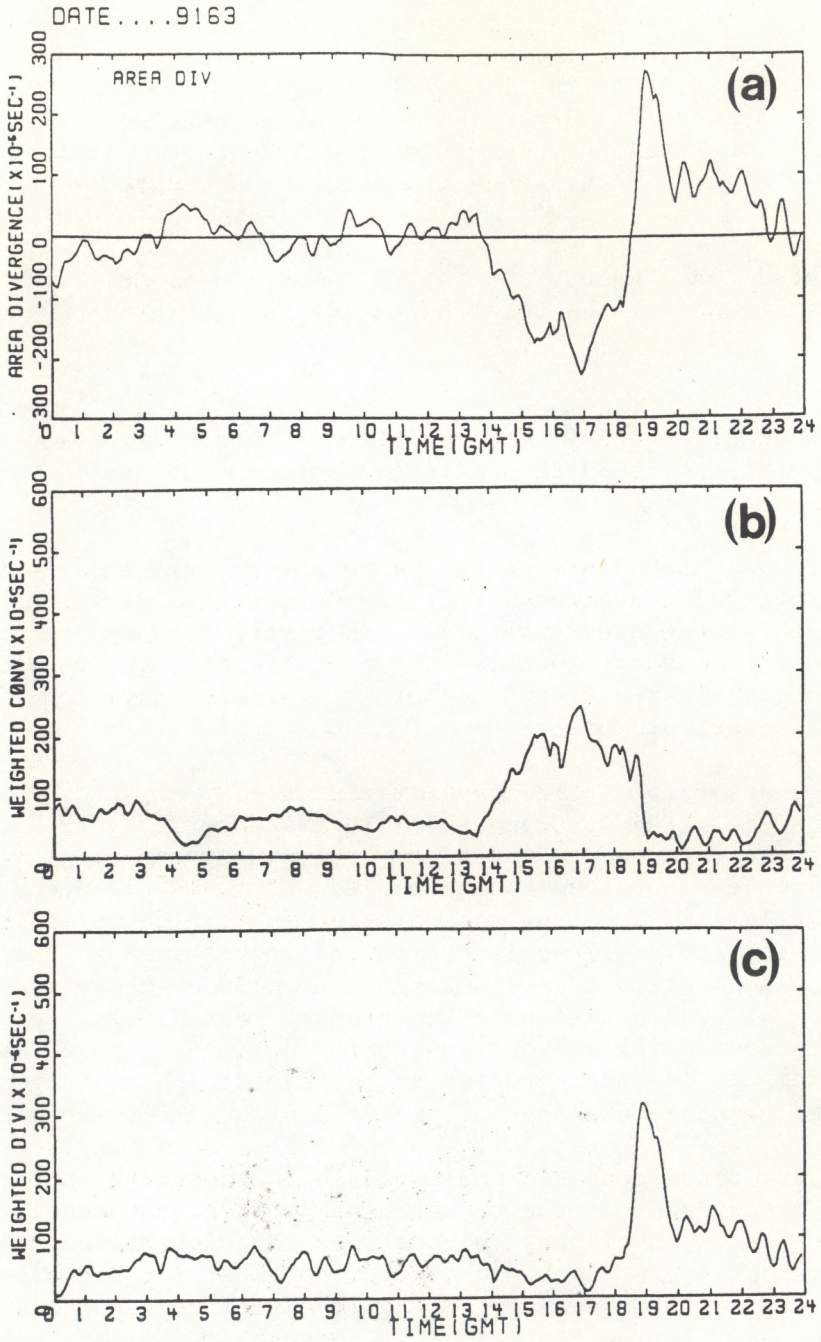

Figure 4. Divergence time profiles for 16 September 1983. (a) Total area divergence; (b) weighted convergence; (c) weighted divergence.

Total area divergence (Fig. 4a) puts together both effects. The complete life cycle of a convective system within the boundaries of the mesonetwork can be viewed. There is a sudden increase in total area divergence when precipitation begins at 1815 GMT. Maximum rain rate probably occurs during the cross-over (0 divergence) from network convergence to network divergence. Rain ends at 2208 GMT when the total area divergence profile returns to quiescence. Only 0.20 in of rain was recorded by the observer at the Shuttle Airport runway. However, this location was somewhat north of the most intense core of the convective cell.

It is important at this point to express some cautions concerning total area divergence. First, since surface convergence identifies convective potential that is forced from the boundary layer, the boundary layer must be sufficiently mixed so that potential temperature, mixing ratio, and momentum remain relatively constant. If the boundary layer is not well-mixed, detecting convective development by means of surface winds will be impossible until downdrafts come in contact with the surface and move out in the form of gust fronts.

At times, the atmosphere may be capped and conditions may not be favorable for deep convection. The sea-breeze circulation, being a convergent zone caused by differential heating between the land and ocean surfaces, will depict moderate convergence in the total area divergence profile as it passes through the mesonetwork. When there is no precipitation and outflow in the network the divergence peak associated with these events will be missing. After peak convergence, the total area divergence time series will gradually adjust itself back to near-zero divergence.

Outflows from distant cumulonimbus systems may traverse the network, causing convergence without triggering new convection. In this case, the sinusoidal pattern of convergence followed by divergence is present in the total area divergence time series without initiating precipitation in the area.

The size of the wind network plays a major role when total area divergence is used to anticipate convective development. The convective system is fueled from the surrounding area and total area divergence is used to measure this process. If the area is too large, the convective entity may be lost, since several systems could grow and die in the area at the same time canceling each other in the averaged divergence field. The reverse is also true, since the network may be too small to describe the convective development. The smaller the network, the greater the chance of only partially recording the development stage; frequently only the dissipation stage appears to be contained in the network. If the system is moving, development and convergence may be in the network while precipitation and dissipation are outside the area; or the reverse could be true. Much of the time, the KSC network (Fig. 1) in its present configuration is probably too small to record all of the stages of development accurately.

Watson et al. (1981) examined variable station separation. It was found that the sinusoidal pattern signal of convective events in total area divergence is quite large within network scales of 1500 to 3000 km^2 and very few stations (8 to 12 mile station separation) are required to detail its characteristics. The problem arises that the exact location of development is

lost with only a few sites. Therefore, a relatively uniform station grid provides a focusing of the location and movement of convergence and divergence centers. Figure 1 describes the KSC situation as having a very dense set of sensors over the Cape, around the VAB, and Pad 39A and B complexes. The remainder of the area is poorly represented by sensors.

Natural variability of convection poses a final and most complicated problem. Convection piercing into a dry mid-troposphere will yield less rainfall than convection tapping a relatively moist mid-troposphere. These two situations may have nearly equal convergence magnitudes while their effects on precipitation, strength of downdrafts and outflows, and lightning may be completely different.

Familiarity with the regional scale meteorological conditions is essential. As surface and upper-air data are updated the forecaster must anticipate the chances of convective development and possible movement. Monitoring by satellite and radar bridges the gap from synoptic to mesoscale. The passage of mid-troposphere troughs and shortwaves must be anticipated; frontal movement, climatological situation, timing for convective temperature and initial vertical development, development of cloud lines on satellite, interaction of gust fronts, and arrival of squall lines must be reviewed. On the smallest scale, mesonetwork data can provide a 30-45 min nowcast as to location and magnitude of convective development. Continued monitoring of total area divergence will give information on the stage of development, i.e., developing, mature, or dissipation stage.

C. Radar Data

The radar data used in this study were obtained from Daytona Beach (DAB) (Fig. 5). This radar was a WSR-74S system belonging to the National Weather Service (NWS) and having a wavelength of 10.39 cm. The antenna beamwidth was 2^{o} and the minimum detectable signal (MDS) was -104 dBm. The radar operated continuously; however, only data from 1000 GMT to 0200 GMT (1500 to 0700 EDT) and from July 15 to September 30, 1983 were recorded. A full 360^{o} scan covering a range from 21 to 450 km was recorded every 5 min. The antenna elevation was kept at a low scanning angle (0.5^{o} to 0.8^{o}) most of the time. Only data from scans at less than 1.5^{o} elevation were used.

The data were digitized and recorded on magnetic tape. The returned power signal was nominally integrated for sectors of 1 km in range and 1^{o} in azimuth. These signals were then digitized on a scale of 0 to 255, using 8 binary digits. Four hundred and fifty such sectors were integrated and digitized along a given 1^{o} azimuth region. A range delay of 20 km was used. Digitizer calibration runs were made and recorded on tape at the beginning, middle, and end of the recording period. Because of the good stability of this radar, the resulting calibration curves did not vary significantly. Accordingly, only one representative curve was used for the entire period.

The first step in processing the data was to distinguish between noise and valid data. The data for several days were inspected to determine the level of the random (non-true-echo) noise fluctuations in detected power. The proper calibration and the radar equation were then used to assign a radar reflectivity to every video data point whose digitized value was above the

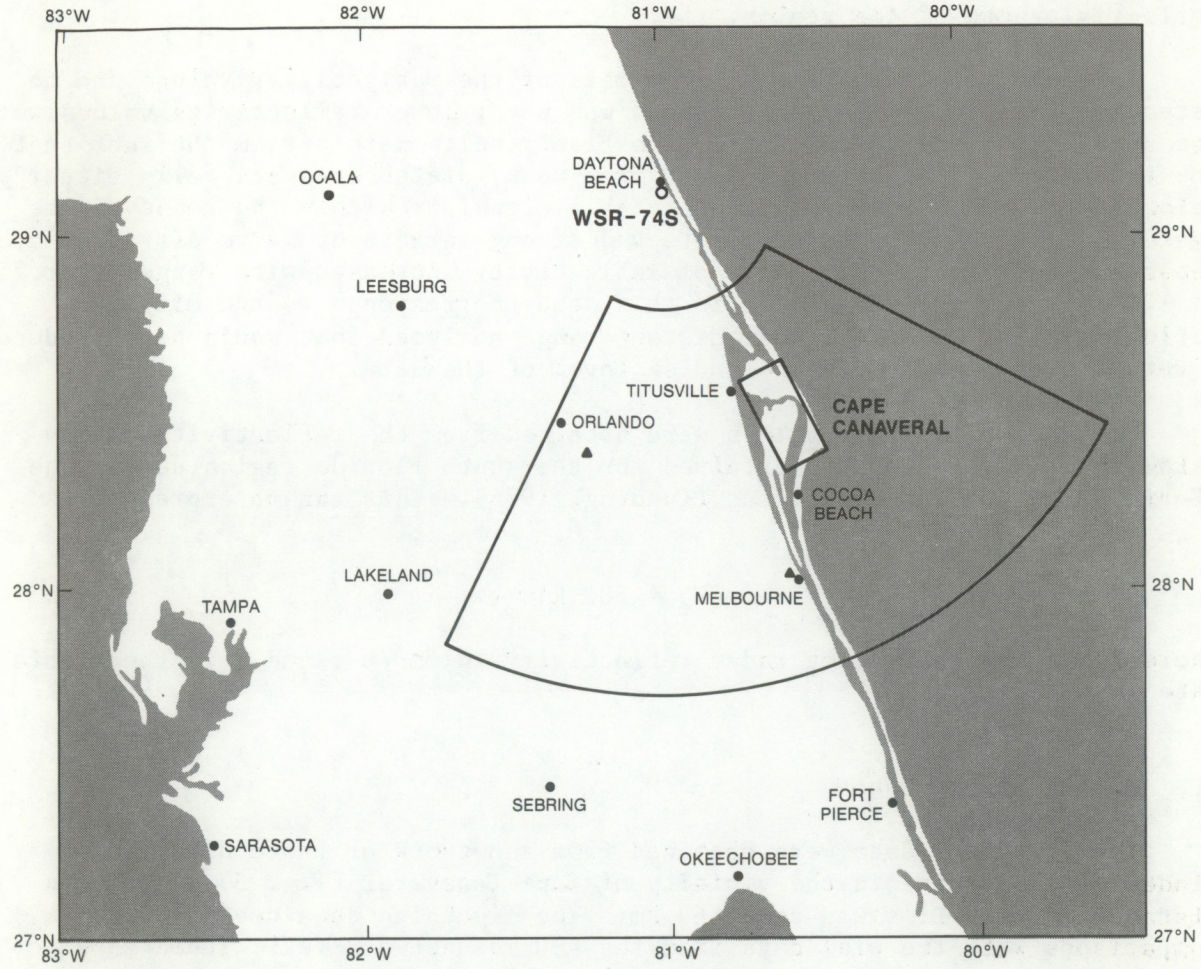

Figure 5. Regional map of central Florida showing location of National Weather Service WSR-74S radar at Daytona Beach (DAB); the truncated cone outlines the principal area of analysis, 31 to 145 km to the south. The Kennedy Space Center wind network is shown by the rectangle, and the three lightning direction finder sites are indicated by triangles.

noise level. Only points in an area bounded by the 31- and 145-km-range circles, and the 123° and 206° azimuths were used in the study (Fig. 5). The resulting values were put into a data matrix that constituted a low-level reflectivity map of the region.

In order to eliminate the range bias of the reflectivity values due to detection failure, a 22-dBz threshold was used; lower reflectivity values were not used in the analysis. This range bias results mainly from the fact that the intensity of the returned power from weak, distant targets falls either below the level of the minimum detectable signal or within the noise of the system. As a result, only moderate and strong targets at large distances are detected, and the average value of reflectivity increases with range after 75 to 100 km. The threshold used in this study corresponds to the minimum reflectivity value at the most distant range analyzed that would have produced a return signal just above the noise level of the data.

Equivalent rainfall values were obtained from the reflectivity map by using the Z-R relationship obtained for the south Florida region during the Florida Area Cumulus Experiment (Cunning, 1976). This can be expressed as

$$Z_e = 300\ R^{1.4}\ ,$$

where Z_e is the equivalent radar reflectivity in mm^6/m^3, and R is the rainfall rate in mm/h.

D. Lightning Data

The lightning data were obtained from a network of three direction finders (DF) located in the vicinity of Cape Canaveral (Fig. 5). The mean distance between DF's was about 69 km. The lightning data used in the comparisons with the wind data from the KSC mesonetwork fell within 76 km of any particular DF (small triangles in Fig. 5). The area represented by the data is a truncated cone with vertex at the Daytona Beach radar and bound by the 123° and 206° azimuths and the 31- and 145-km-range circles. Thus, flashes within this region were not more than 85 km away from a DF, and in most cases were much closer.

The information from the DF's was transmitted to a central processing site where cloud-to-ground (CG) flash positions were computed and displayed. The original DF data (containing the time, azimuth, signal strength, and number of return strokes of the detected flashes) were recorded on cassette tapes. These data were used in the present study to recompute the flash locations. The system operated continuously during the day. Data for this study were obtained for the entire summer of 1983 except for days when a malfunction of the system occurred.

The description of this lightning-mapping system, manufactured by Lightning Location and Protection, Incorporated (LLP), has been presented by Krider et al. (1976) and Krider et al. (1980). Basically, the DF's consist of a wideband system of two orthogonal magnetic-loop antennas and a flat-plate electric antenna. The magnetic field of a lightning flash produces a signal in the circuit of each of the loops which is proportional to the field

strength and the cosine of the angle between the plane of the loop and the direction of the field. From the ratio of the signals of the two loop antennas, the direction of the flash can be determined. The 180° ambiguity of the direction is resolved by the use of the flat-plate electric antenna which detects the polarity of the charge brought to ground.

The system discriminates against cloud-to-cloud discharges and background noise by comparing the field waveshapes of the observed flash against those shapes typical of CG discharges. Subsequent strokes after the initial one are distinguished in a similar way. The location of the ground contact point is assured (rather than some elevated position along, or branching from, the channel) by using the information of the flash field at just the time of the first peak, when the stroke current is still about 100 m from the ground. Only negative flash information was available at the time that the present data were collected.

The positions of the flashes were obtained by triangulation, using the quasi-simultaneous (within 100 ms) direction vectors of the DF's. When the discharge occurred near the baseline (10°) of two DF's, and the third did not detect the flash, the supplementary angles and the ratio of the detected first stroke signal strengths were used to compute the flash position.

The angular accuracy of the DF system has been estimated at 1°-2° or better (Krider et al., 1976). This accuracy at the ranges employed has also been determined to be adequate to resolve individual cells of electrical activity within larger cloud systems. Assuming this angular accuracy, the lightning locations in the present area of study would have a corresponding linear displacement error of 1 to 2 km, depending on the distance of the flashes to the different DF's.

The detection efficiency of these systems has been estimated as 80% to 90% in the 20- to 120-km range for a medium gain DF system with a baseline of 50 km (Maier et al., 1983). Thus, this nominal range of 120 km for a detection efficiency of 90% covers well the data region used in the present study.

Other factors can affect the performance of the DF system. One is the alignment of the crossed-loop magnetic antennas. Normally the accuracy of this alignment can be kept within ±0.5° (Maier et al., 1983). However, large deviations (up to 11°) did occur on some of the sites. The manufacturing company (LLP) checked the misalignment and provided the appropriate corrections.

Another factor consists of systematic angle errors that are associated with non-uniform terrain and large conducting objects near the antenna sites. Again LLP obtained the necessary corrections by subjecting the data to an iterative objective analysis that used the lightning signal amplitudes and angles at all the DF sites for thousands of flashes to minimize the systematic angle errors. These corrections, as well as those for antenna rotation were used to recalculate the flash locations used for this study.

The raw data were subjected to an editing and location-computation process that produced a basic data base of lightning stroke positions within the area of analysis. From this, time series of 5-min flash rates, as well as flash location maps, were constructed for the different study days.

At times when the lightning mapping system was unavailable or when it was believed necessary to compare the data, the KSC electric field mill system was used. The field mills measure the vertical component of the atmospheric potential gradient at ground level. Currently there are 29 field mills on KSC and CCAFS. The system has been described in detail by Jacobson and Krider (1976) and Piepgrass and Krider (1982). Two methods for determining lightning flashes are used. Lightning is assumed to occur when very rapid charges in field values are detected. Thresholds are 600 V m^{-1} field change detected by at least two sites and 850 V m^{-1} change detected by at least three sites.

4. 1983 KSC CASE STUDIES

The three August days examined in detail were chosen because of their active convection. Discussion of the mean thermal and moisture characteristics for the whole month provides a general background for the three case studies, and two additional examples.

A. Mean Conditions

Figure 6 is a time cross section of temperature difference from the mean, i.e., the temperature at 50-mb increments for soundings taken at the Cape between 0900 and 1200 GMT each day subtracted from the mean temperature at those levels for the month of August 1983. Figure 7 is a time cross section of mixing ratio difference from the mean.

The early part of the month shows little temperature and moisture variation as a uniform tropical airmass provides rather deep south-southeasterly flow across east-central Florida. On the 4th and 5th, warmer temperatures near the surface and moist conditions throughout the column provide fuel for considerable convective development over the mainland west of KSC. Beginning on the 6th, warmer temperatures at upper levels descend through the column and decrease stability by the 11th. During this period the Atlantic ridge slips southward and low- to mid-tropospheric winds veer from southeast to almost directly west by the 9th. Increasing moisture at middle-levels begin on the 6th, reach a maximum on the 9th, but maintain high values through the 12th. Finally, warming below and cooling aloft make the 11th and 12th unstable.

Westerly flow continues through the 14th with somewhat cooler than normal temperatures in the mid-troposphere. Drying from below begins on the 12th, the driest conditions, extending to 450 mb, occurring on the 16th. The 15th, 16th, and 17th continue to be weakly unstable with development only on the 15th and 16th.

Moisture begins to increase on the 17th and reaches a maximum on the 19th, which is countered by very warm temperatures aloft that effectively put a lid on any development. Suppression continues through the 22nd. Dry conditions result during the latter part of the suppressed period ending about the 23rd.

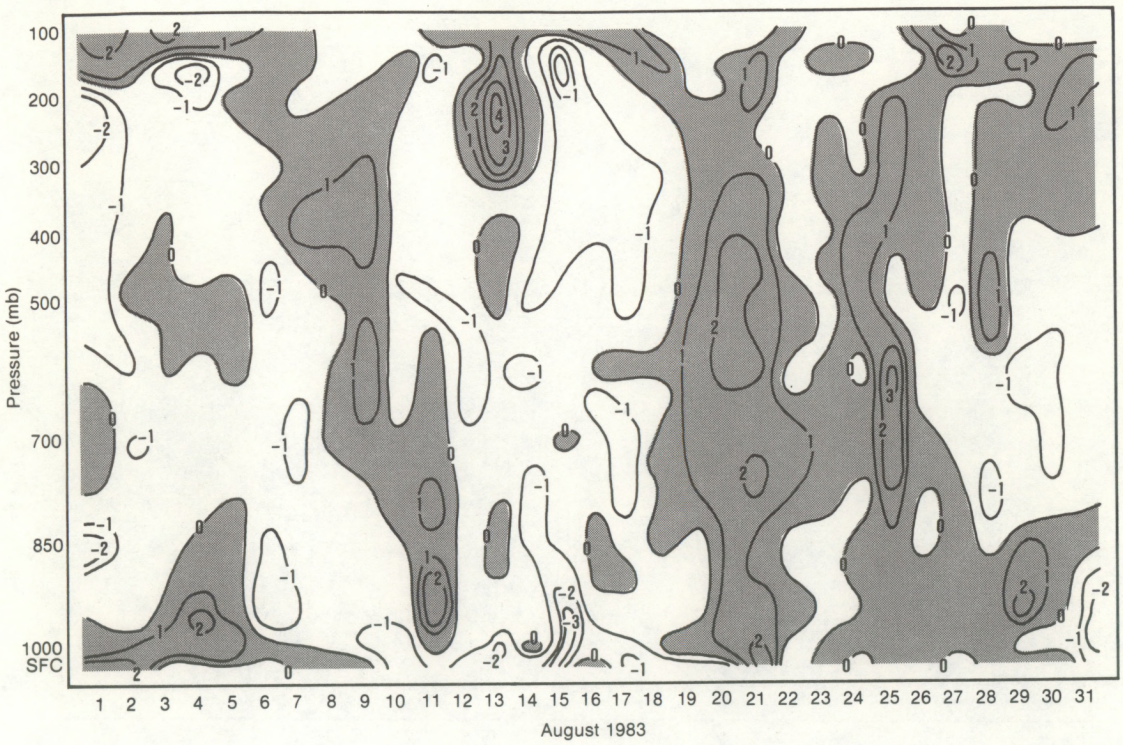

Figure 6. Temperature difference from the mean at 50-mb increments for soundings taken at Cape Canaveral between 0900 and 1200 GMT during August 1983. Shading denotes temperatures greater than the mean.

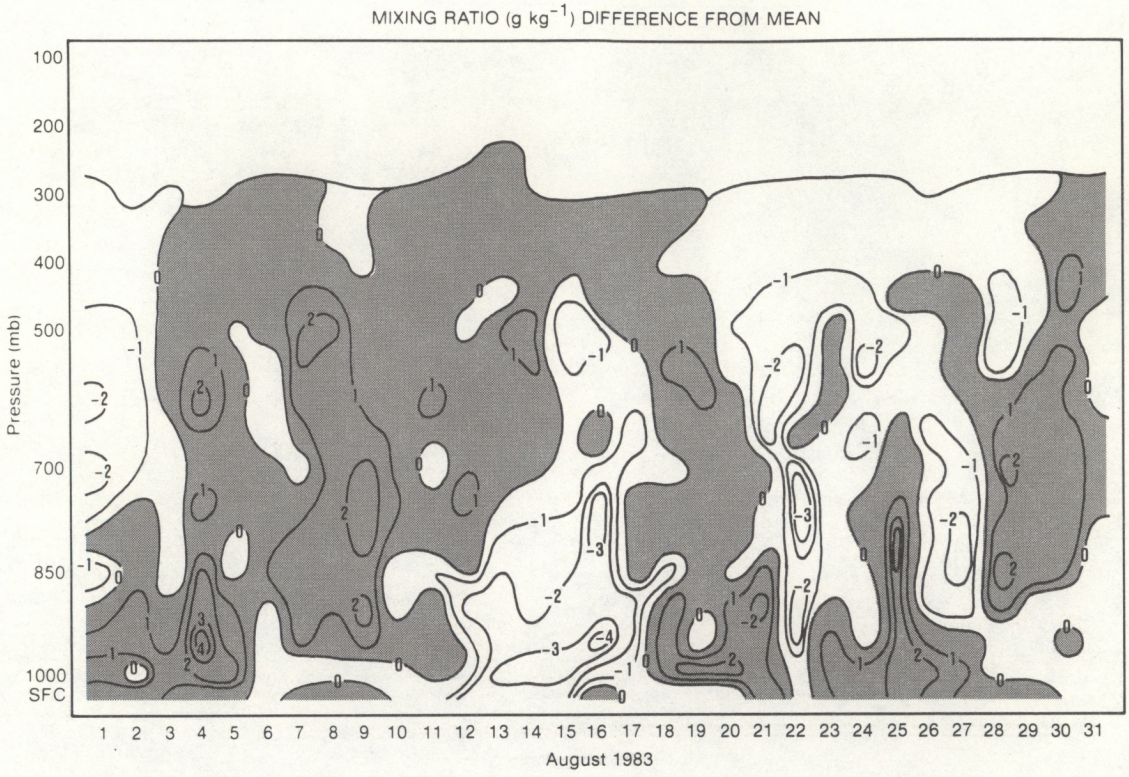

Figure 7. Mixing ratio difference from the mean at 50-mb increments for soundings taken at Cape Canaveral between 0900 and 1200 GMT during August 1983. Shading denotes moisture greater than the mean.

On the 25th, tropical storm Barry traverses the area; temperatures are warmer, and moisture is at low to middle levels. Destabilization begins again on the 26th, and cooler temperatures aloft reach a peak on the 29th and 30th. Middle-level moisture appears again on the 29th as a mid-tropospheric disturbance is in the vicinity.

Figure 8 presents the maximum 5-min CG lightning (LLP) flash rate for each day of August 1983, in the 430 km^2 region in and around KSC (Figs. 1/ and 5). Two strong maxima are noted during the month: 10-12 August and 30-31 August. Therefore, for the case studies, we have selected 10 and 30 August. If the data for 7 August were not missing, they would probably show another peak. August 7 was selected as a case study day because the largest convergence and divergence signals for August and September of 1983 were recorded during this day.

B. Case Study 1: 7 August 1983

The dominant meteorological influence on 7 August is troughing over the southeast United States in which a convective pulse intensified by afternoon heating moved across central Florida. Figure 9 illustrates the surface situation at 1200 GMT, 7 August. Weak ridging extends westward over south-central Florida from the Atlantic high. Troughing extends across the southeast United States into the Gulf of Mexico.

Figures 10a-d are the constant pressure charts for 850, 700, 500, and 300 mb at 1200 GMT. A north-south trough is quite evident at 850 and 700 mb through central Georgia extending southward just east of Apalachicola, Florida. At 500 mb (Fig. 10c), the flow is generally weak westerly to southwesterly over Florida, and the trough is farther northwest, oriented east-west across central Georgia to southern Louisiana. At 300 mb (Fig. 10d), the flow is very weak with ridging across Florida. Notice that moisture is abundant at all levels.

Figure 11 is a sequence of satellite imagery for the period.

0930 GMT (Fig. 11a). This is an infrared (IR) image with MB enhancement, which is a standard curve used to enhance convective activity. The interesting feature here is a line of weak showers extending from north-central Florida southward across Tampa, continuing into the Gulf of Mexico.

1631 GMT (Fig. 11b). This visible imagery shows the weak line of showers near Daytona Beach and extending down to the southern tip of Florida.

2300 GMT (Fig. 11c). The enhanced IR image shows that convection has exploded, and the major portion of the line is now offshore Cape Canaveral, extending southward over Miami and the upper Keys.

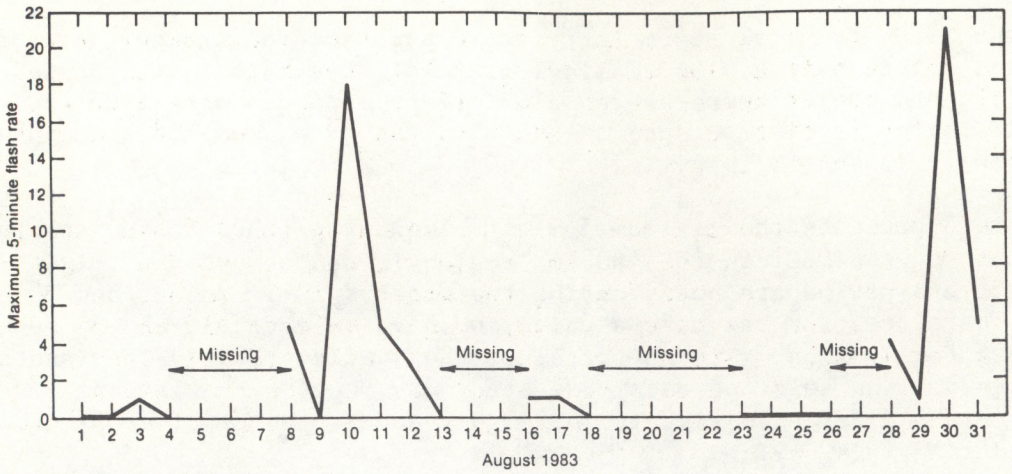

Figure 8. The maximum 5-min cloud-to-ground (CG) lightning flash rate for days during August 1983, in the 430-km^2 region of the KSC mesonetwork.

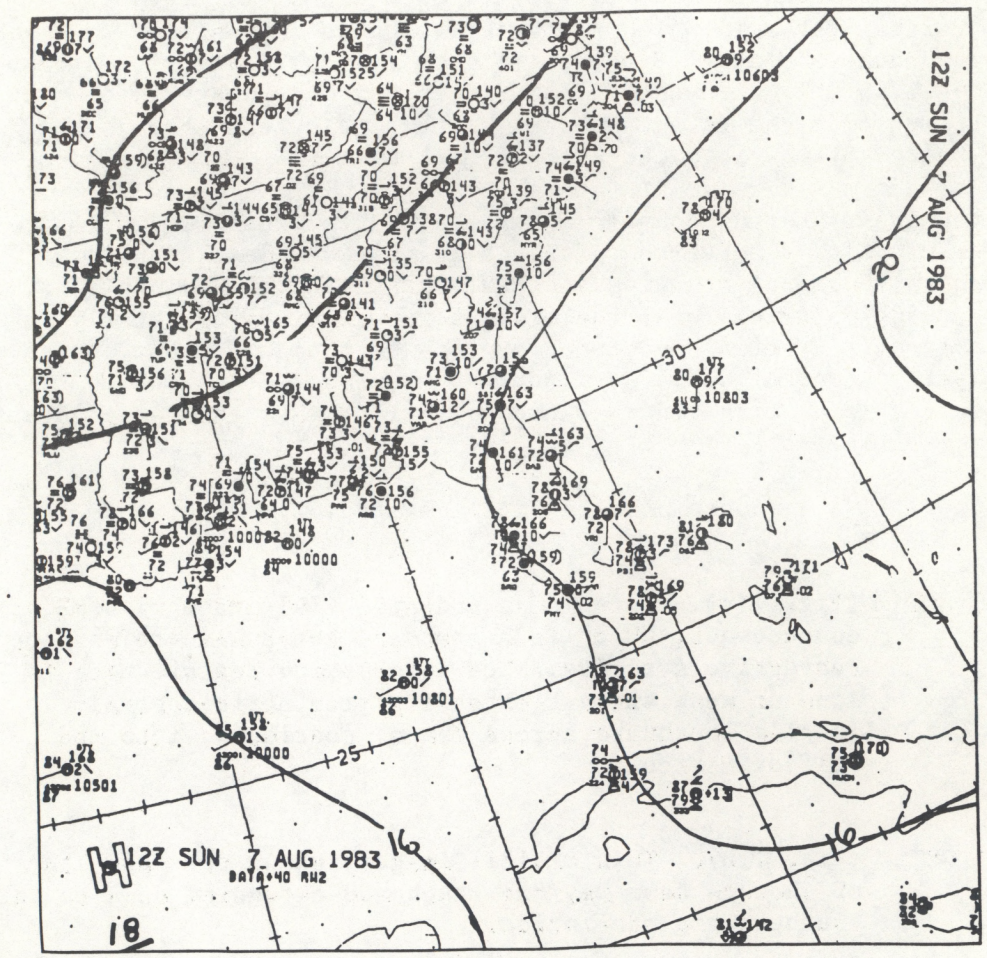

Figure 9. National Meteorological Center (NMC) surface analysis for 7 August 1983 at 1200 GMT.

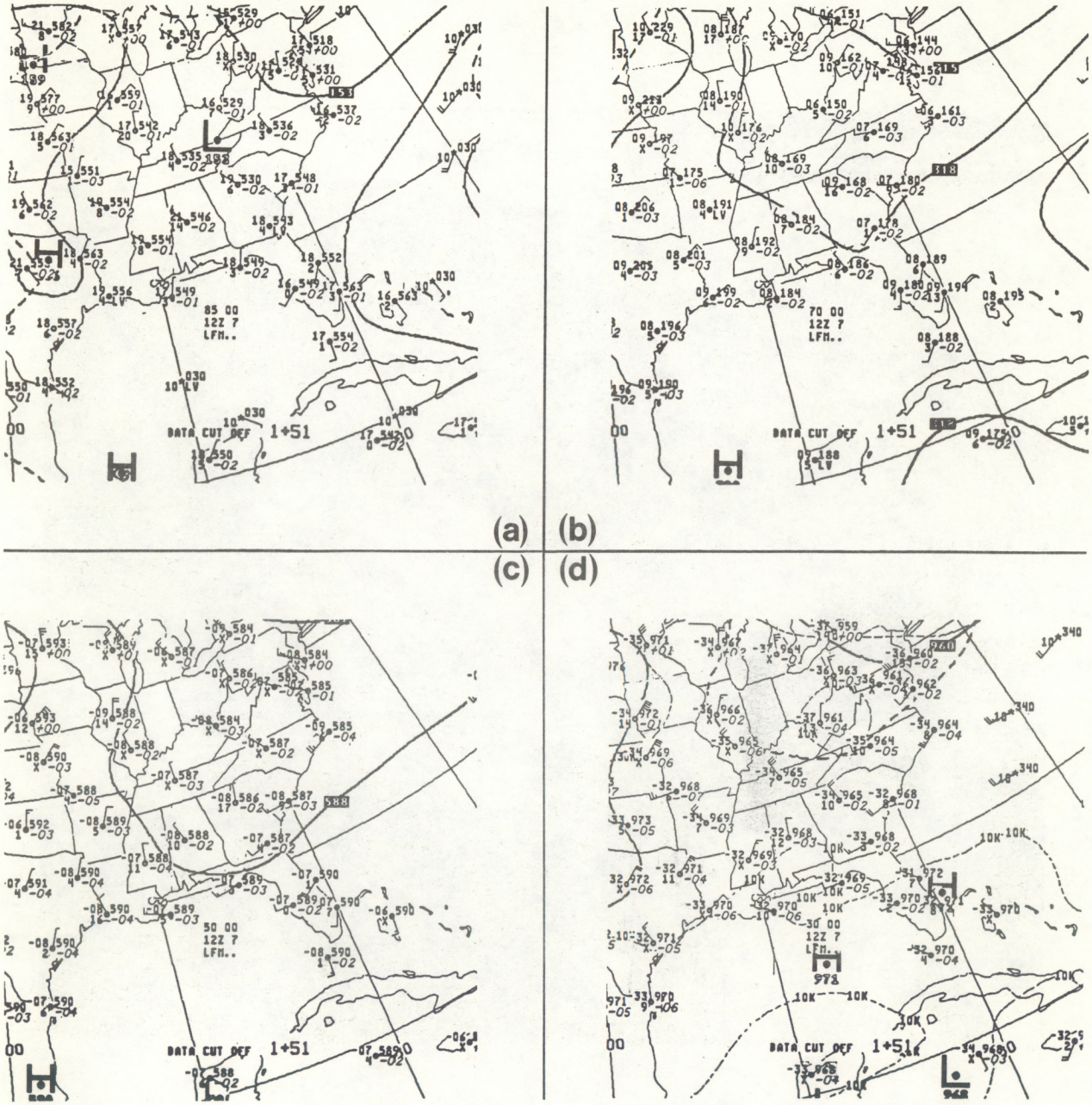

Figure 10. NMC upper-air analyses for 7 August 1983 at 1200 GMT for (a) 850 mb, (b) 700 mb, (c) 500 mb, and (d) 300 mb.

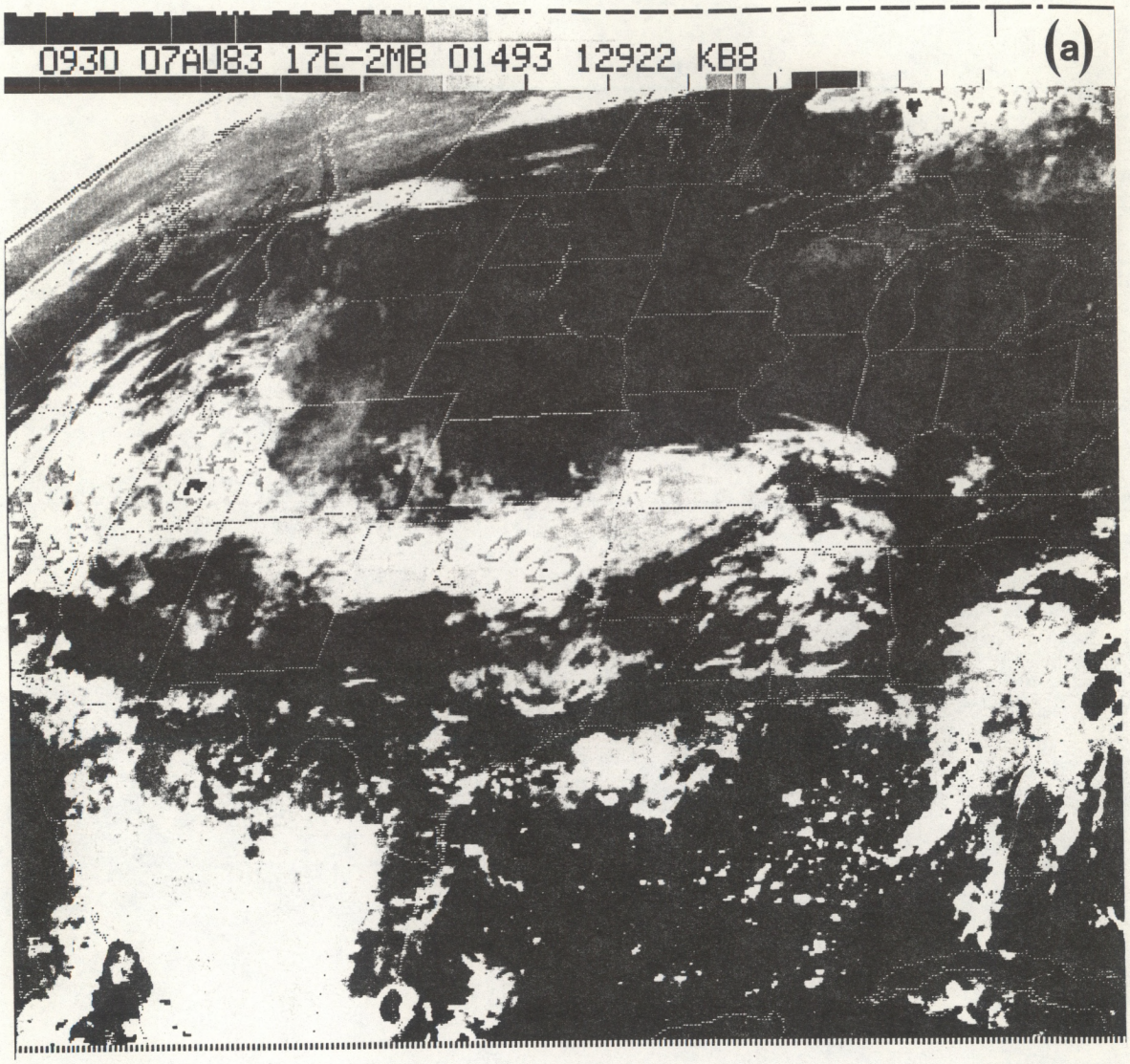

Figure 11. Satellite imagery for 7 August 1983. (a) 0930 GMT IR image with MB enhancement.

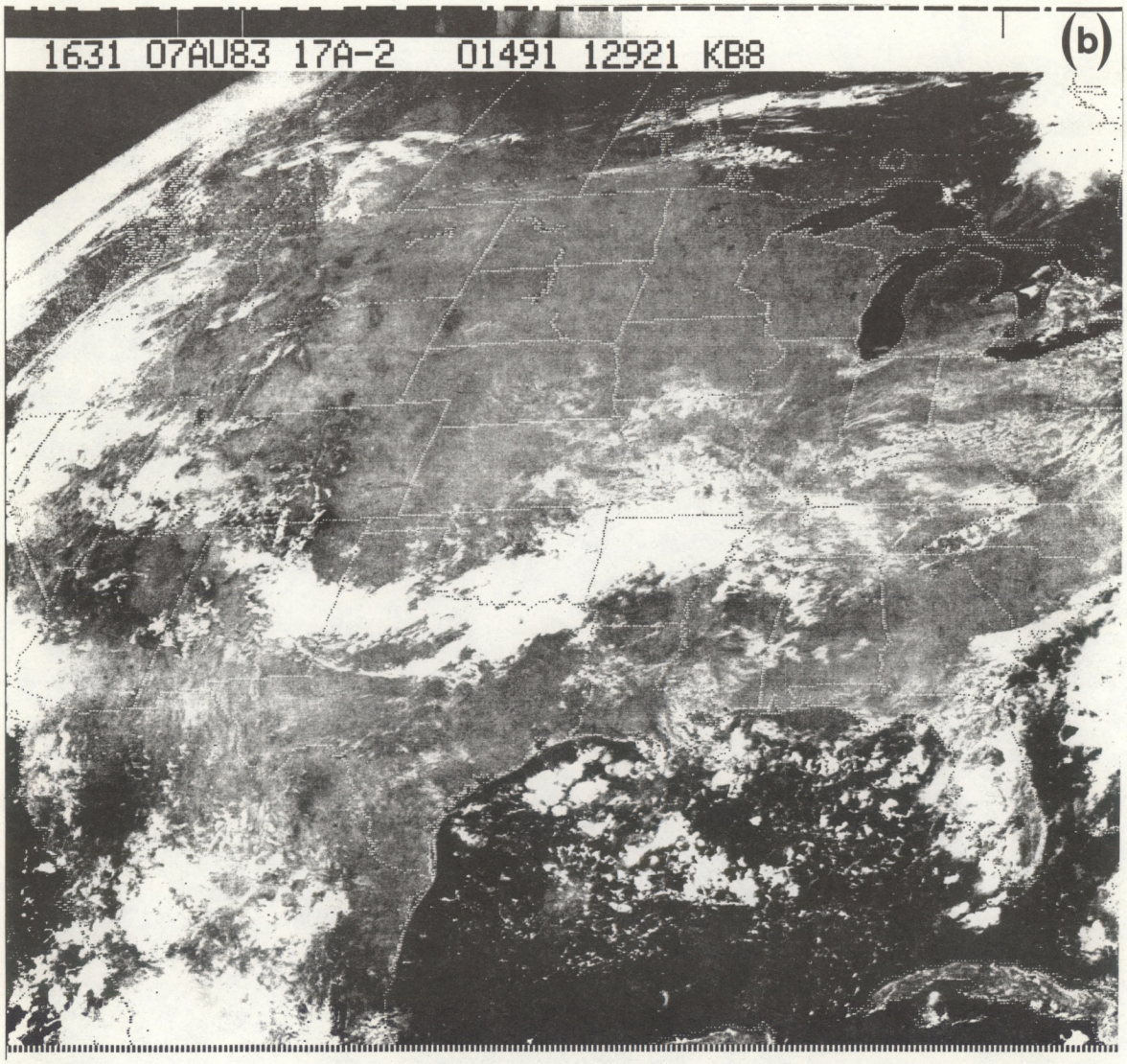

Figure 11. (Continued). (b) 1631 GMT visible image.

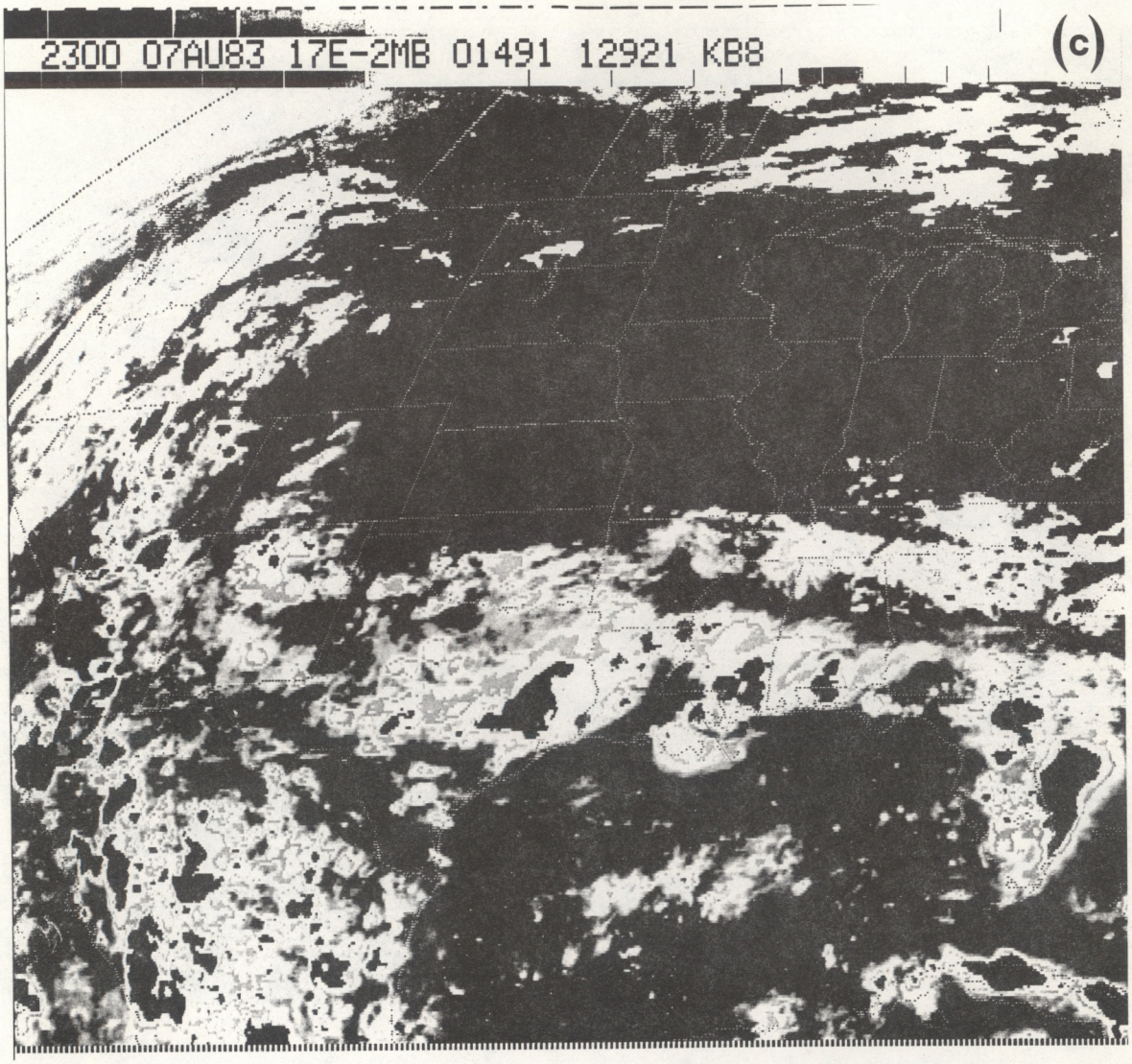

Figure 11. (Continued). (c) 2300 GMT IR image with MB enhancement.

Coming down in scale, examination of the local and neighboring soundings is critical as part of the total assessment of the local and large-scale situation. Figure 12 is the sounding taken at Cape Canaveral at 1200 GMT, 7 August, represented on a skew-T, log P diagram. Moisture is abundant at all levels. Mainly weak winds are southwesterly in the lower levels, becoming northwesterly at upper levels. The total-totals index is 48; the lifted index is -7, an unstable sounding for Florida, indeed. Therefore, the forecast for thunderstorms is necessary; only timing remains a question.

The predicted high temperature (850 mb temperature extrapolated dry-adiabatically to surface pressure) and the average mixing ratio for the lowest 100 mb was used to determine the LCL (lifted condensation level), LFC (level of free convection), positive buoyant energy, and negative area above the equilibrium level. This is graphically displayed on the skew-T plot in Fig. 12. The expected maximum top for thunderstorms in this case would be above 100 mb.

Figure 13 shows hourly reflectivity scans from the Daytona Beach National Weather Service radar (DAB). The area covered lies between 123^{o} and 206^{o} in azimuth, and between 31 and 145 km in range from Daytona Beach (Fig. 5). The Florida coastline and KSC surface network boundary are included for reference.

1600 GMT (Fig. 13a). The convective line seen by satellite is approaching the east coast from the mainland to the west of the Cape.

1700 GMT (Fig. 13b). The convective line continues to move eastward at 20 km h^{-1}. Weak activity is developing over the KSC network.

1800 GMT (Fig. 13c). The line is approaching the northwest corner of the KSC network. It is possible that a weak gust front lies just ahead of the convective line, providing the additional lift to an environment primed for convective development. The new line of showers begins to develop just to the east and in the same orientation as the old convective line to the northwest.

1900 GMT (Fig. 13d). All activity has consolidated over KSC in a north-south configuration.

2010 GMT (Fig. 13e). Level 3's and 4's are exiting the southeast corner of the KSC network.

2100 GMT (Fig. 13f). The convective line has continued eastward into the Atlantic at 20 km h^{-1}, leaving only dissipating anvil precipitation (level 2) in its wake.

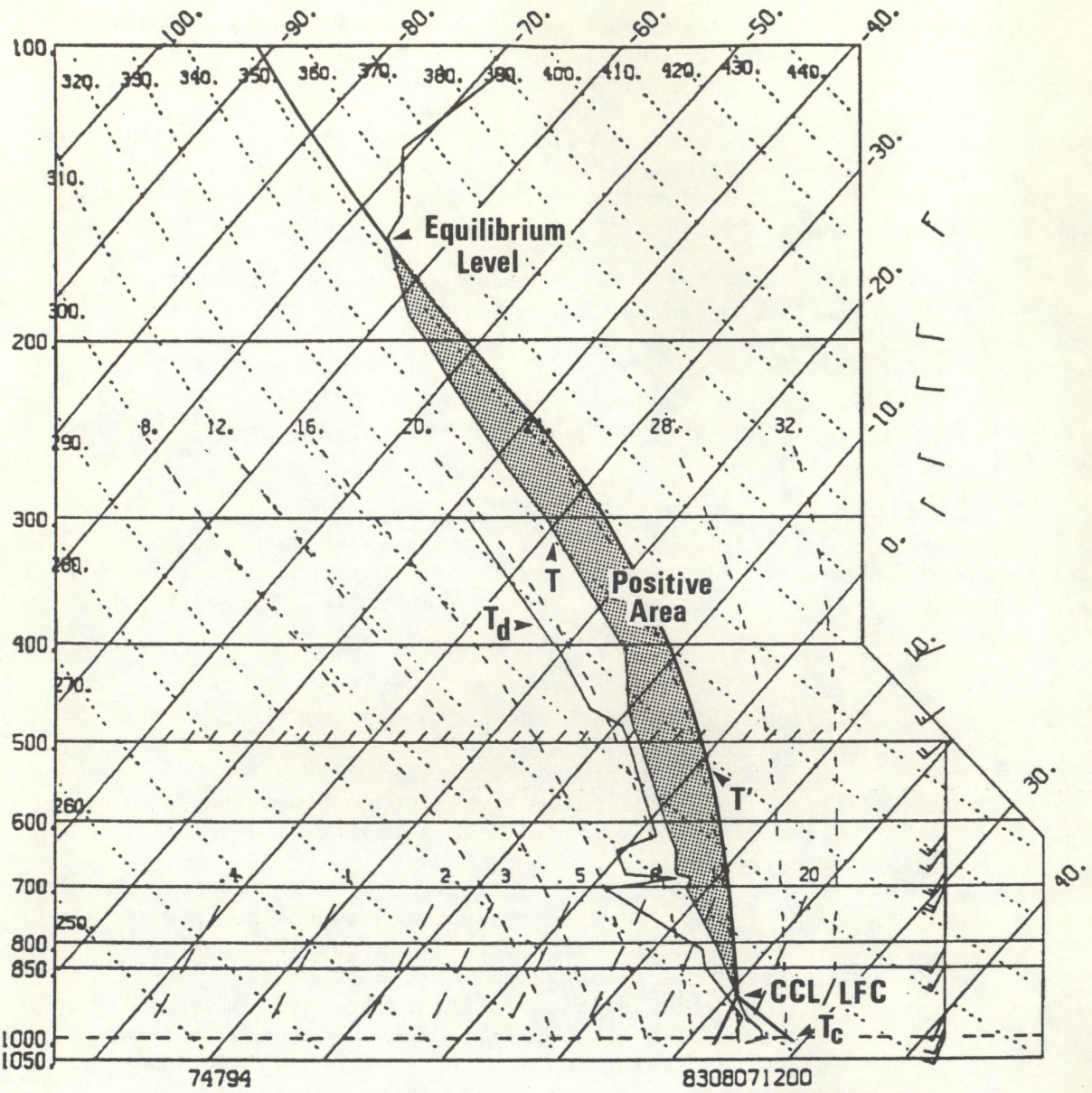

Figure 12. Rawinsonde sounding for Cape Canaveral at 1200 GMT, 7 August 1983, plotted on a skew-T, log P diagram.

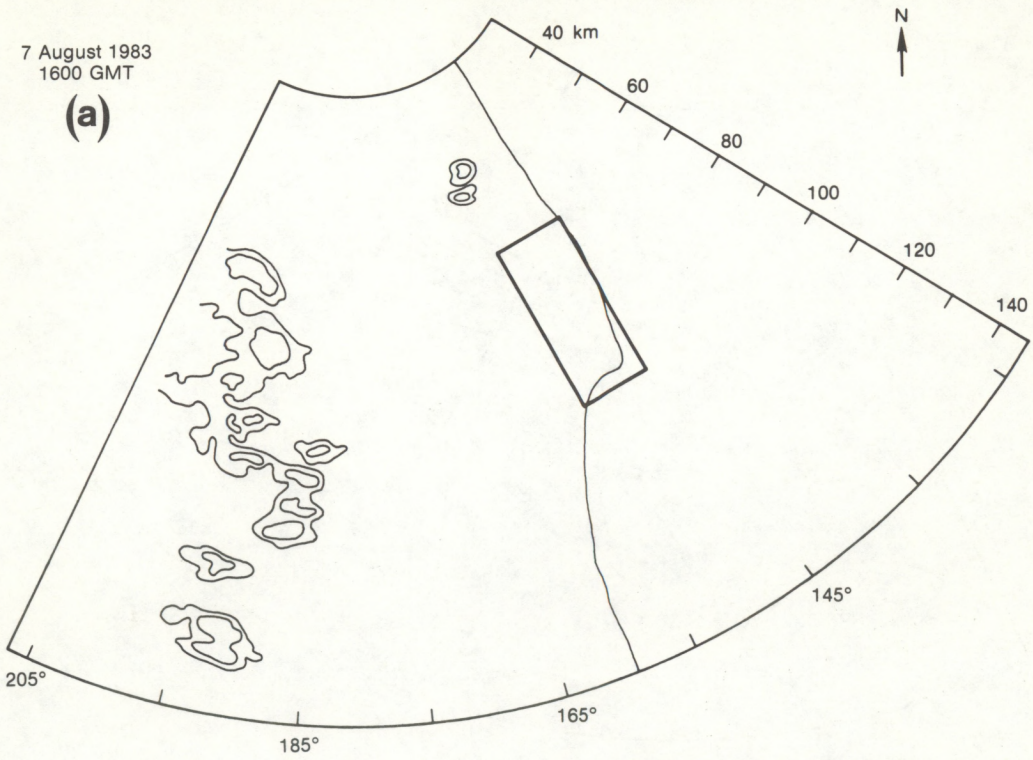

Figure 13. Regional radar patterns for 7 August 1983. DVIP levels are shown: Level 1 $\tilde{\sim}$ 20-28 dBz, level 2 $\tilde{\sim}$ 28-40 dBz, level 3 $\tilde{\sim}$ 40-45dBz, level 4 $\tilde{\sim}$ 45-50 dBz, level 5 $\tilde{\sim}$ 50-54 dBz, level 6 > 54 dBz. (a) 1600 GMT.

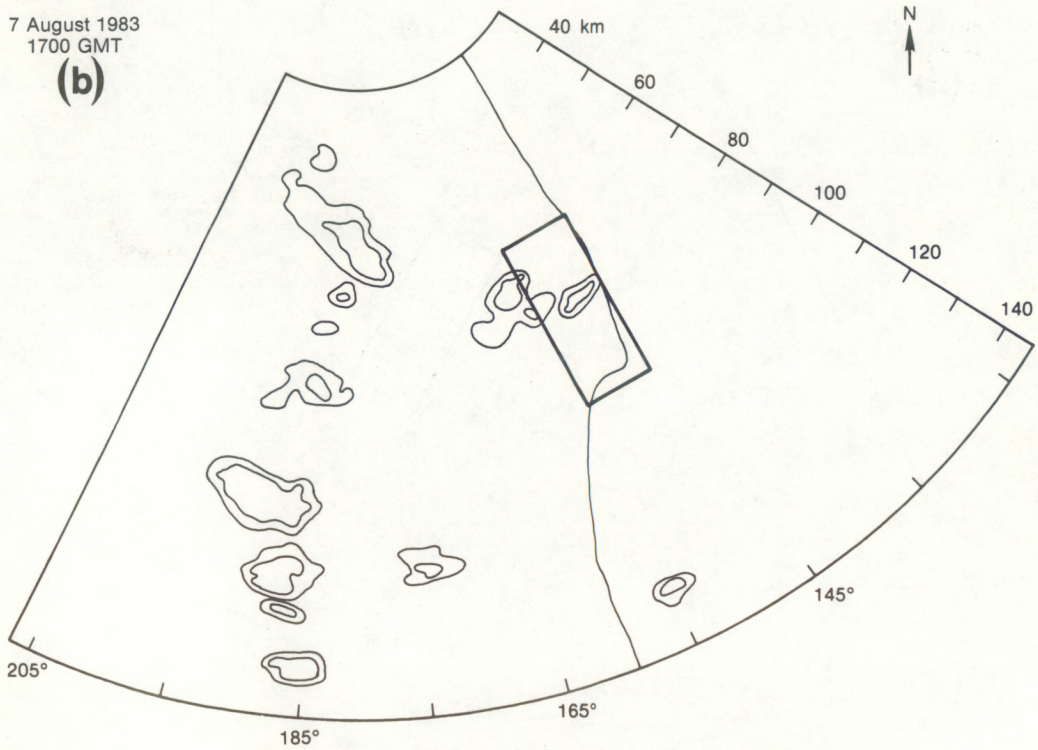

Figure 13. (Continued). (b) 1700 GMT.

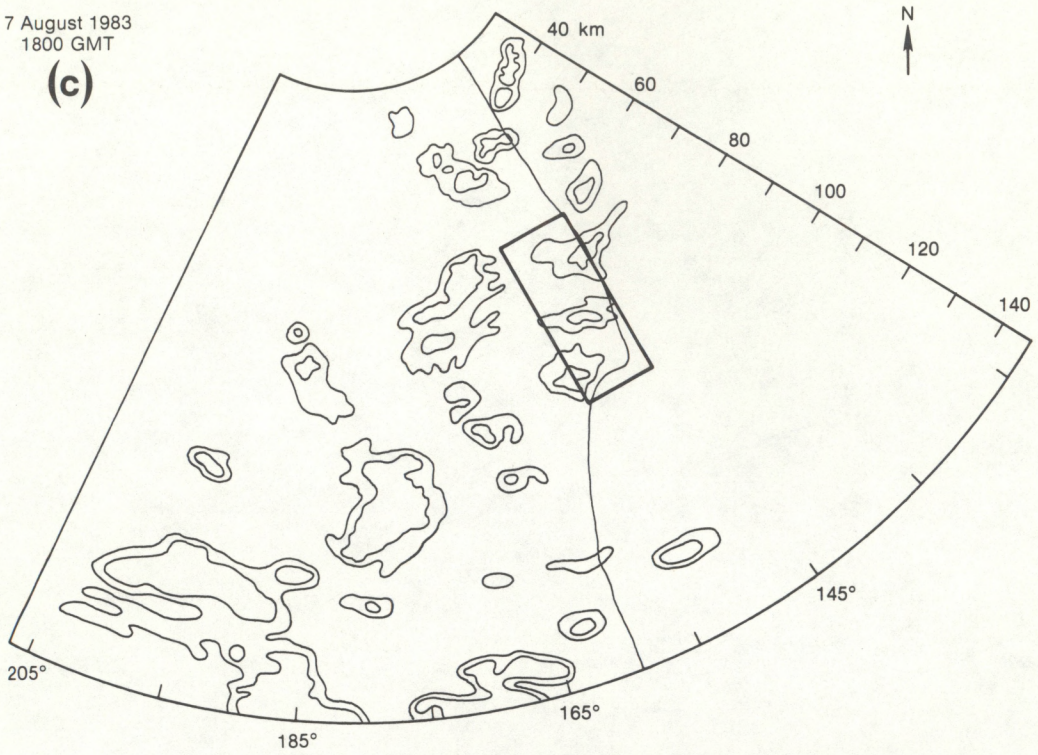

Figure 13. (Continued). (c) 1800 GMT.

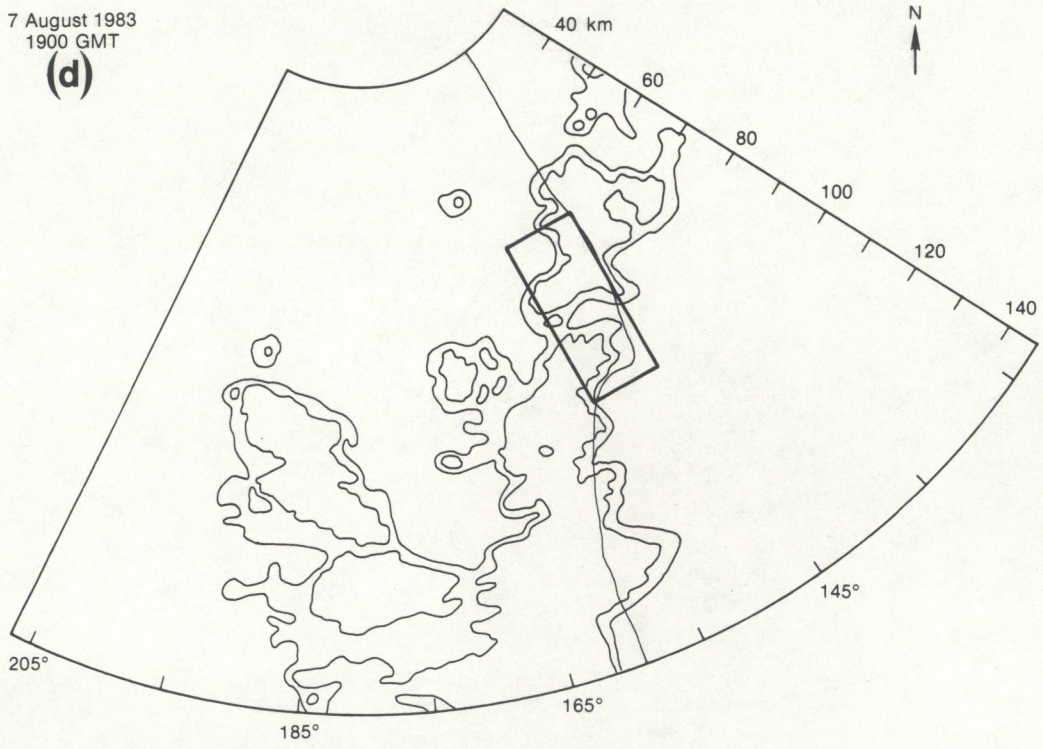

Figure 13. (Continued). (d) 1900 GMT.

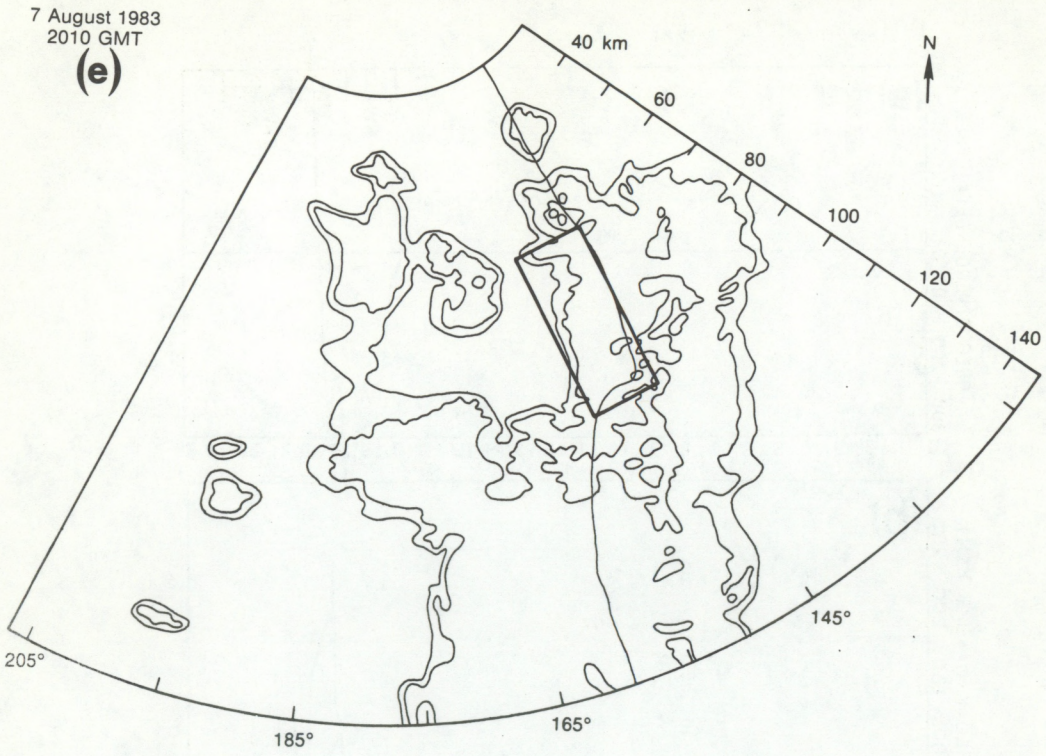

Figure 13. (Continued). (e) 2010 GMT.

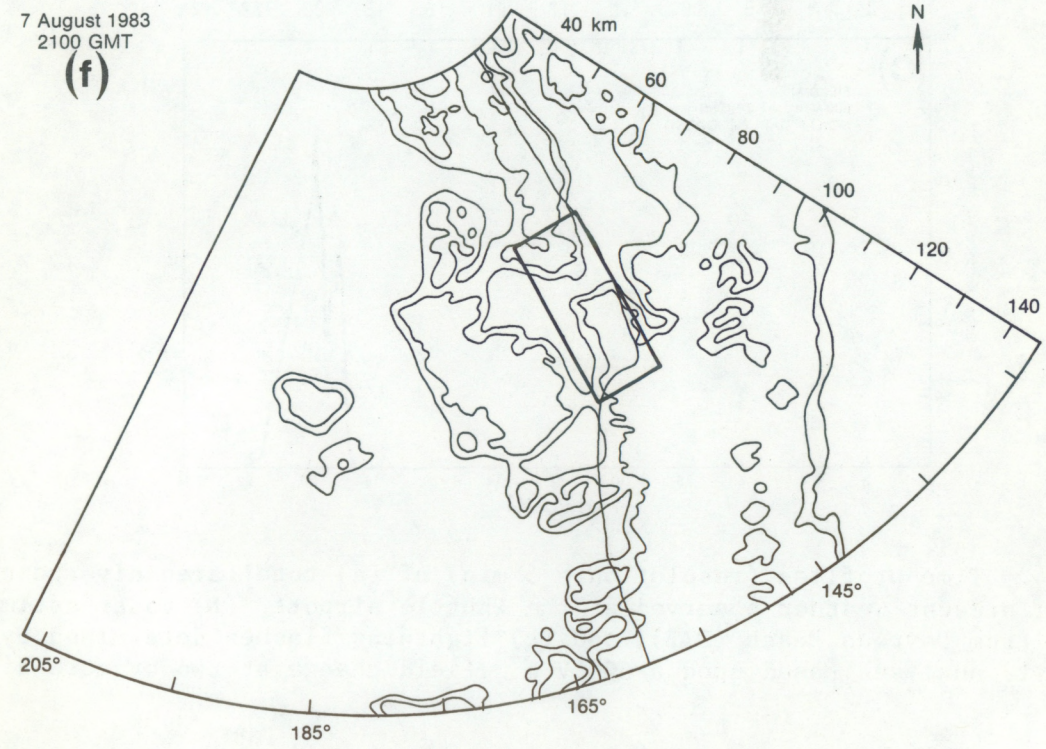

Figure 13. (Continued). (f) 2100 GMT.

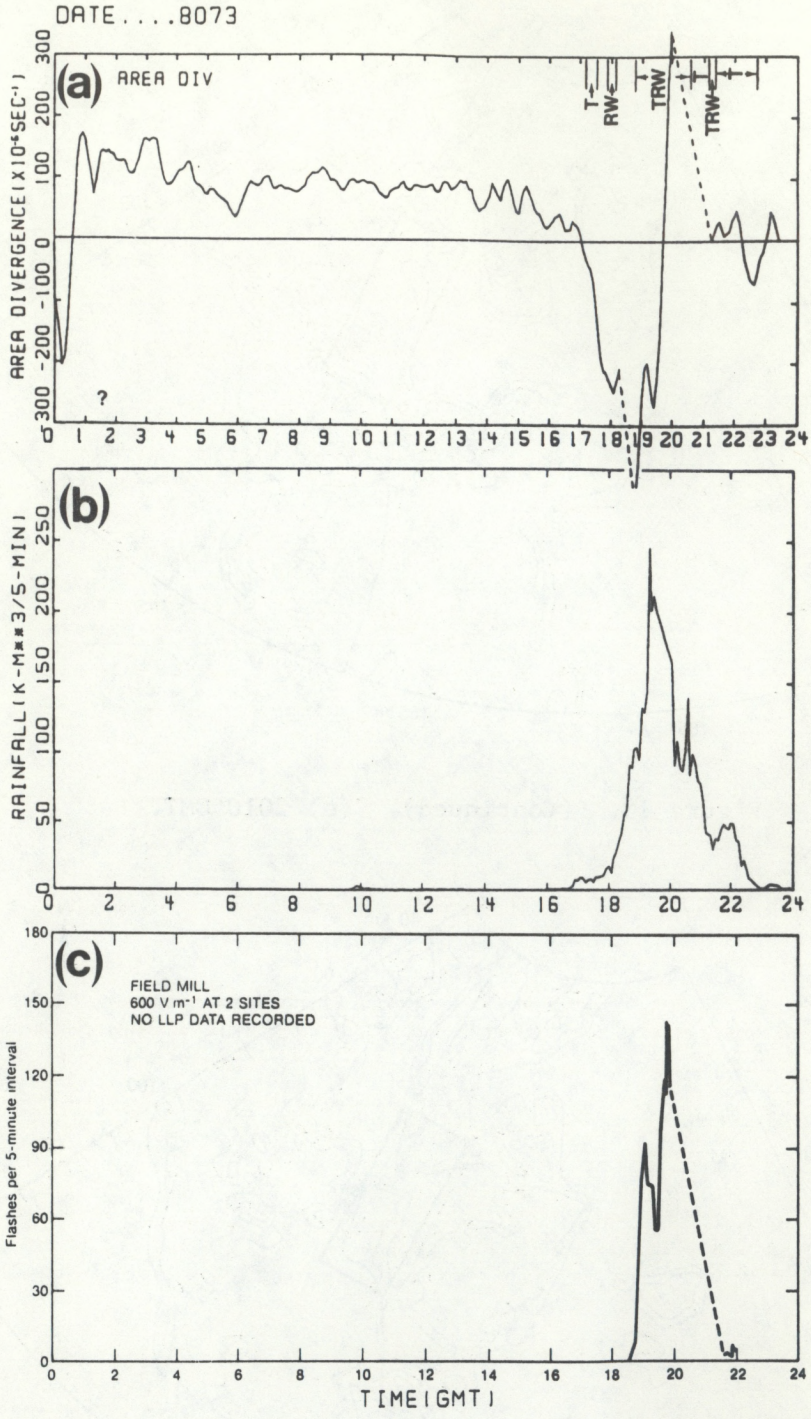

Figure 14. Time profiles (resolution = 5 min) of (a) total area divergence including present weather observed at the Shuttle airport, (b) radar-estimated rainfall from Daytona Beach (DAB), and (c) lightning flashes determined by field mills analyses based upon a 600 V m^{-1} field change at two or more sites.

Finally, we seek to understand what is happening on the network scale (see Fig. 1). Can we see convective development in the surface wind field? The time profile of total area divergence and radar-estimated rainfall are presented in Fig. 14. No CG lightning location data from the LLP system were recorded on this day. Instead, the field mill analysis has been substituted. The criterion for determining lightning flashes is a field change of 600 V m^{-1} at two or more sites.

Strong convergence (Fig. 14a) begins at 1700 GMT, peaking near 1845 GMT. Dashed lines indicate missing mesonetwork data, probably due to power outages resulting from the proximity of electrical activity. Significant precipitation (Fig. 14b) begins at 1800 GMT, reaching a maximum at approximately 1900 GMT. Notice that the present weather at the Shuttle Airport runway is also depicted on Fig. 14a. Although thunder is heard by the observer at the Shuttle Airport at 1708 GMT, no lightning flashes are detected by the field mills until 1835 GMT. The flash peak (Fig. 14c) occurs at 1945 GMT. A divergence peak is cut short by the power failure at 2000 GMT. By 2100 GMT, when the ARMS system comes back on line, the total area divergence profile has returned to normal. The field mill system, at this time, is reporting a few flashes, and probably has no CG reports since the weather observer at the Shuttle runway has reported only inner-cloud or cloud-to-cloud flashes after 2036 GMT.

Figure 15 compares the time profiles of weighted convergence and weighted divergence with total area divergence. Significant convergence begins in the weighted convergence profile (Fig. 15b) at 1700 GMT and climaxes in a powerful peak at 1945 GMT, comparing exactly with the convergence maximum in total area divergence. Notice a convergence period between 0000 and 0100 GMT associated with weak convection. During the night, the convergence signal is weak or nonexistent. In the weighted divergence profile (Fig. 15c), moderate divergence values continue through the evening hours. At approximately 1730 GMT, divergence drops considerably as convergence covers the entire network. After a short power outage between 1815 and 1830 GMT, weighted divergence is again on the rise as peak weighted convergence occurs. The maximum in weighted divergence then occurs during the main power failure.

Figure 16 displays the horizontal analyses of streamlines and isotachs, divergence, and radar reflectivities at selected milestones during the total area divergence and area precipitation time profiles (Fig. 14).

1700 GMT (Fig. 16a). Initial convergence. There are weak southeast to south winds across the KSC network. A weak convergence zone (-4×10^{-4} s^{-1}) is situated in the center of the network, resulting from speed convergence. Several weak level-2 radar reflectivity cores are found over the northern half of the network.

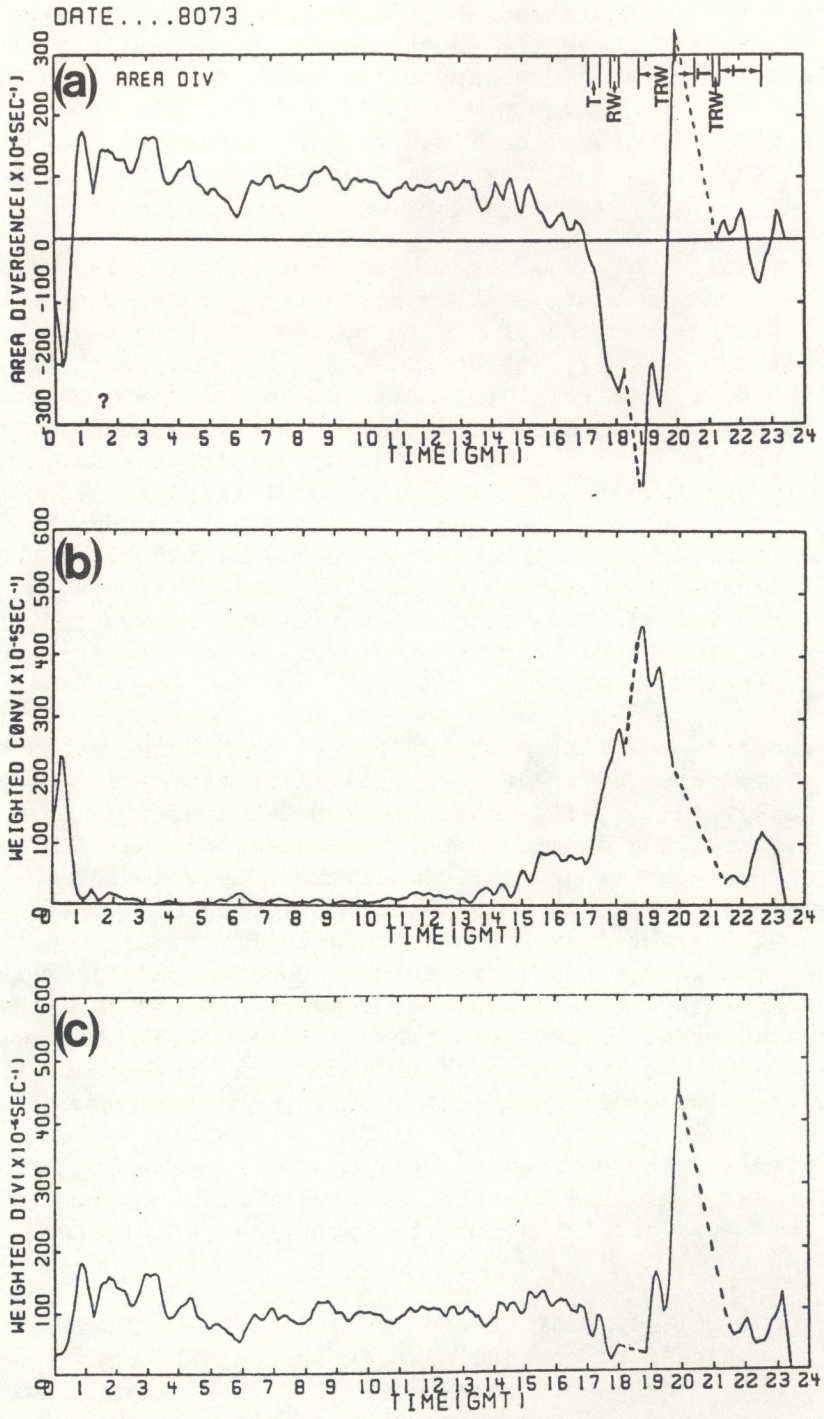

Figure 15. Time profiles of (a) total area divergence, (b) weighted convergence, and (c) weighted divergence for 7 August 1983.

1800 GMT (Fig. 16b). Beginning rain. According to the radar, reflectivities are large enough for precipitation to have begun. Precipitation has not affected any surface winds sites as yet. Weak northwesterly flow is recorded by two wind tower sites near the northern border. This is possibly the first sign of outflow from the north-south weakening squall line traversing the peninsula. Strong convergence ($-1 \times 10^{-3} s^{-1}$) is noted under the developing line shown by the radar.

1845 GMT (Fig. 16c). Maximum convergence. A nearly pure convergence zone is found in the wind field near the VAB on KSC. A very strong convergence maximum ($-2.4 \times 10^{-3} s^{-1}$) and level-3 echo (40-45 dBz) are found at that same location.

1900 GMT (Fig. 16d). Maximum rain. Heavy rain and strong outflow are located near the VAB building. Strong convergence lies along the new gust front boundary over eastern Merritt Island, developing between the cool moist downdraft air and southeast flow across the Cape. The wide zone of convergence southeast of the gust front is probably indicative of vertical motion viewed in the wind field as speed convergence.

1955 GMT (Fig. 16e). Maximum divergence. Now, there is nearly pure divergence; the outflow is almost symmetrical over northern Merritt Island. Maximum divergence is approximately $1.8 \times 10^{-3} s^{-1}$. The gust front is now crossing the eastern tip of the Cape. The strongest reflectivity core, indicative of the heaviest precipitation, lies just behind the gust front boundary. The largest divergence values have yet to occur (and may have occurred a short time later during the power failure, as the gust front exited the network moving offshore). As the main convective core moves eastward, only anvil rain remains over the network.

On this day redevelopement occurred over KSC ahead of a dissipating line of showers. A very strong convergence signal was followed by heavy precipitation and lightning. Thunder was heard at 1708 GMT from the dissipating system to the west. According to the time profiles, significant precipitation began shortly after 1800 GMT, 1 hour after beginning convergence. Field mill data detected first lightning flashes at 1835 GMT, 1 hour and 35 min after initial convergence. The total area divergence profile also portrayed the stages of convective evolution. Stages of development, maturity, and dissipation are evident (even though dissipation data are missing) in the sinusoidal pattern of total area divergence. Note also that the horizontal analyses of divergence and winds provided the location, magnitude, and timing of the evolution of the cumulonimbus over the network.

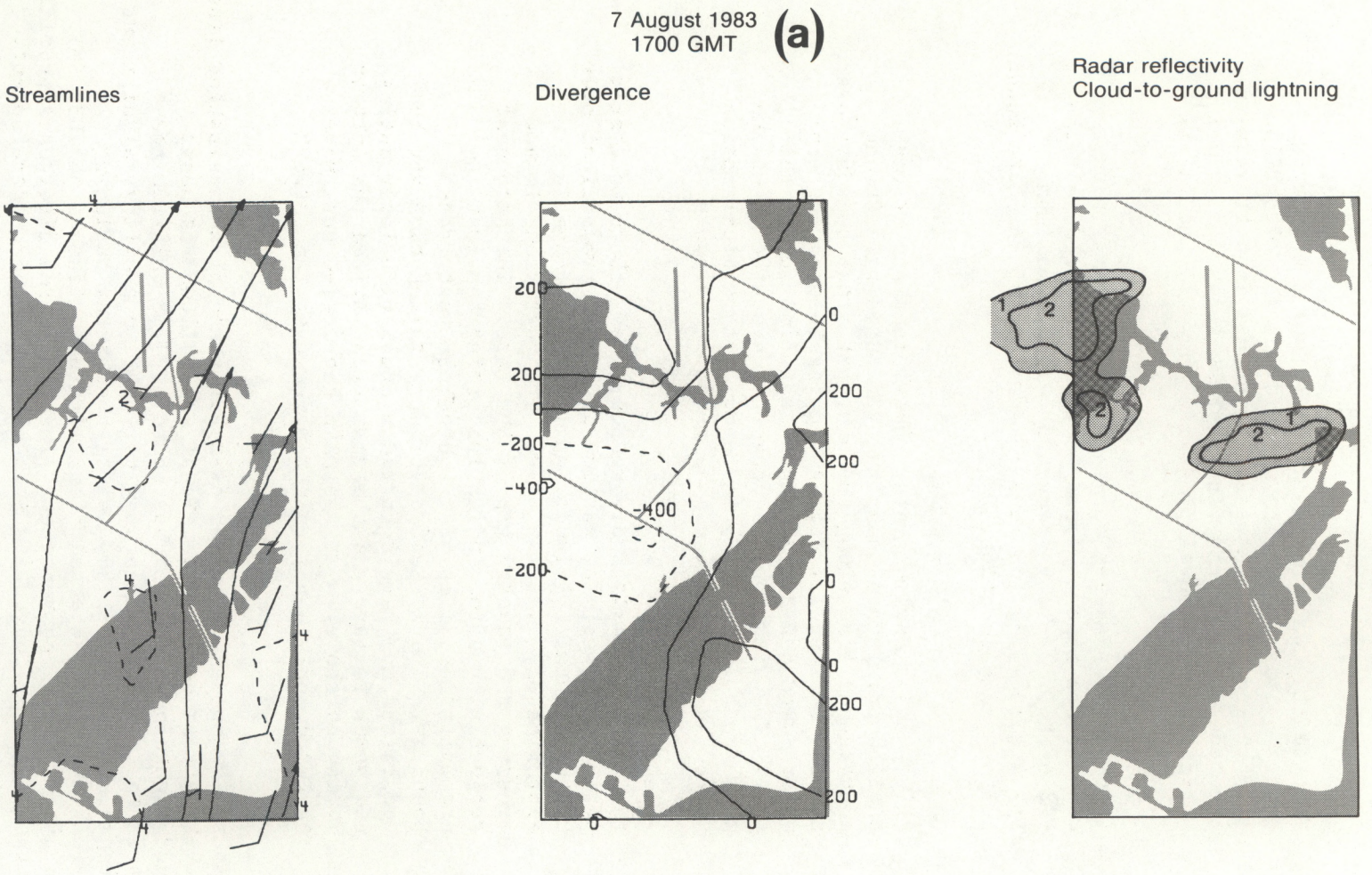

Figure 16. KSC mesonetwork analyses of winds, divergence, and radar and CG lightning for 7 August 1983. (a) 1700 GMT, initial convergence.

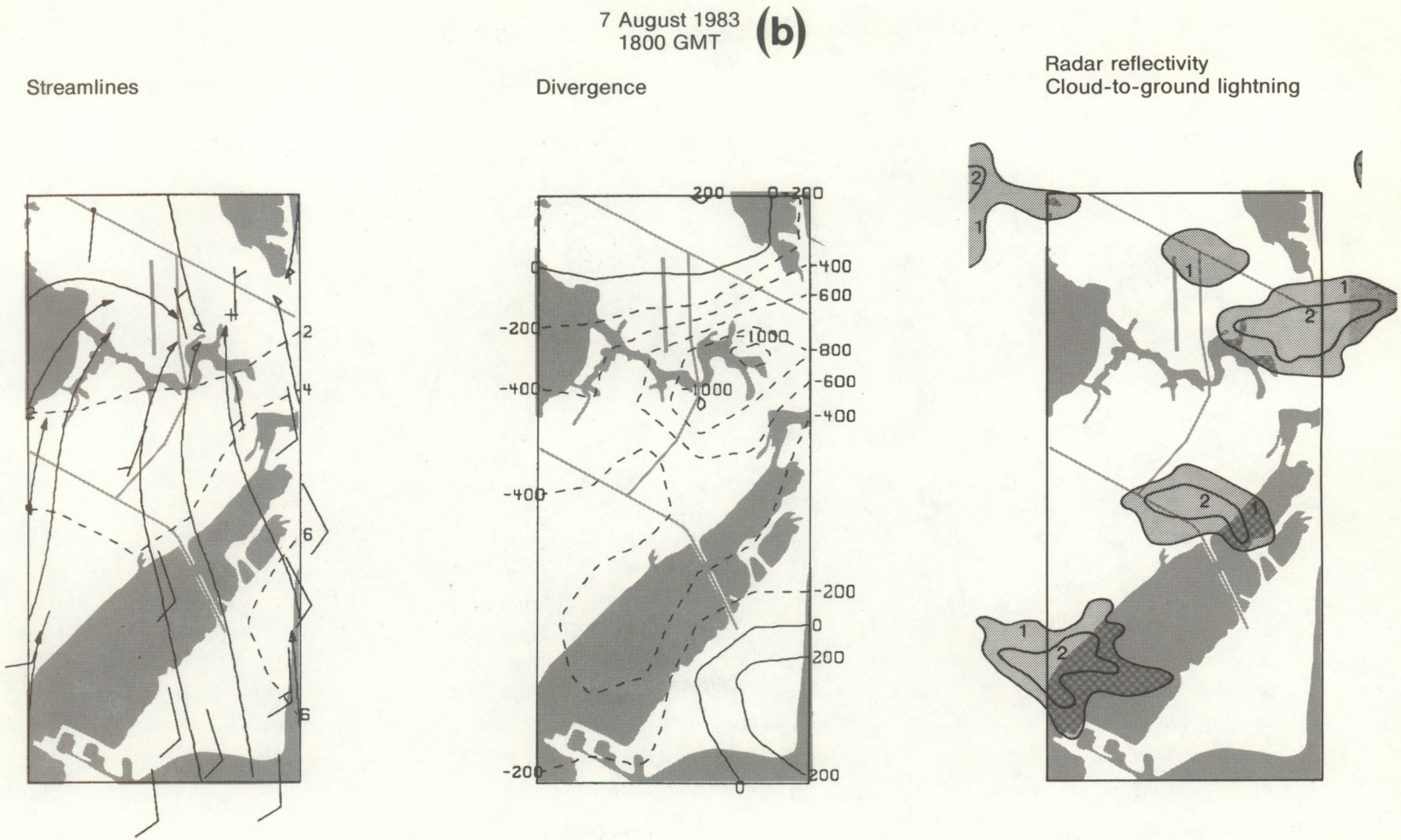

Figure 16. (Continued). (b) 1800 GMT, beginning rain.

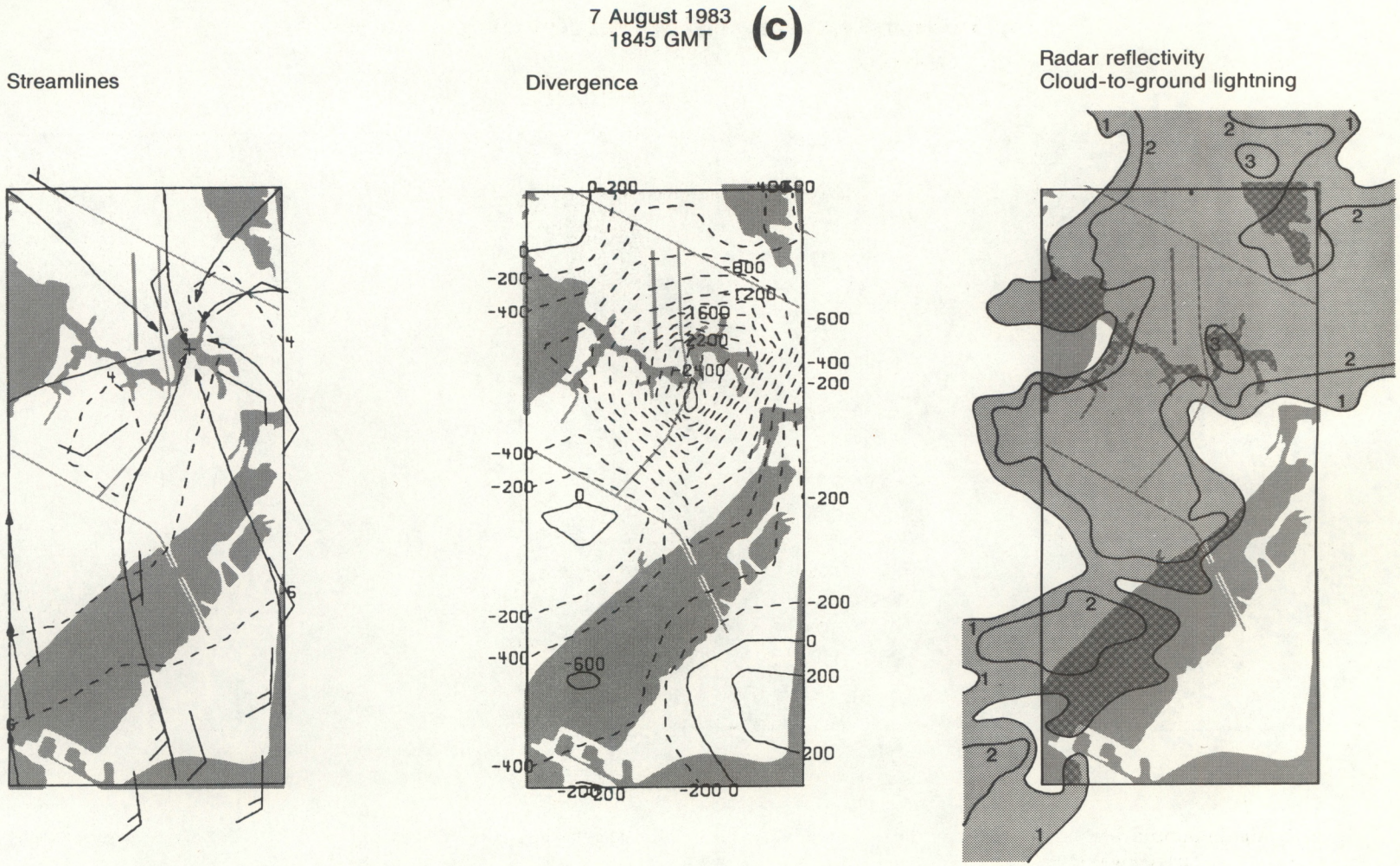

Figure 16. (Continued). (c) 1845 GMT, maximum convergence.

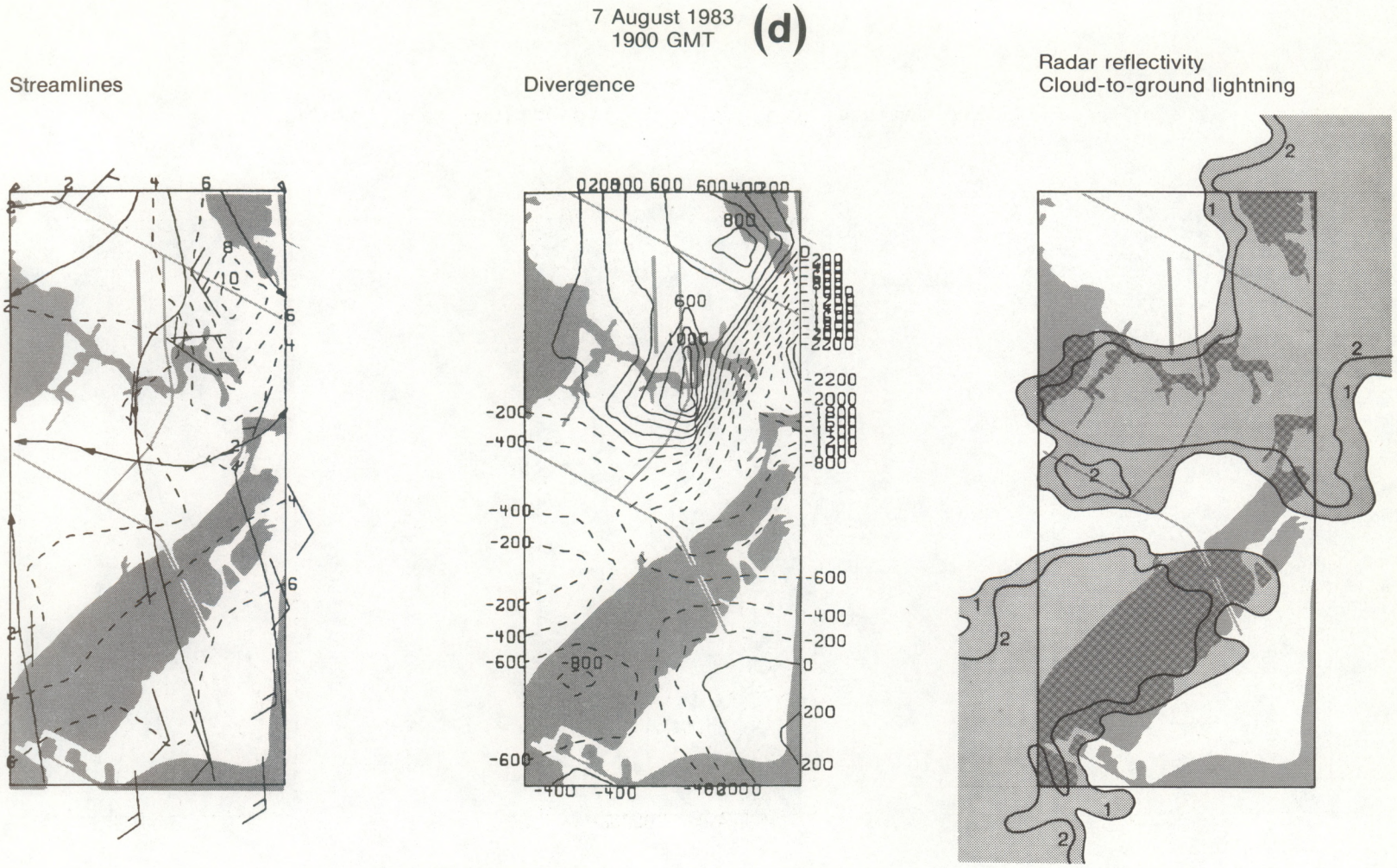

Figure 16. (Continued). (d) 1900 GMT, maximum rain.

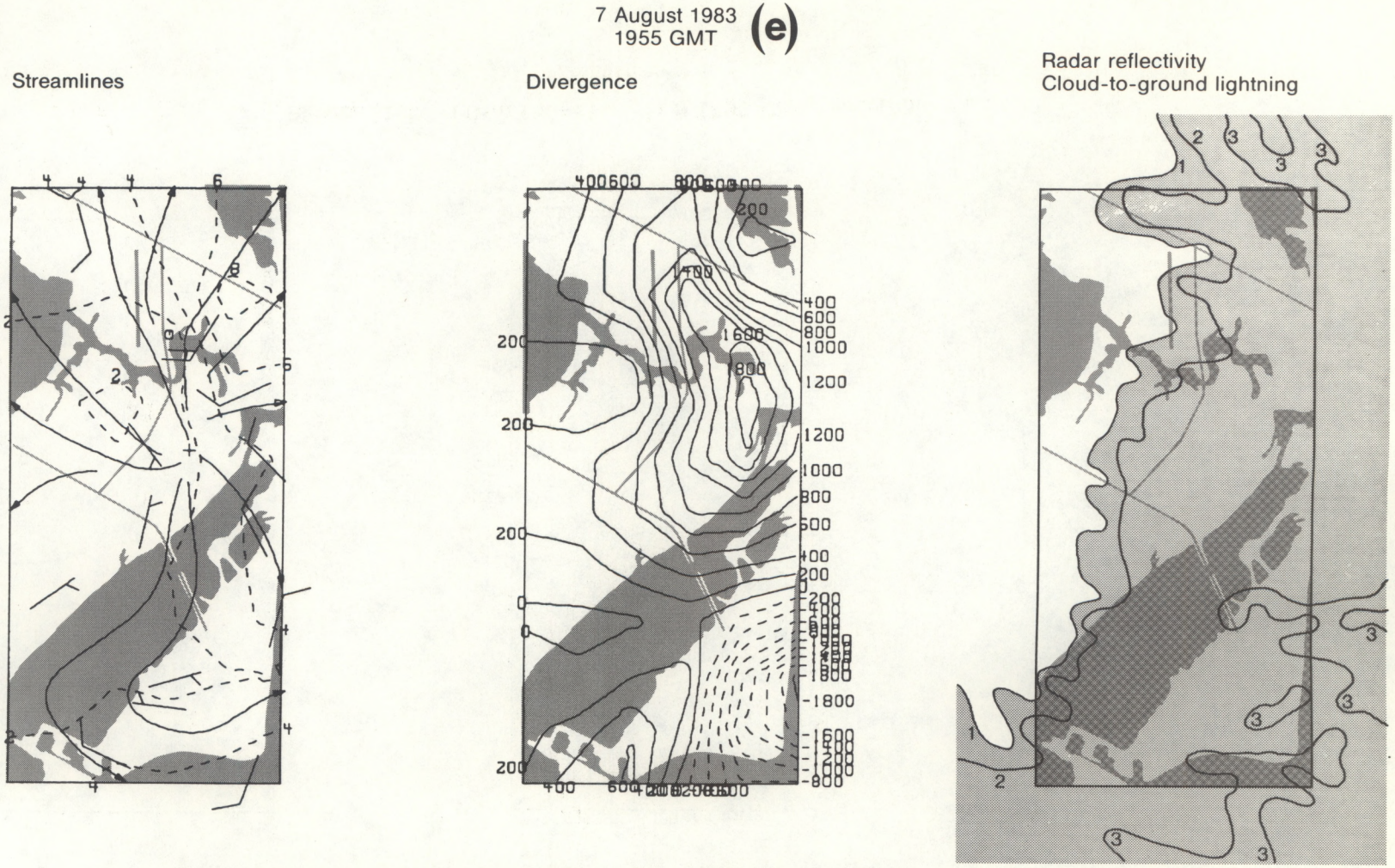

Figure 16. (Continued). (e) 1955 GMT, maximum divergence.

C. Case Study 2: 10 August 1983

The tenth of August was a day when the flow was weak but significant in some respects. It was a day when gust fronts and outflows contributed greatly to secondary convection (Holle and Maier, 1980; Cunning et al., 1982). The low- to middle-level winds were southwest to westerly. Therefore, the west-coast sea breeze would be the dominant mechanism in modulating the convective activity while the east-coast sea breeze would be mainly weak. How far would the west-coast sea breeze progress before the peninsular heating ceased? In this case, the west-coast sea breeze fired quite early and extended rapidly eastward along two east-west confluence zones, some of the heaviest convection passing near the Cape Canaveral area.

The day dawned with a summer weather situation typical over the southeastern United States. The surface features at 1200 GMT, 10 August are presented in Fig. 17. The westward extension of the Atlantic high has spread ridging across south Florida and into the Texas Gulf Coast. A frontal system in the Carolinas was beginning to retreat northward in advance of a developing system in the upper Midwest.

Figure 18 gives the upper-air pattern at 1200 GMT. Moisture is abundant at all levels over most of Florida. Heights at most levels are steady or at least showing minimal height rises of 10 meters. At 850 mb (Fig. 18a), winds over Georgia are northwesterly, defining the southern extremity of a trough in the vicinity of Jacksonville and Daytona Beach. With westerly winds over central Florida, northwest flow over Georgia, and west-southwest winds in south Florida, an east-west confluence zone is situated in the central portion of the state. The Atlantic ridge at 850 mb appears to pass through the Bahamas, across the Florida Keys, and into the southern Gulf of Mexico. At 700 mb, winds remain westerly across the state with the ridge defined in a narrow band across south Florida.

A mid- and upper-tropospheric low is first defined at 500 mb in Fig. 18c in the Florida Panhandle. A trough is shown along the Gulf coast eastward into the main middle-latitude trough lying off the Atlantic seaboard. The temperature gradients are weak with slightly cooler temperatures (1^{o}) at West Palm Beach and Cape Canaveral. The east-west trough and closed low depicted first at 500 mb are also reflected at 300 mb.

The satellite imagery (Fig. 19) shows the development of convection during the day.

1731 GMT (Fig. 19a). West-coast sea breeze convection has started. Convective development is also seen along the Gulf coast, associated with the upper trough. Two small east-west enhanced cloud lines are visible across north central Florida; one line extends westward from the vicinity of the Cape. Notice the cloud-free suppressed area downstream from Lake Okeechobee.

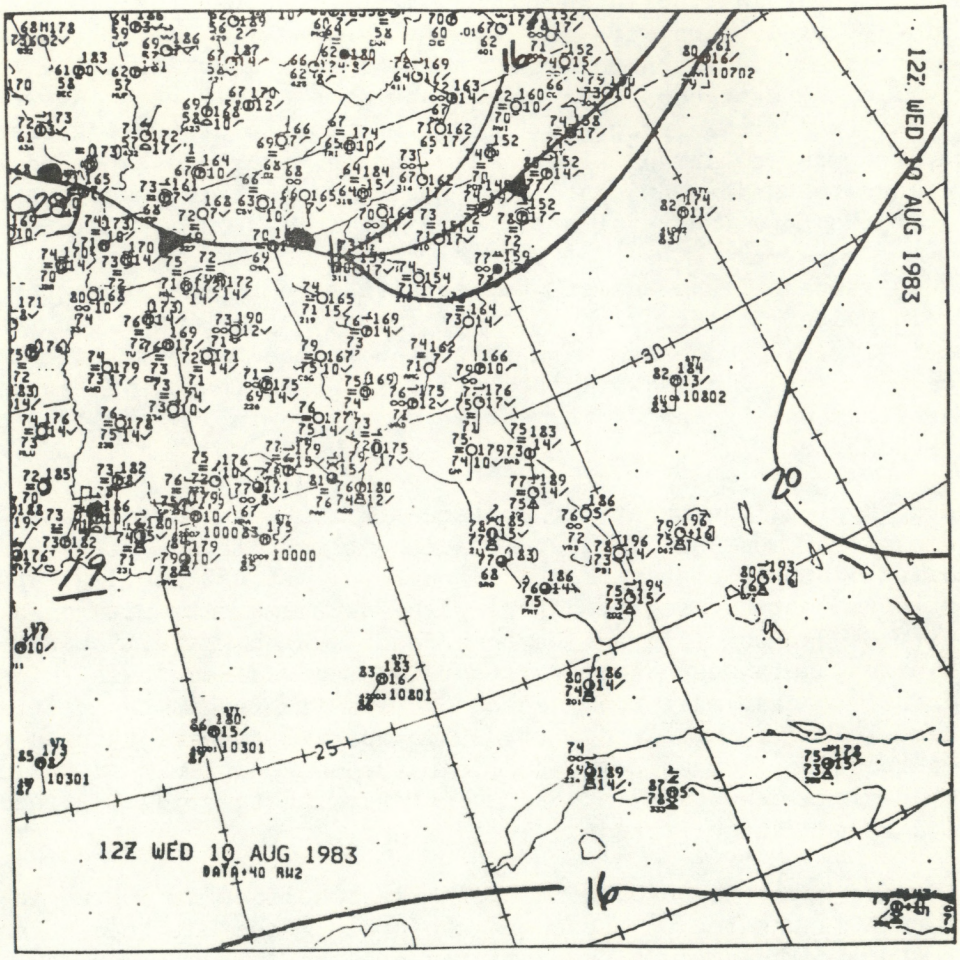

Figure 17. NMC surface analysis for 10 August 1983 at 1200 GMT.

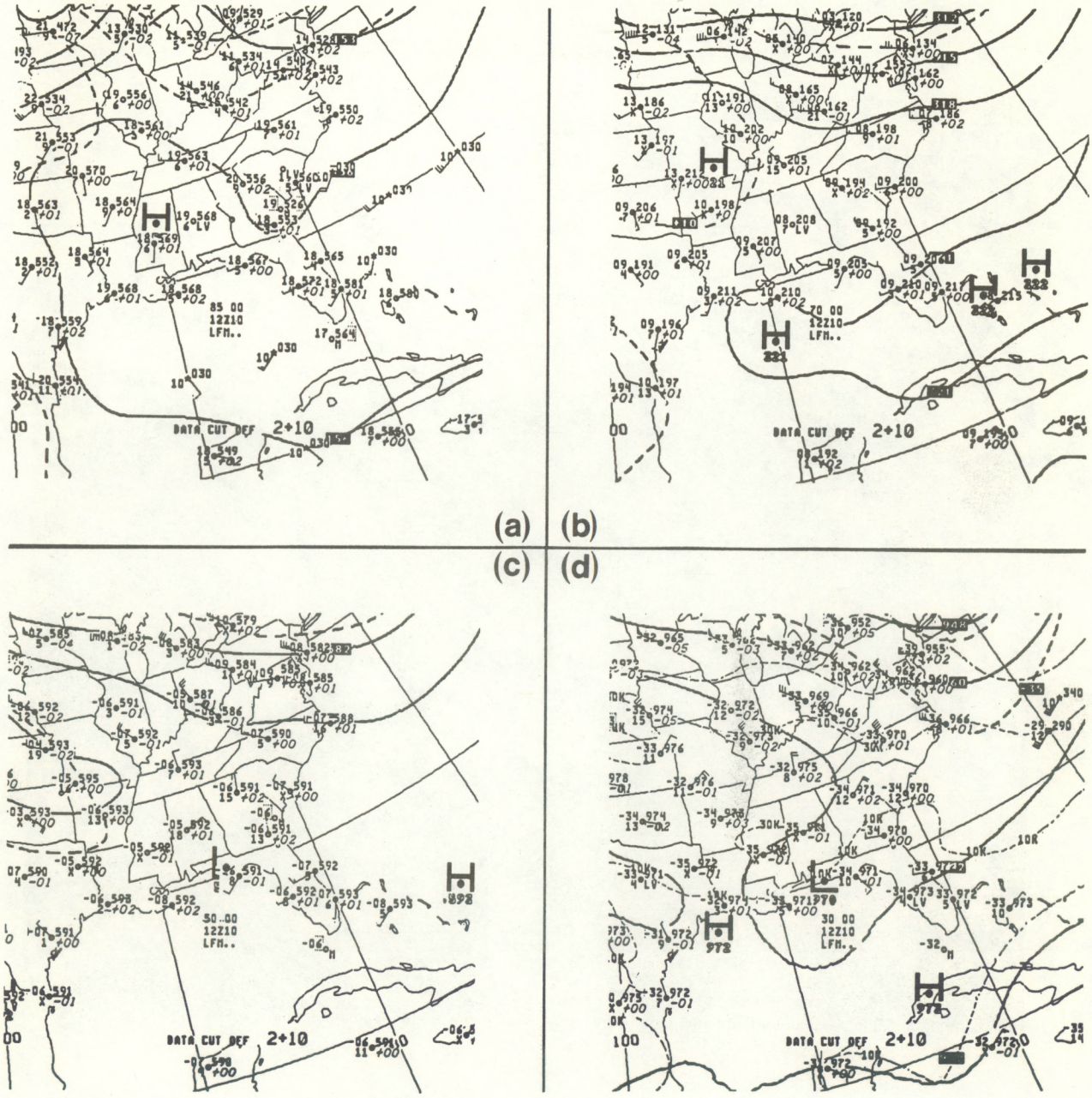

Figure 18. NMC upper-air analyses for 10 August 1983 at 1200 GMT for (a) 850 mb, (b) 700 mb, (c) 500 mb, and (d) 300 mb.

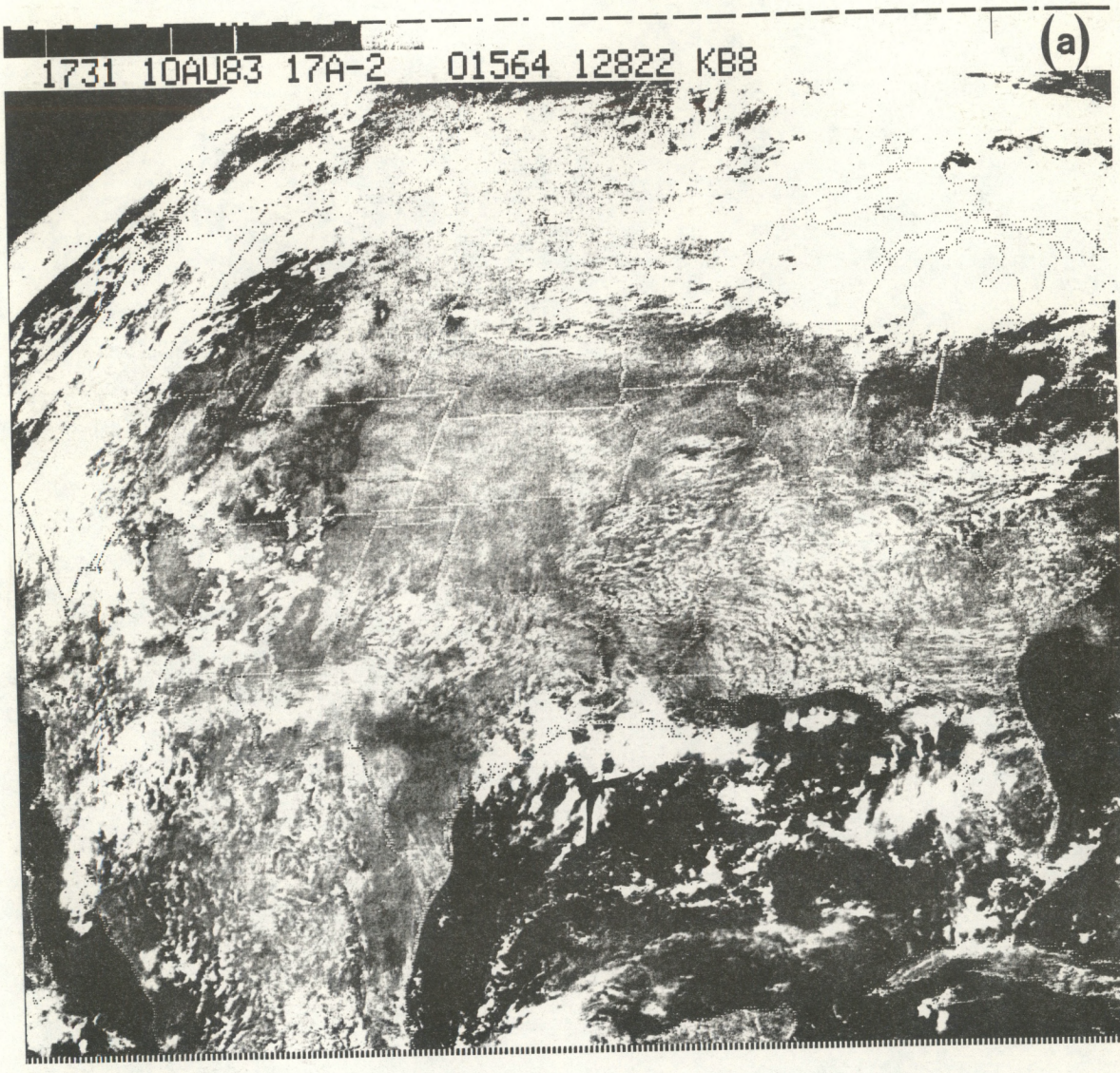

Figure 19. Satellite imagery for 10 August 1983. (a) 1731 GMT visible image.

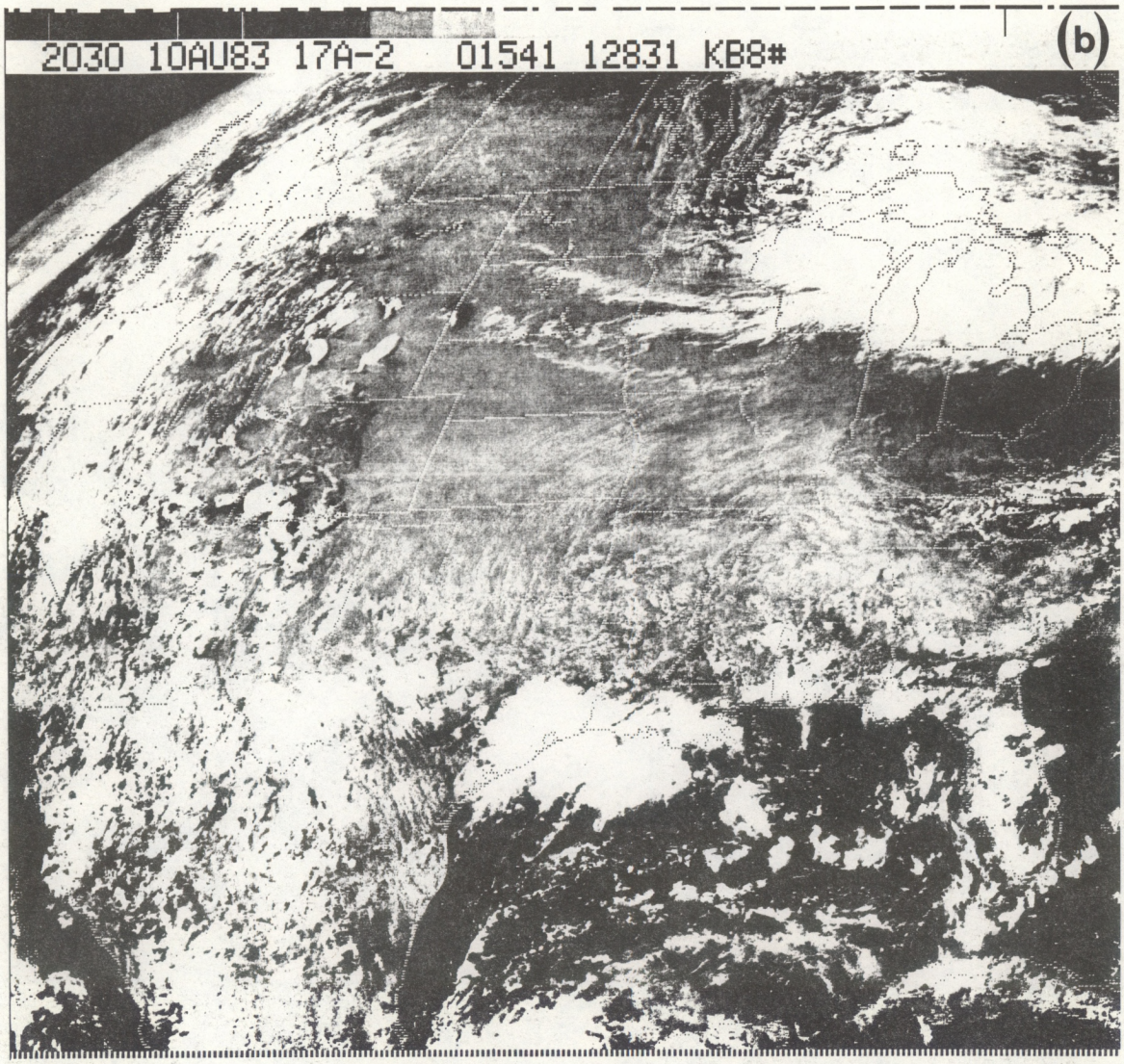

Figure 19. (Continued). (b) 2030 GMT visible image.

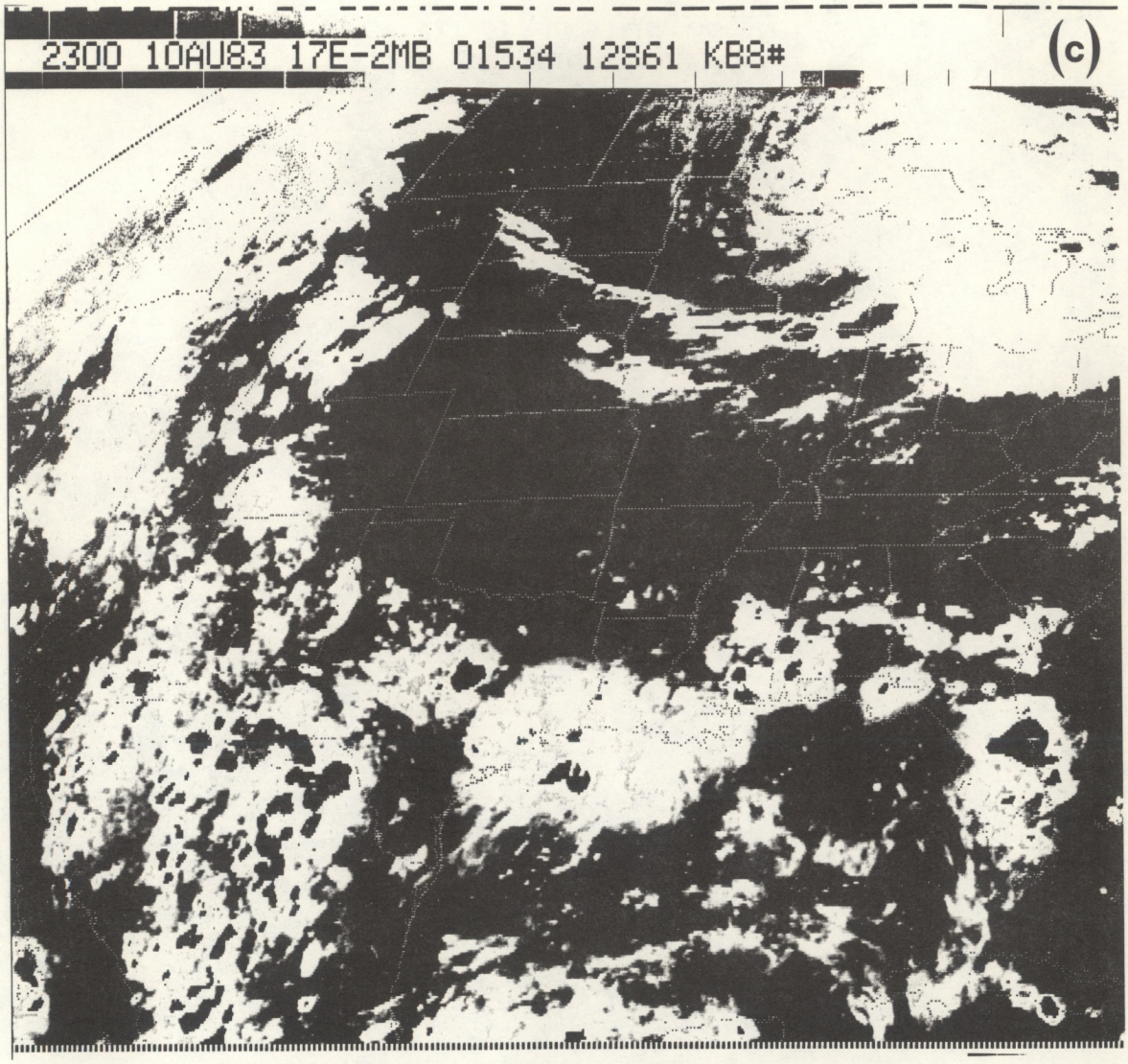

Figure 19. (Continued). (c) 2300 GMT IR image with MB enhancement.

2030 GMT (Fig. 19b). The west-coast sea-breeze has begun to move inland. Development is also occurring in central Florida. The two confluence lines in central Florida have blossomed with convection now found along the east coast.

2300 GMT (Fig. 19c). This is an IR image with MB enhancement. The coldest top ($<-62^{\circ}C$) in the southeast United States is located just north of KSC.

The Cape Canaveral sounding for 0900 GMT, 10 August in Fig. 20 shows that the atmosphere is conditionally unstable and quite moist throughout its depth. The winds are mainly westerly, and no observations are greater than 15 kn. The predicted high temperature is $33^{\circ}C$ ($\tilde{}92^{\circ}F$). Actually, the high temperature was $89^{\circ}F$. Using the expected maximum temperature and average mixing ratio for the first 100 mb gives a lifted index of -4.5. The LCL and LFC are at 850 mb, equilibrium level is at 190 mb, and the expected maximum top of thunderstorms is slightly above 100 mb. Totals index is 46. Therefore, provided that surface heating gives the initial boost, deep vigorous convection with a slight eastward drift can be expected.

Figure 21 reviews hourly radar scans from the Daytona Beach radar. Cloud-to-ground (CG) lightning that occurred in this area is also shown. Lightning locations depict flashes for the 5-min period centered on the radar observation time.

1600 GMT (Fig. 21a). No echoes are reported in the vicinity of KSC.

1705 GMT (Fig. 21b). Showers are beginning to develop about 50 km west of the Cape. Orientation is a slightly east-west, possibly because of the convergence zone in the vicinity. First CG strokes were recorded 10 min later in the area (at 1715 GMT).

1800 GMT (Fig. 21c). The activity has spread eastward into the KSC mesonetwork. A level-3 core is currently on the western boundary of the network. Three CG flashes can be seen in convection 50 km west of the Cape along the confluence line.

1900 GMT (Fig. 21d). East-west orientation of convection continues. Two level-3 echoes are now in the network, showing little movement. New convection is developing northward near the coast while additional cells are appearing south of the Cape and extending southwestward into the interior of the state. Initial lightning activity in the KSC mesonetwork occurred at 1830 GMT;

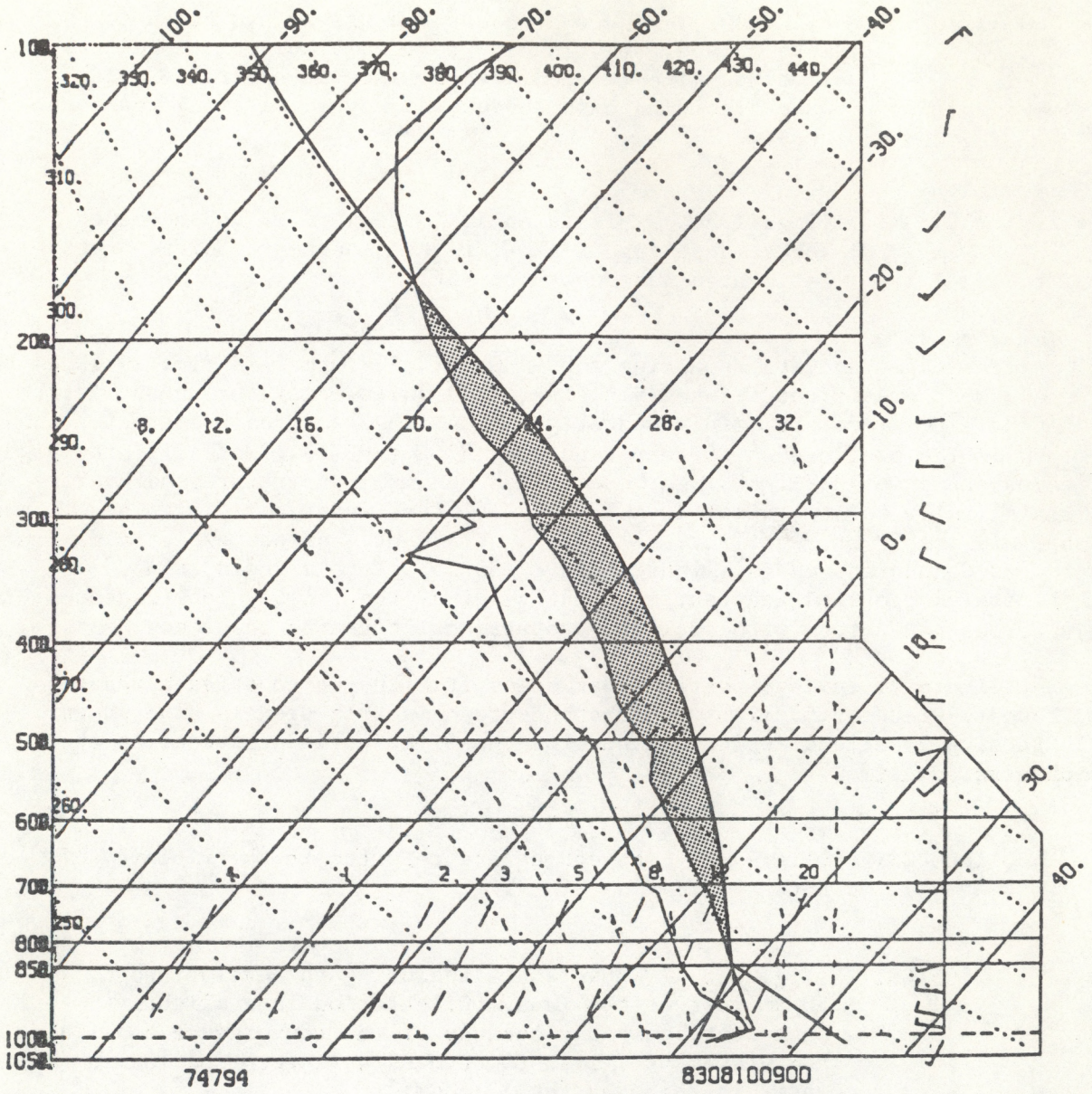

Figure 20. Cape rawinsonde sounding at 0900 GMT, 10 August 1983, plotted on a skew-T, log P diagram.

two CG lightning strikes were reported in that 5-min period. At 1900 GMT, nine lightning flashes were reported in or very near the network.

2000 GMT (Fig. 21e). The east-west line appears to be weakening while the development to the south has consolidated into a more organized system. Five strokes are recorded in the network. The strongest lightning activity occurred between 1900 and 2045 GMT; 17 strokes were recorded for the 5-min period around 1928 GMT. At 2030 GMT (not shown), the Daytona Beach radar detected a gust front moving away from the activity over the Cape.

2100 GMT (Fig. 21f). The gust front is quite visible as a weak north-south narrow band of level-1 echoes about 10 to 20 km west of the northwest corner of the mesonetwork. Approximate speed is 20 km h^{-1} toward the northwest. The activity south of the network has continued to intensify during the hour. A relatively strong CG lightning center is located in the level-3 core just adjacent to the western boundary of the KSC network. Redevelopment apparently has occurred farther west with two level-3 cores.

2200 GMT (Fig. 21g). A large echo now lies west of KSC where the gust front was traversing only 1 hour earlier. Therefore, there is a distinct possibility that the gust front was the trigger required to initiate this cell. An "X" marks the spot where two outflows seen on the radar film have just come together. One outflow came from the cell just to the west; the other came from the vicinity of KSC and had been tracking northwest for quite some time.

2300 GMT (Fig. 21h). A small line segment is found just northwest of the network extending northward offshore, probably as a result of the intersection of the two gust fronts. Activity over KSC is weakening now. Another line that developed during the hour west of KSC is showing signs of dissipating.

Time profiles of the total area divergence, radar-derived rainfall, and lightning for 10 August 1983 are found in Fig. 22. Total area divergence through much of the night illustrates weakly divergent conditions becoming convergent after 1400 GMT. Moderate convergence signals begin after 1500 GMT, and strong convergence begins at 1700 GMT. Maximum convergence occurs at 1840 GMT, 10 min after first lightning in the network. The weather observer at the Shuttle airport runway recorded a thunderstorm beginning at 1849 GMT.

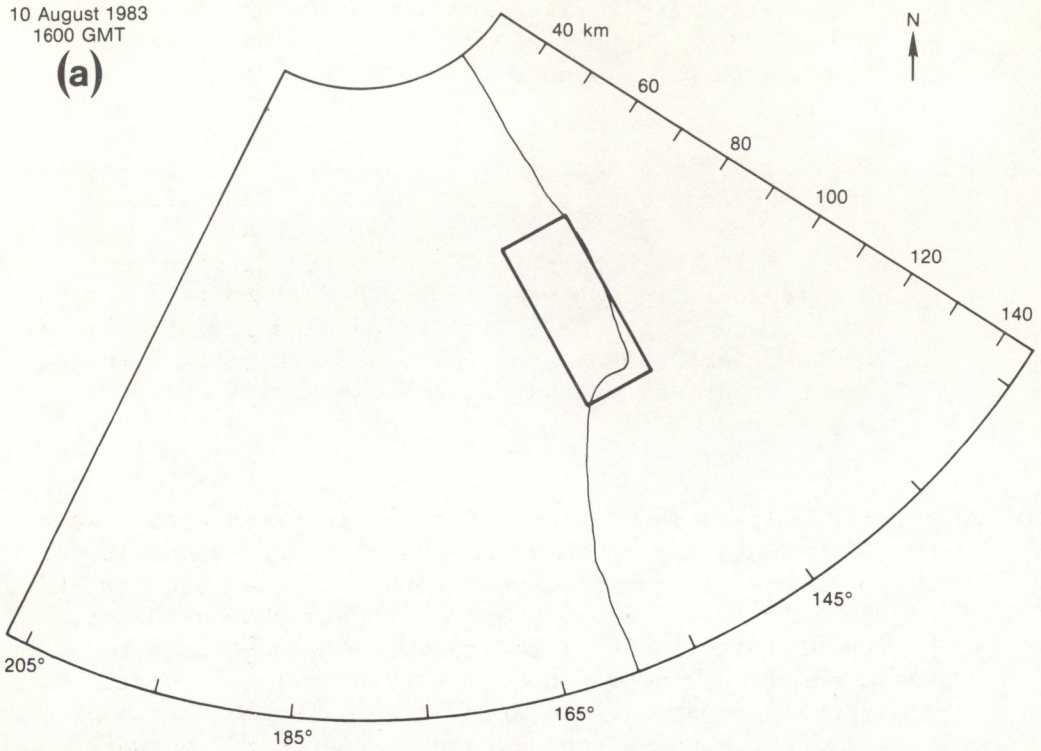

Figure 21. Regional radar and CG lightning pattern for 10 August 1983. Lightning locations are indicated by plus or number of CG flashes in approximately the same location. DVIP levels are shown as described for Fig. 13. (a) 1600 GMT.

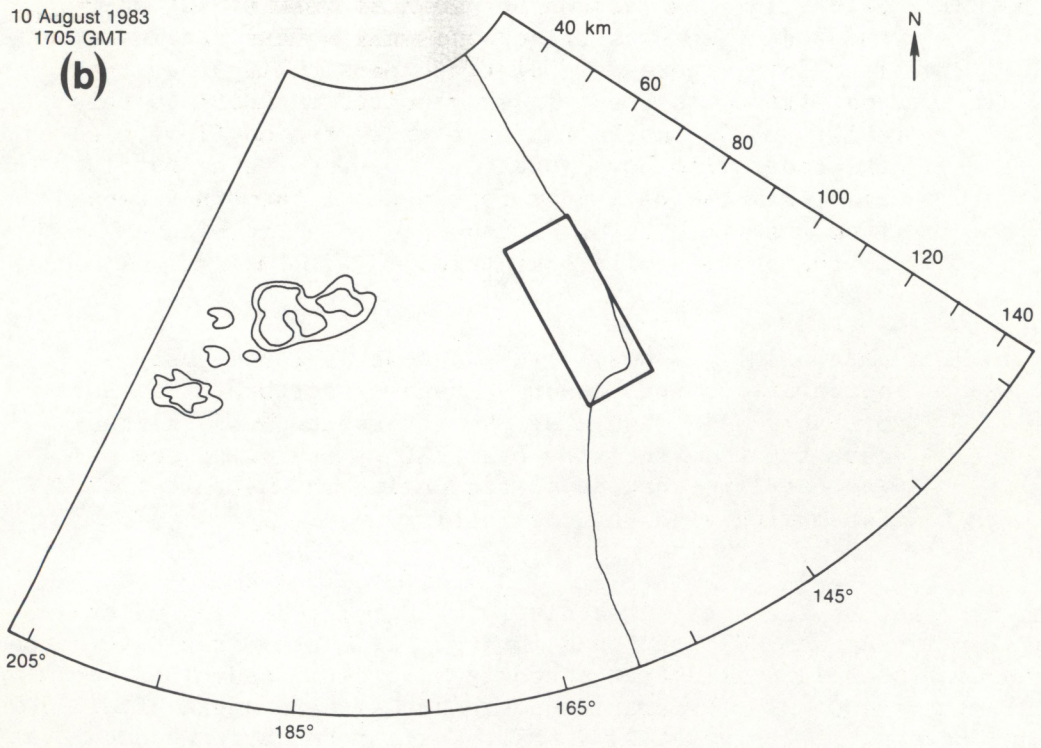

Figure 21. (Continued). (b) 1705 GMT.

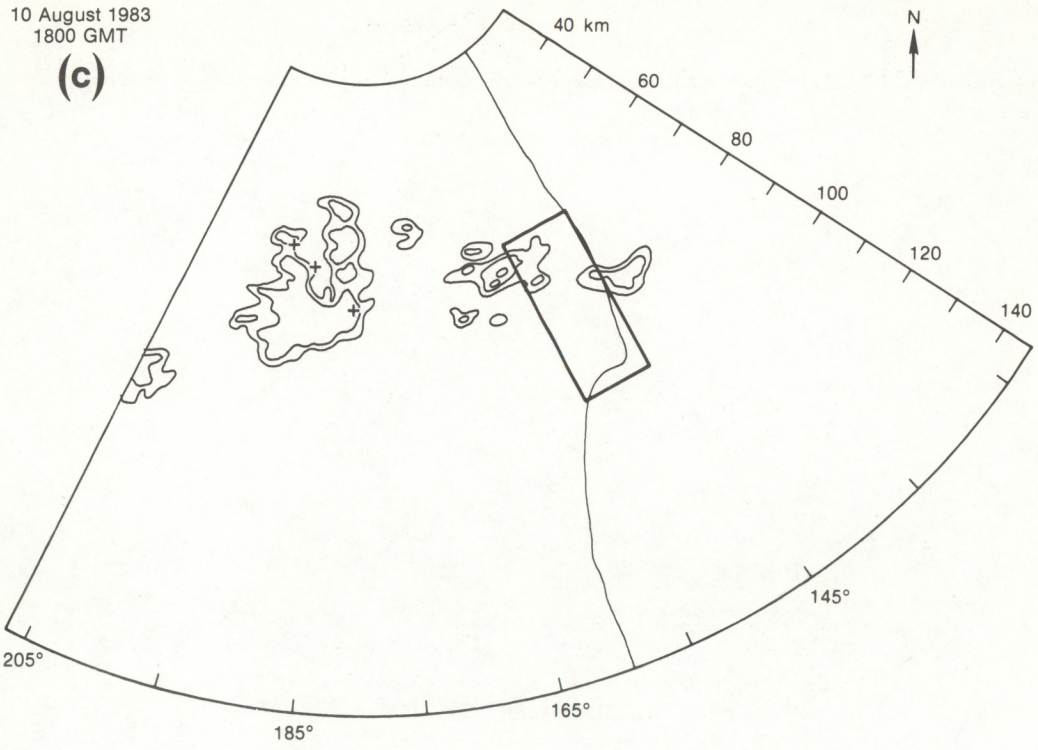

Figure 21. (Continued). (c) 1800 GMT.

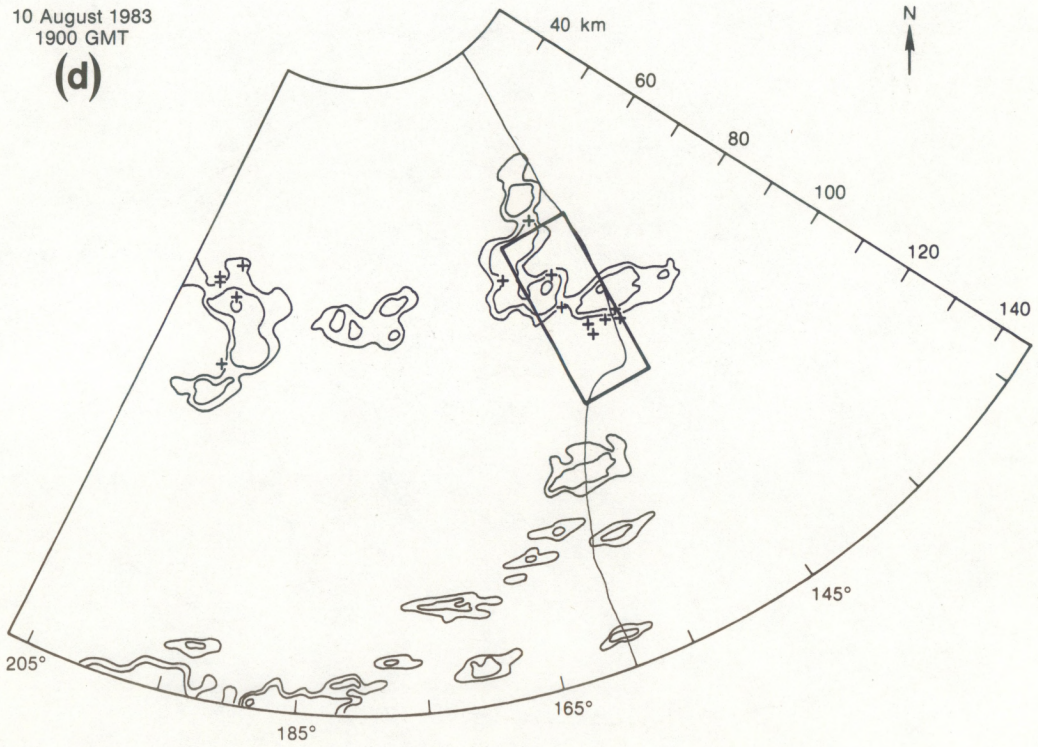

Figure 21. (Continued). (d) 1900 GMT.

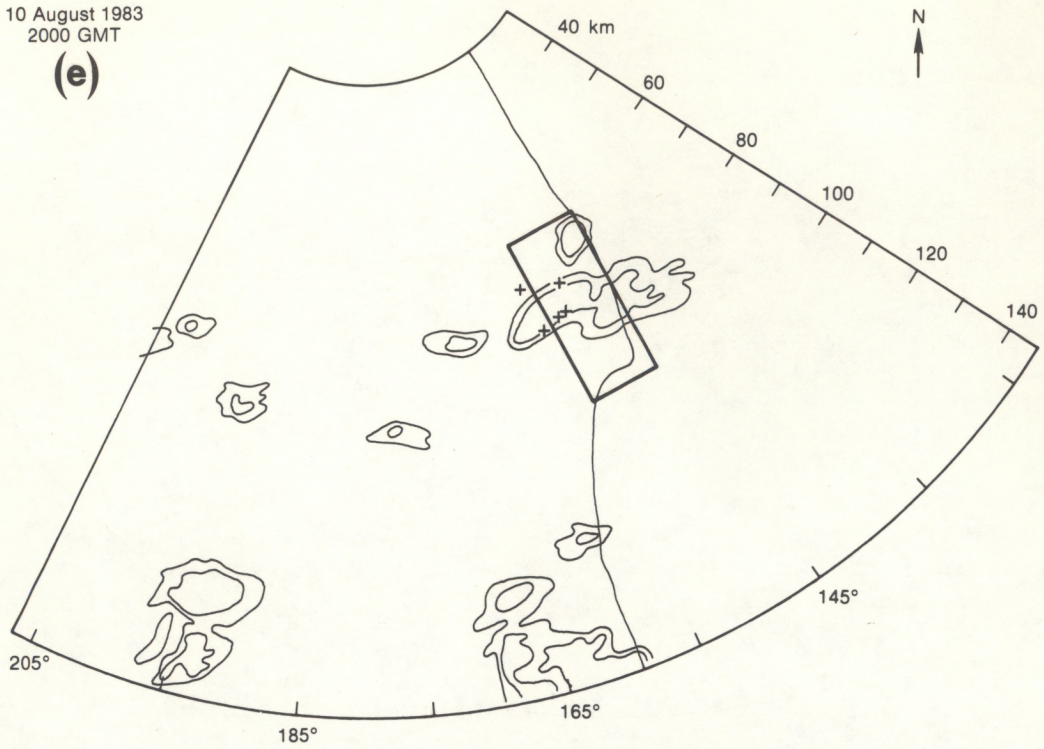

Figure 21. (Continued). (e) 2000 GMT.

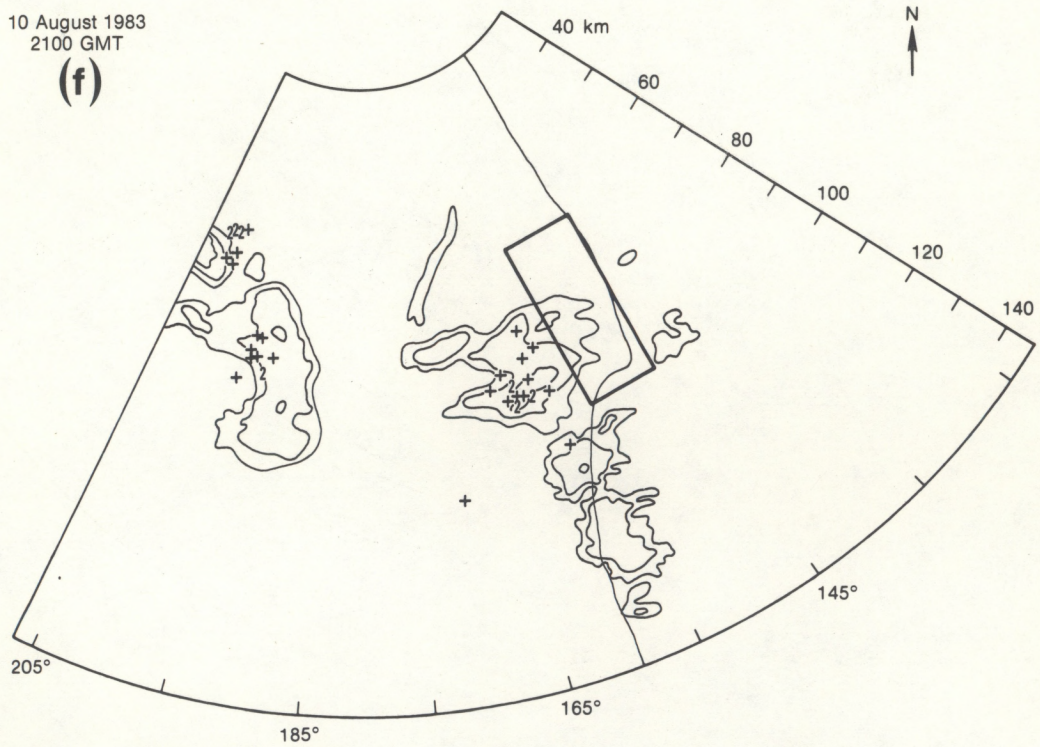

Figure 21. (Continued). (f) 2100 GMT

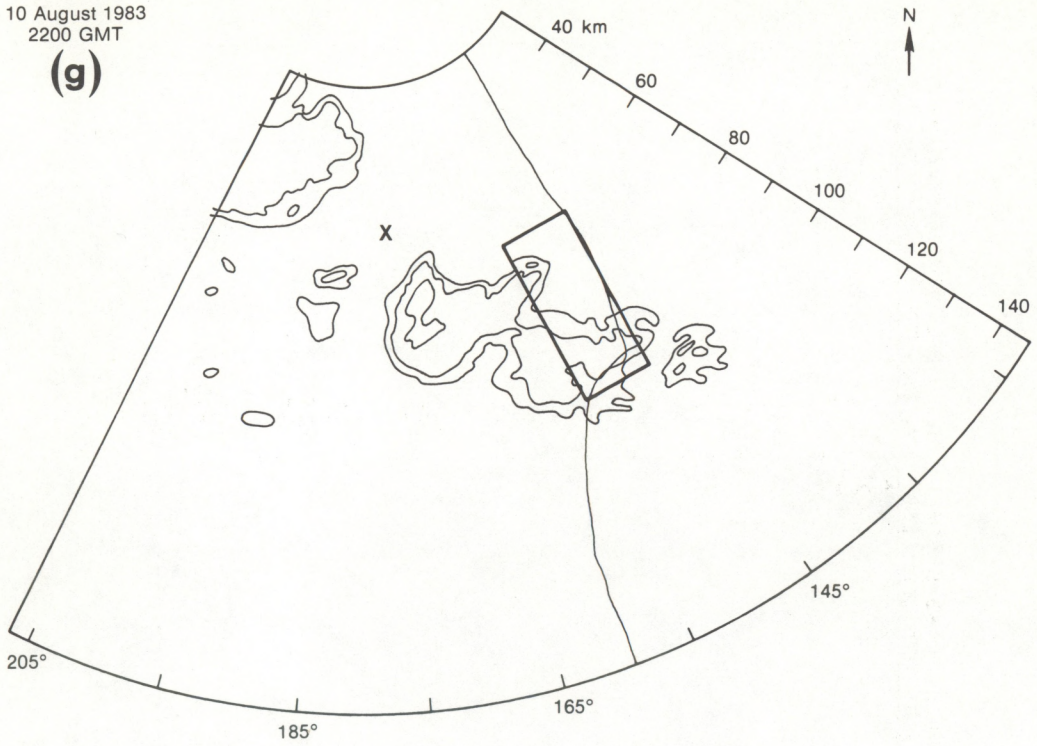

Figure 21. (Continued). (g) 2200 GMT.

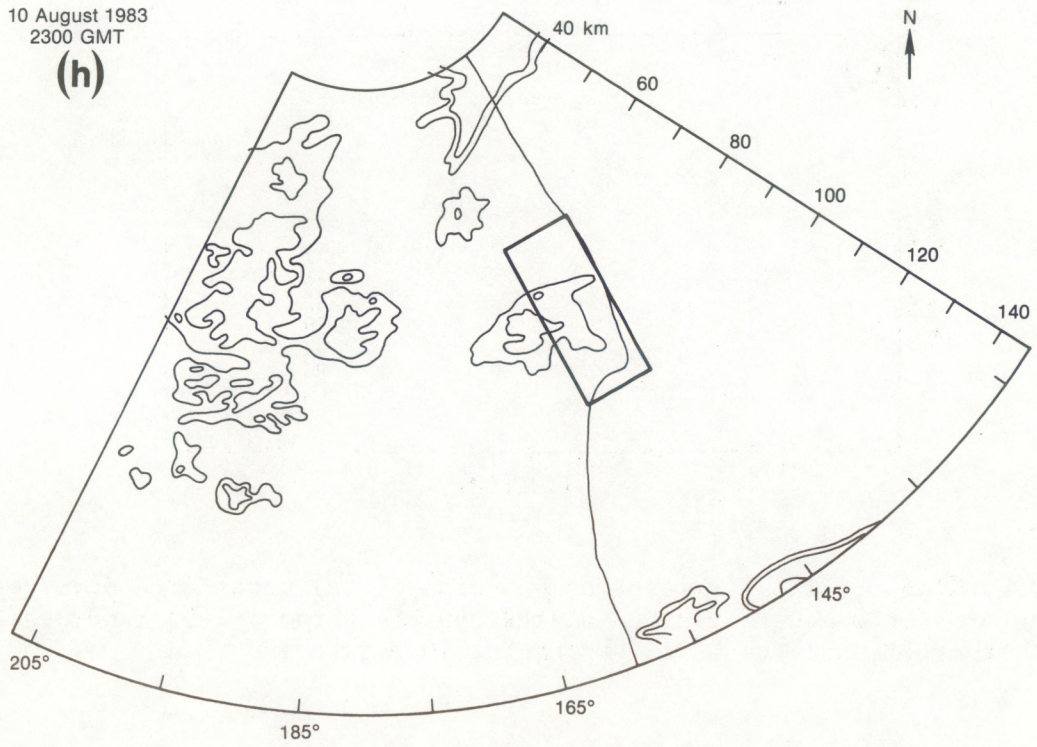

Figure 21. (Continued). (h) 2300 GMT.

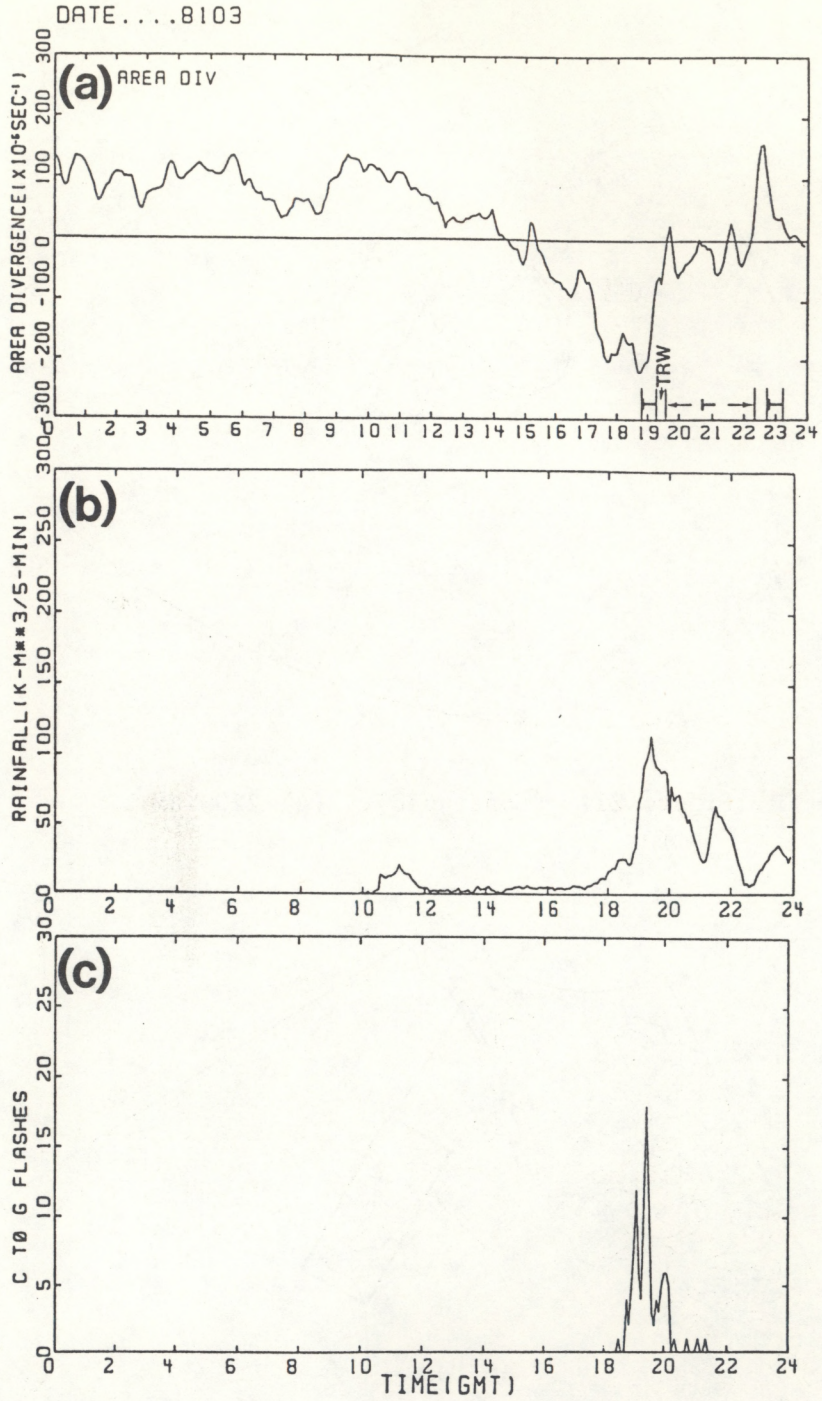

Figure 22. Time profiles (resolution = 5 min) of (a) total area divergence including present weather observed at the Shuttle airport, (b) radar-estimated rainfall from DAB, and (c) CG lightning for 10 August 1983.

A significant maximum in divergence was never detected from this system, probably because a significant amount of precipitation never occurred in the network. However, a small amount of precipitation began in the network at about 1800 GMT and reached a peak at 1930 GMT. Lightning began at 1830 GMT and reached a peak at 1930 GMT; occasional CG flashes continued until 2120 GMT.

Figure 23 presents the meteorological conditions within the mesonetwork boundaries for significant milestones during the afternoon.

1530 GMT (Fig. 23a). Significant convergence is beginning in the network. The east-west confluence zone evident across the state is noticeable; winds are from the west to west-northwest in the northern half of the network and from the southwest in the southern half of the network. Of course, there are no echoes or lightning at this time.

1800 GMT (Fig. 23b). Beginning rain. A moderate convergence zone ($10^{-3}s^{-1}$) has developed over northern Merritt Island; nearly symmetric inflow is depicted by the wind field. Southeast winds are found over the Cape, becoming easterly farther to the north along the coast. The convergence maximum is just on the edge of a group of cells with two small areas of level 3. No lightning is reported in the network as yet.

1840 GMT (Fig. 23c). Maximum convergence. Several regions of weak convergence are displayed over the northern two-thirds of the network. The winds remain southeast over the Cape, becoming easterly to the north along the coast. Notice the northwest wind in the northwest corner of the network, indicating inflow into the updraft region of the cell nearby. Level-2 echoes are found in the area. Lightning began in the network at 1830 GMT, but no strikes were recorded during this 5-min period.

1915 GMT (Fig. 23d). Maximum rain. Precipitation can also be inferred from the wind field at this time. A 25-kn wind is found at wind tower 110 about midway up the coast. Other wind sites near this location continue southeasterly. The divergence signal derived from the wind field is quite strong at $1.6 \times 10^{-3}s^{-1}$. A level-2 reflectivity core lies just south of the divergence maximum. Two CG lightning strokes are found at that location. Two other lightning flashes occurred along the western border of the network during this 5-min period.

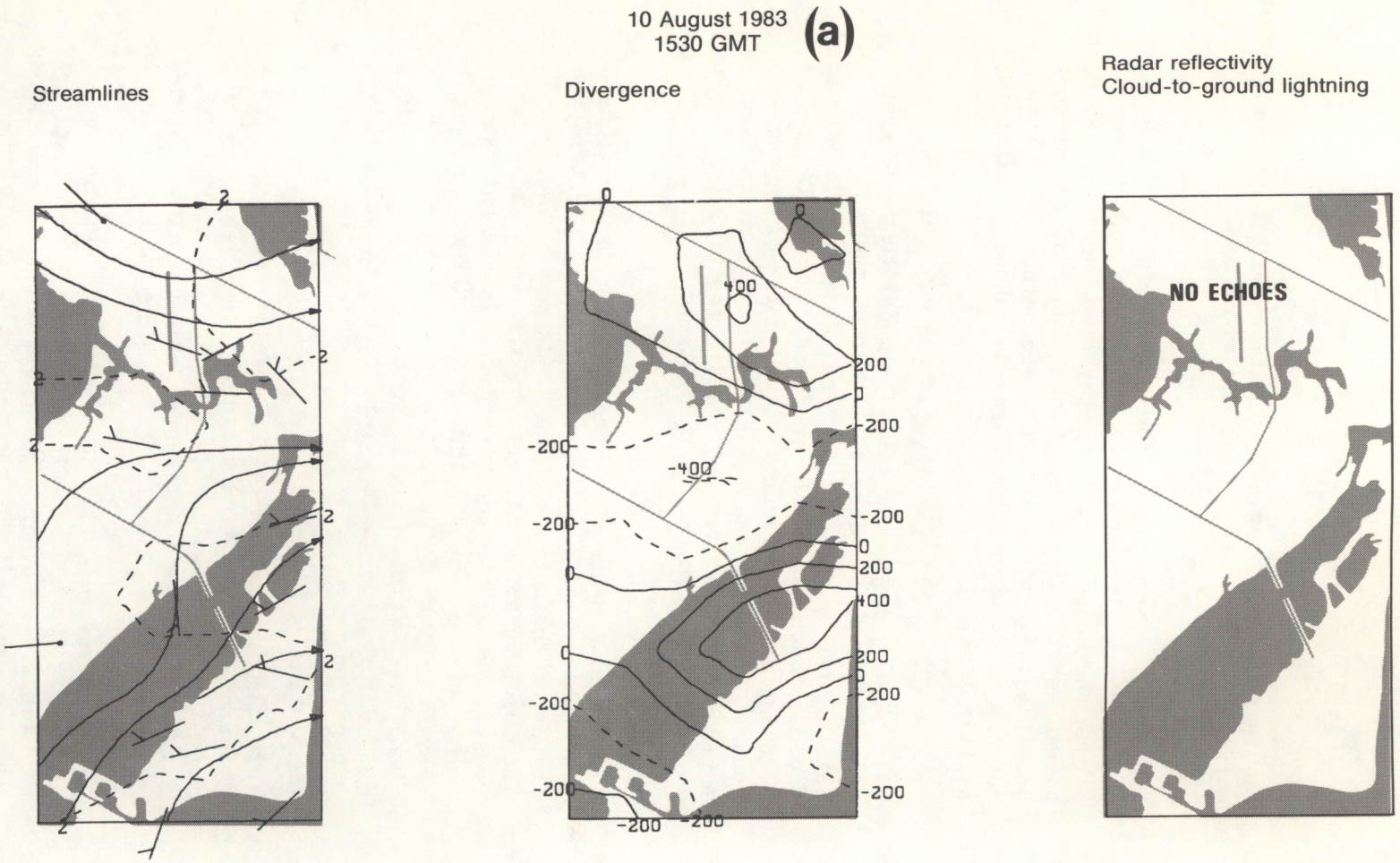

Figure 23. KSC mesonetwork analyses of winds, divergence, and radar and CG lightning locations for 10 August 1983. (a) 1530 GMT.

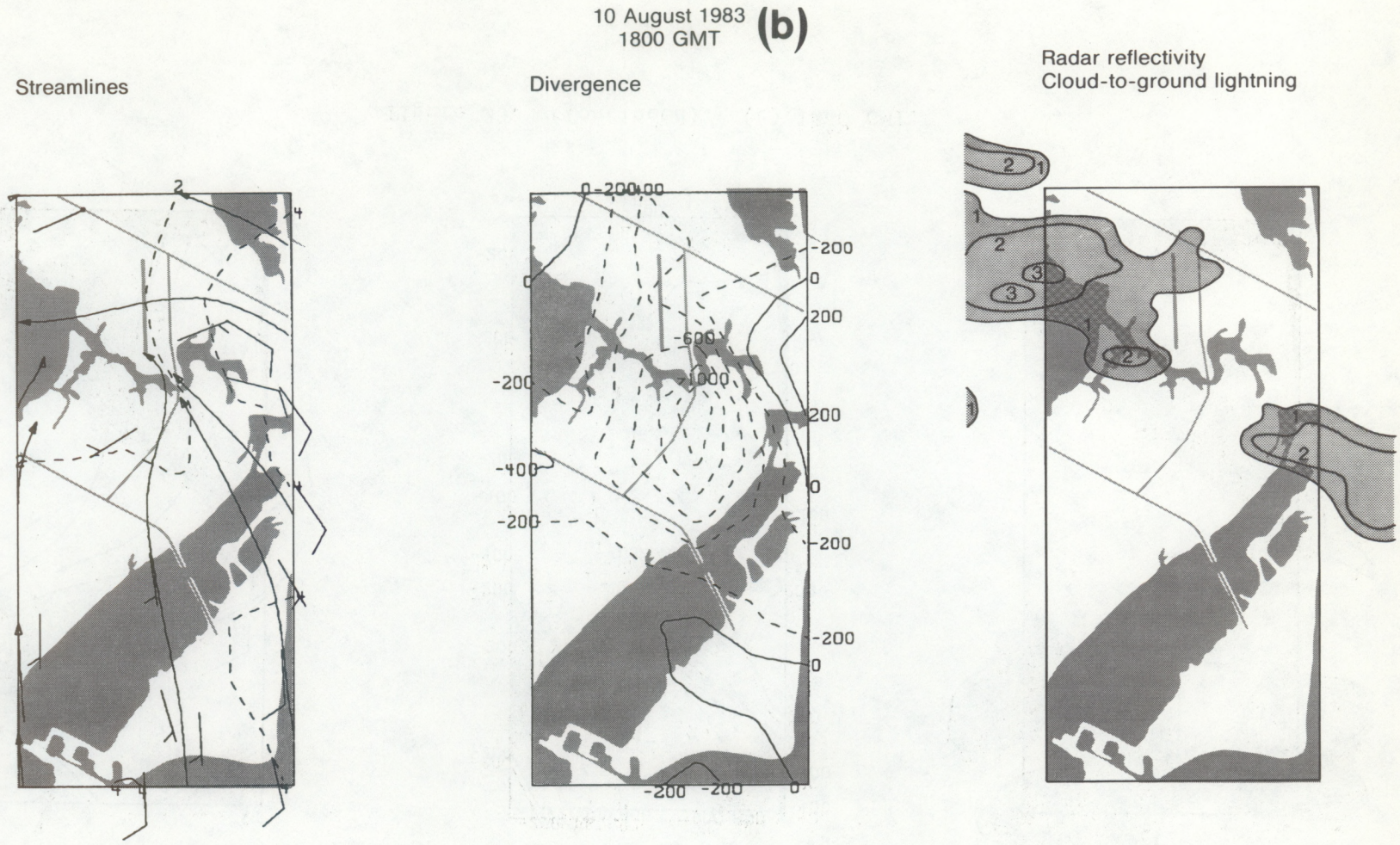

Figure 23. (Continued). (b) 1800 GMT.

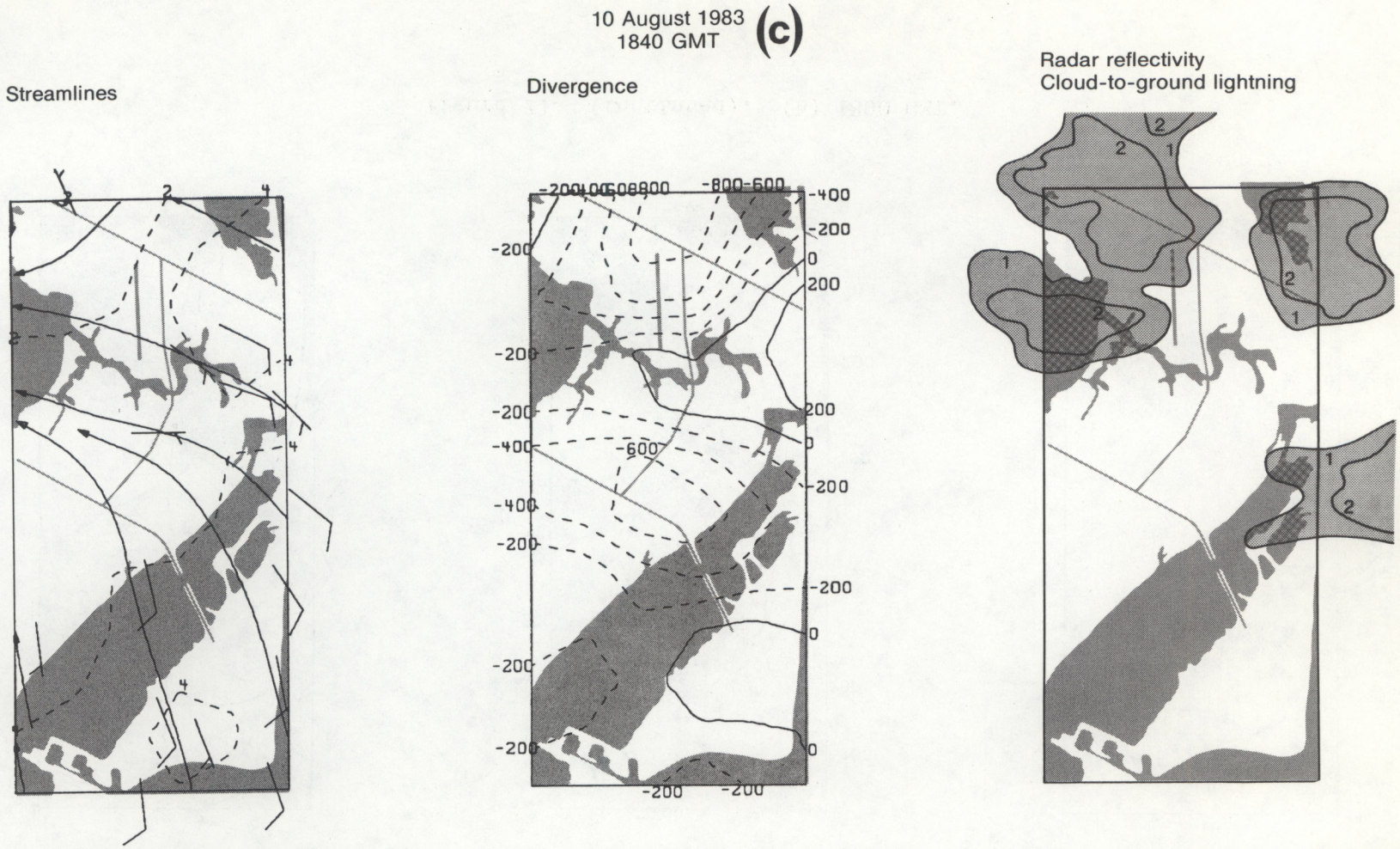

Figure 23. (Continued). (c) 1840 GMT.

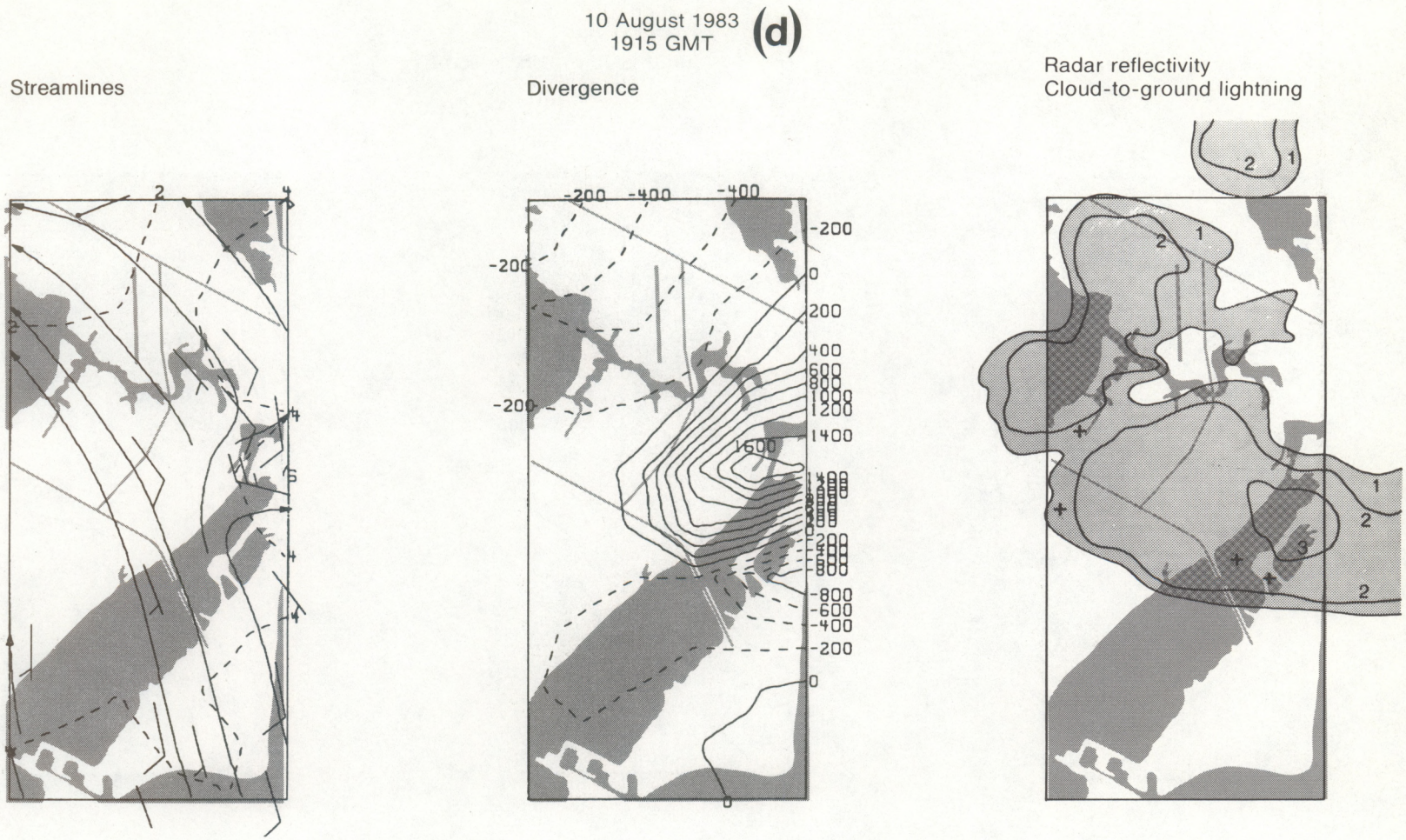

Figure 23. (Continued). (d) 1915 GMT.

10 August 1983
2155 GMT (e)

Streamlines

Divergence

Radar reflectivity
Cloud-to-ground lightning

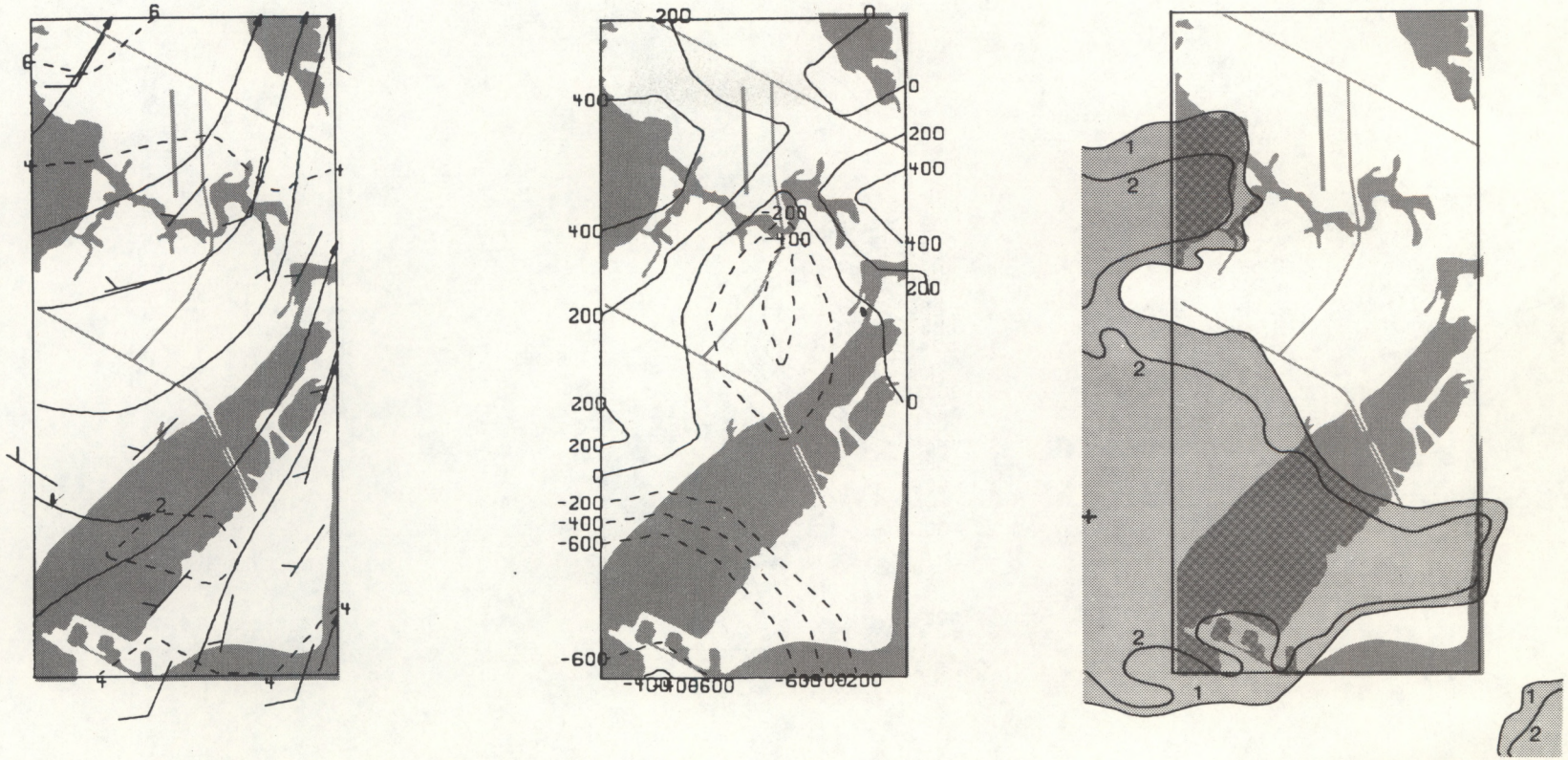

Figure 23. (Continued). (e) 2155 GMT.

2155 GMT (Fig. 23e). Dissipation. The reflectivity shows a sizable area of level 2 over the southwest corner of the network. No lightning has been reported in the network since 2115 GMT. A weak gust front/outflow is defined by the winds from just east of the Shuttle runway southward to west of Port Canaveral on the Banana River. Weak convergence is also shown in the same region. The echo remains in the vicinity for the next several hours but it appears to be only anvil. Figure 21h at 2300 GMT shows that the area has weakened even more. The Shuttle runway observer has reported a ceiling estimated at 25,000 ft since 2033 GMT.

This day illustrates the importance of satellite images. On a day when forcing mechanisms other than heating are weak, the forecaster has determined very early in the day that deep convection will occur, from which direction the activity will move, and how high the tops will be. From that point forward he becomes a short-range mesoscale forecaster. The satellite image becomes a very important tool defining subtle boundaries, confluence zones, and enhanced cloud features. As those areas develop, gust fronts and outflow boundaries and their intersections define new development regions. Then cirrus canopies begin to hide many features, and radar begins to upstage the satellite features. Finally, when convergence is detected in the mesonetwork, the time lead for convection is short. Locations can be pinpointed, movement can be noted. If conditions warrant, it is time for watches, advisories, and warnings. The strength of the convergence signal is proportional to the strength of the convection. On this particular day, there was little in the way of a divergence signature. Therefore, determining dissipation by means of total area divergence would be difficult. However, radar and lightning data clearly showed the demise of the system.

D. Case Study 3: 30 August 1983

The meteorological conditions posed considerable problems in forecasting for the STS-8 launch on the evening of 30 August 1983. A trough moving west across the Florida Peninsula and a developing mid-tropospheric low appeared to be the main factors.

The surface analysis (Fig. 24) at 0000 GMT reveals a very weak frontal zone undergoing frontolysis over the southeastern United States. The pressure gradient indicates mainly weak westerly to southwesterly winds across Florida. Upper-air analyses for 0000 GMT (Fig. 25) show a trough just off the east coast of Florida on both the 850- and 700-mb charts. At 500 mb, the trough appears to be very near Cape Canaveral and extends southward west of West Palm Beach and a little east of Key West. Twenty meter height falls have been experienced across the state in the past 12 h. At 300 mb, winds are mainly light northerly around the high center to the west.

To show the movement of the trough and development of a closed circulation aloft, the upper-air analyses 12 h later at 1200 GMT on 30 August are presented in Fig. 26. At 850 mb, the trough is now west of Tampa, moving west across the state. There is a closed low over the Big Bend area along the

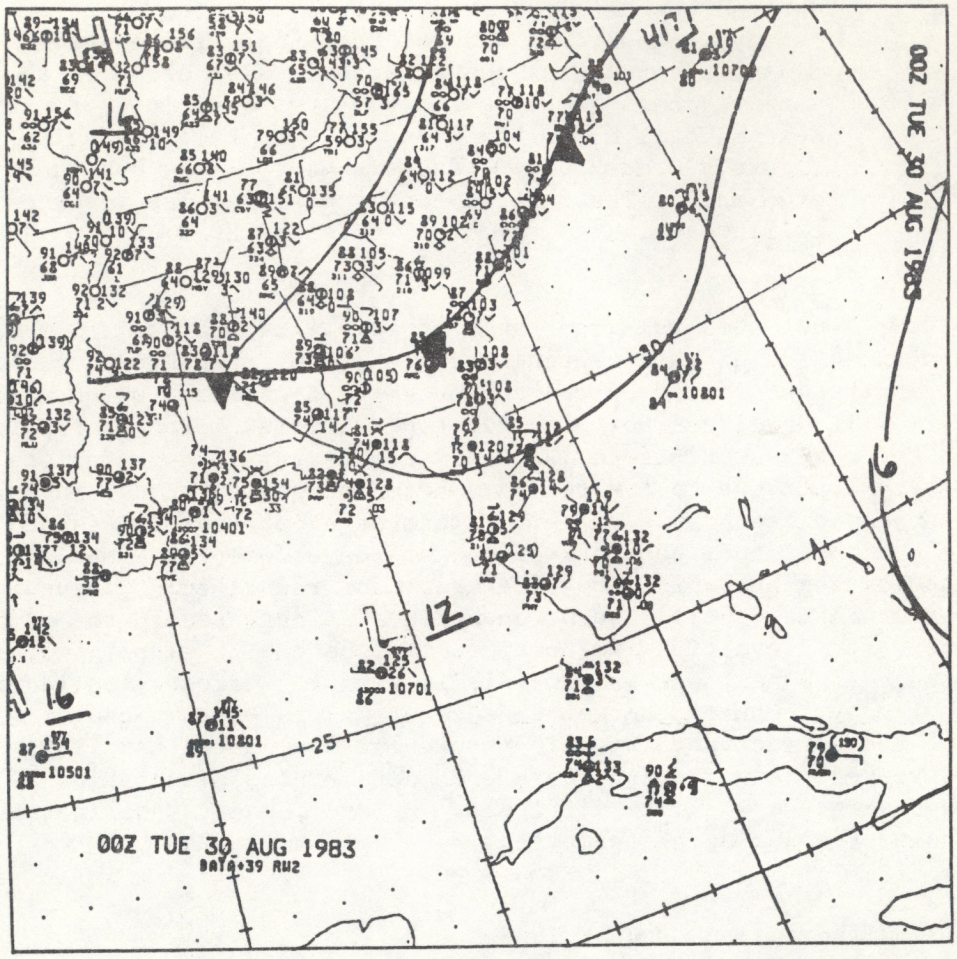

Figure 24. NMC surface analysis for 30 August 1983 at 0000 GMT.

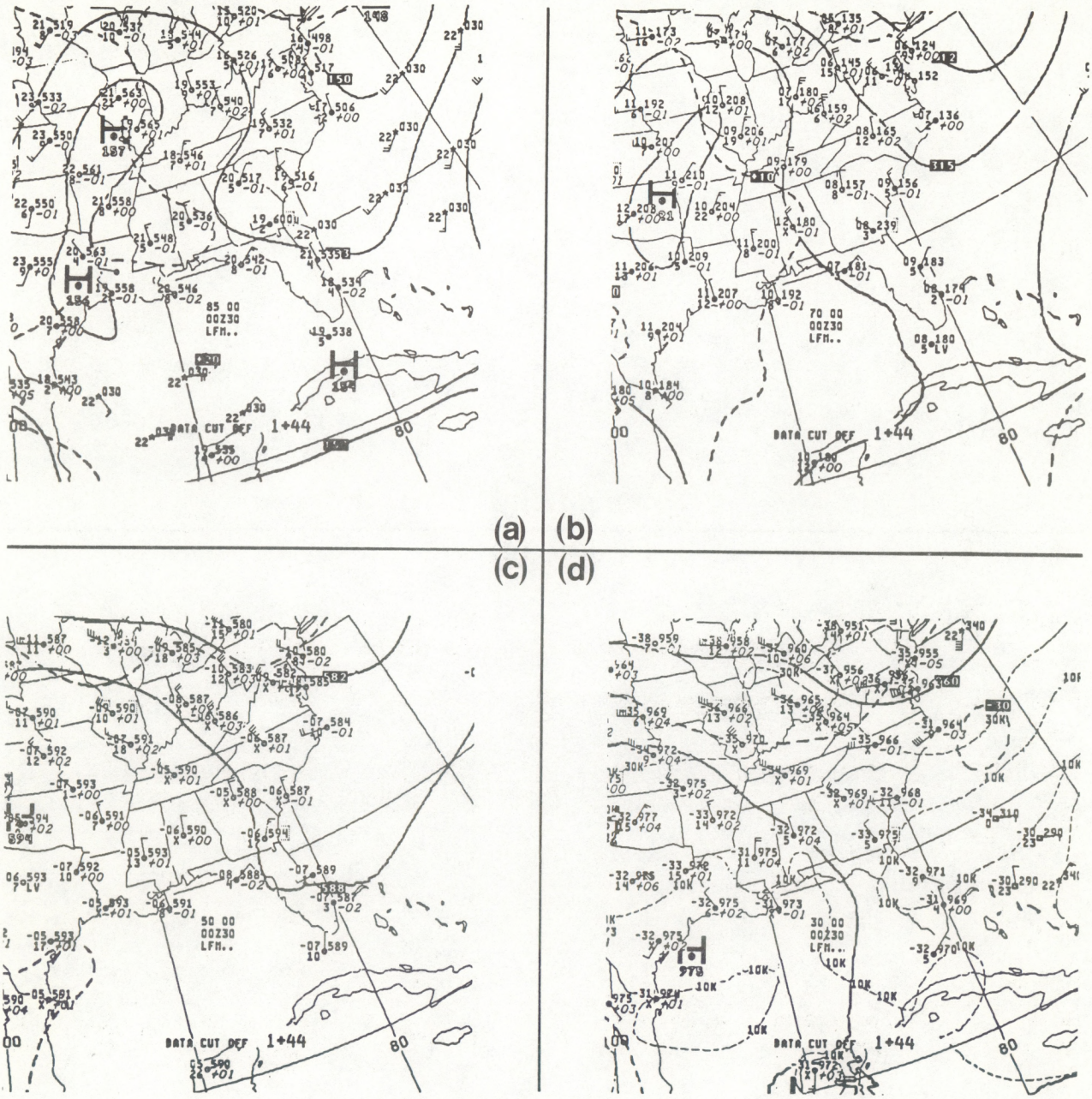

Figure 25. NMC upper-air analyses for 30 August 1983 at 0000 GMT for (a) 850 mb, (b) 700 mb, (c) 500 mb, and (d) 300 mb.

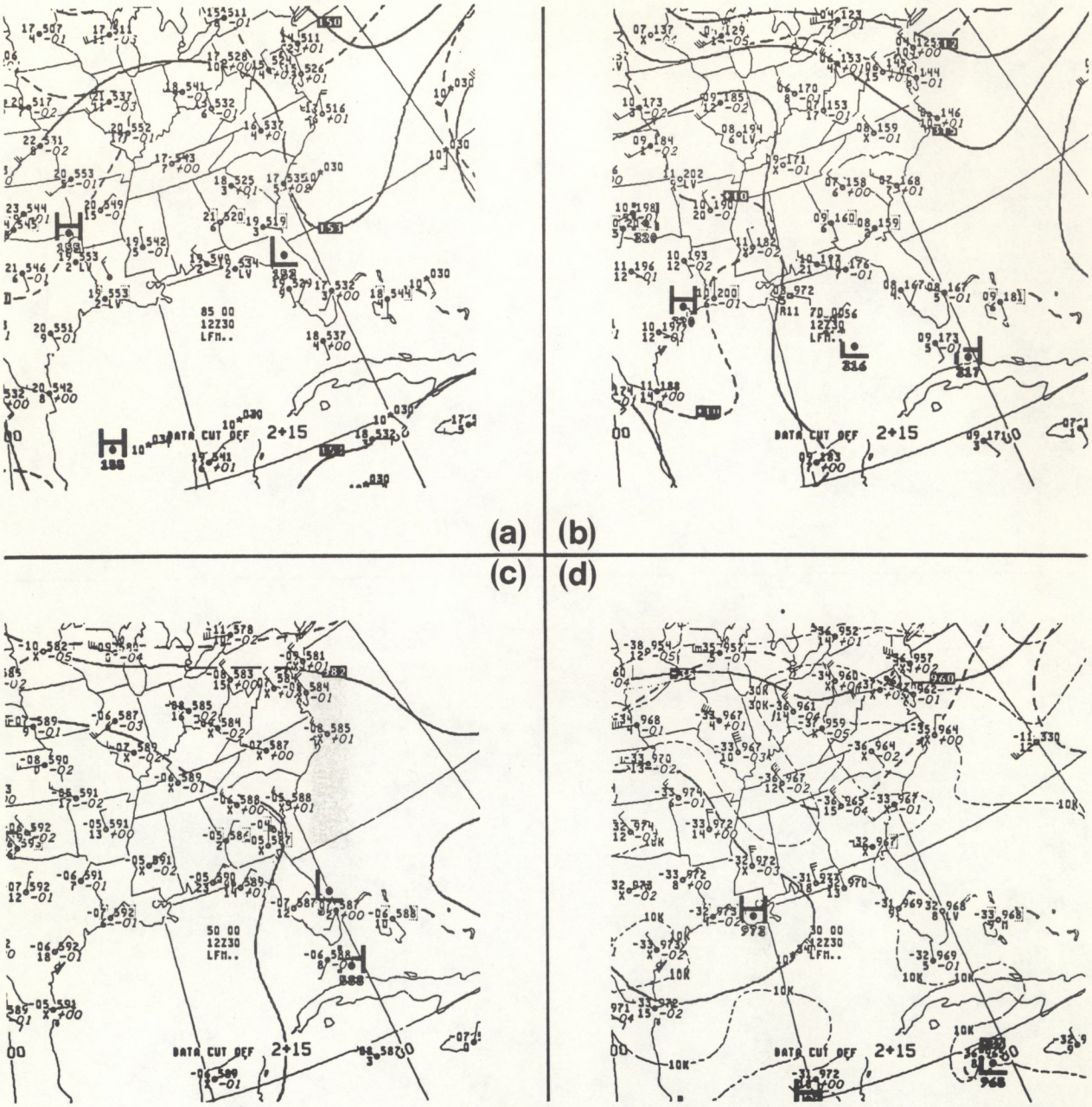

Figure 26. NMC upper-air analyses for 30 August 1983 at 1200 GMT for (a) 850 mb, (b) 700 mb, (c) 500 mb, and (d) 300 mb.

Gulf Coast of Florida. Winds are southerly to southwesterly near Tampa and points south, easterly in Georgia and Alabama, and northerly near Pensacola, Florida. At 700 mb, the circulation is somewhat confused, and it is not clear whether there is a closed circulation. An inverted trough is situated near Apalachicola extending southward into the Gulf. At 500 mb, only the orientation of the trough has changed in 12 h. At 0000 GMT, the trough was defined in a more north-south direction, but by 1200 GMT the trough has shifted into a northeast-southwest position pivoting on central Florida as the middle-latitude system has moved east and the subtropical portion drifted westward. Height falls have stabilized by 1200 GMT.

Infrared satellite imagery for the period 0100 to 0300 GMT is shown in Fig. 27.

0100 GMT (Fig. 27a). Along the Gulf Coast there is a large weakening complex. There is also a hint of a middle-level circulation in the Gulf of Mexico west of Tampa. Over northeast Florida just north of KSC, there is a small convective cell, which is possibly a second generation of the dissipating cell northwest of Daytona Beach.

0200 GMT (Fig. 27b). At this time, the system is located over the northern fringes of KSC. It has grown considerably and has IR temperatures as cold as $-62^{\circ}C$.

0300 GMT (Fig. 27c). The system has grown somewhat in area but there is little change in coldest temperatures and location.

The Cape Canaveral rawinsonde sounding for 2200 GMT, 29 August is displayed in Fig. 28. The sounding, as usual, is conditionally unstable with a rather large amount of available moisture. At face value, the northerly winds recorded by the sounding would be indicative of subsidence and lack of convective activity. However, the development of a mid-tropospheric disturbance in the Gulf modified this "rule of thumb." The total-totals index is substantial at 52. The lifted index, assuming the surface temperature at 2200 GMT and average mixing ratio for the lowest 100 mb, is -5.5 which is quite large for this region. When the same surface conditions are used, the LFC is at 770 mb and the equilibrium level is approximately 185 mb. Therefore, deep vigorous convection still can be expected, given a means of lift.

The lift is provided by the outflow boundary moving away from the dying system northwest of Daytona Beach. Figures 29a through 29g are the Daytona Beach radar and CG lightning displays at hourly increments beginning at 0000 GMT and ending at 0600 GMT. Initial convective development occurred at approximately 2300 GMT on 29 August east of Daytona Beach.

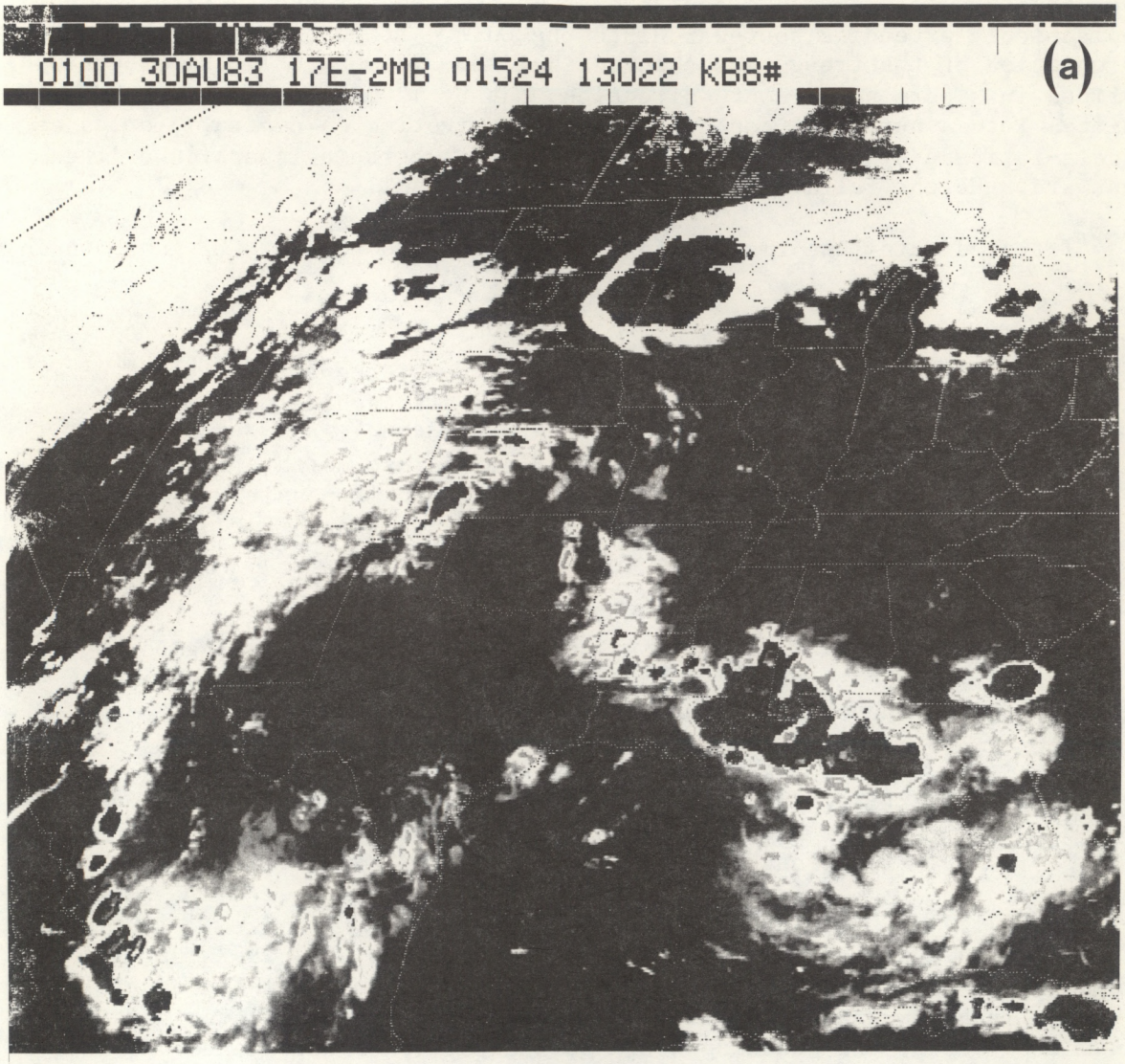

Figure 27. IR satellite imagery with MB enhancement for 30 August 1983. (a) 0100 GMT.

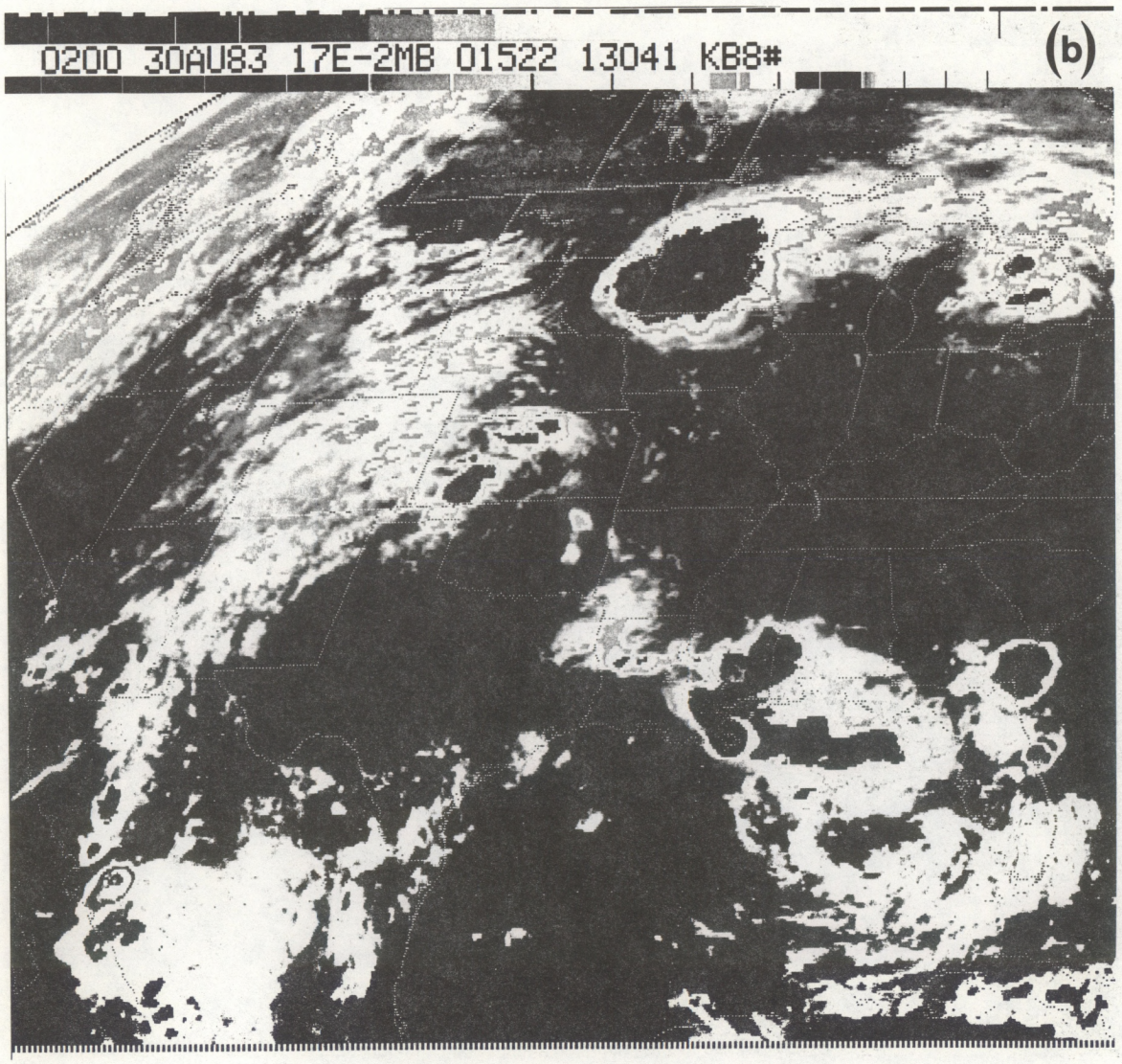

Figure 27. (Continued). (b) 0200 GMT.

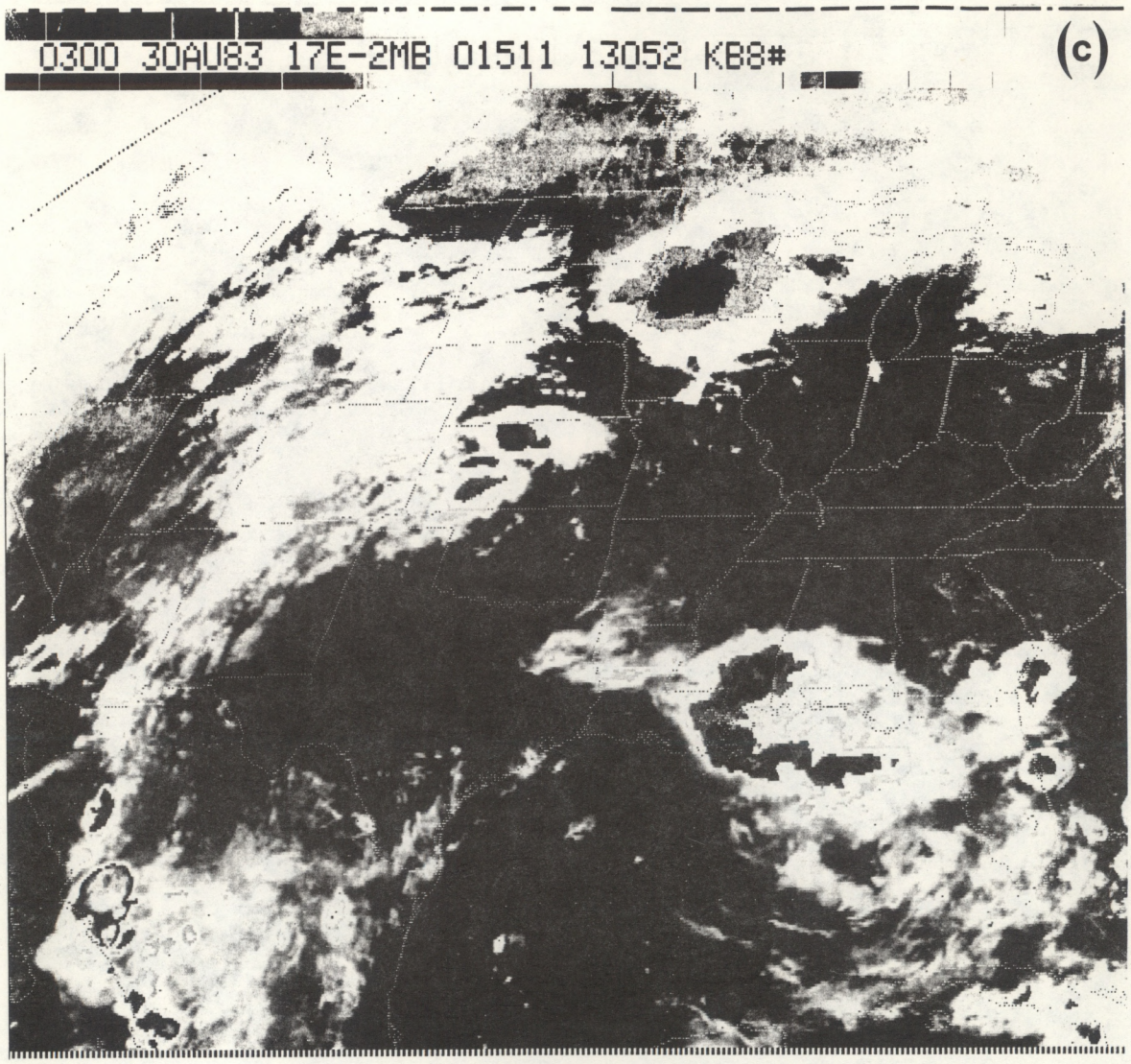

Figure 27. (Continued). (c) 0300 GMT.

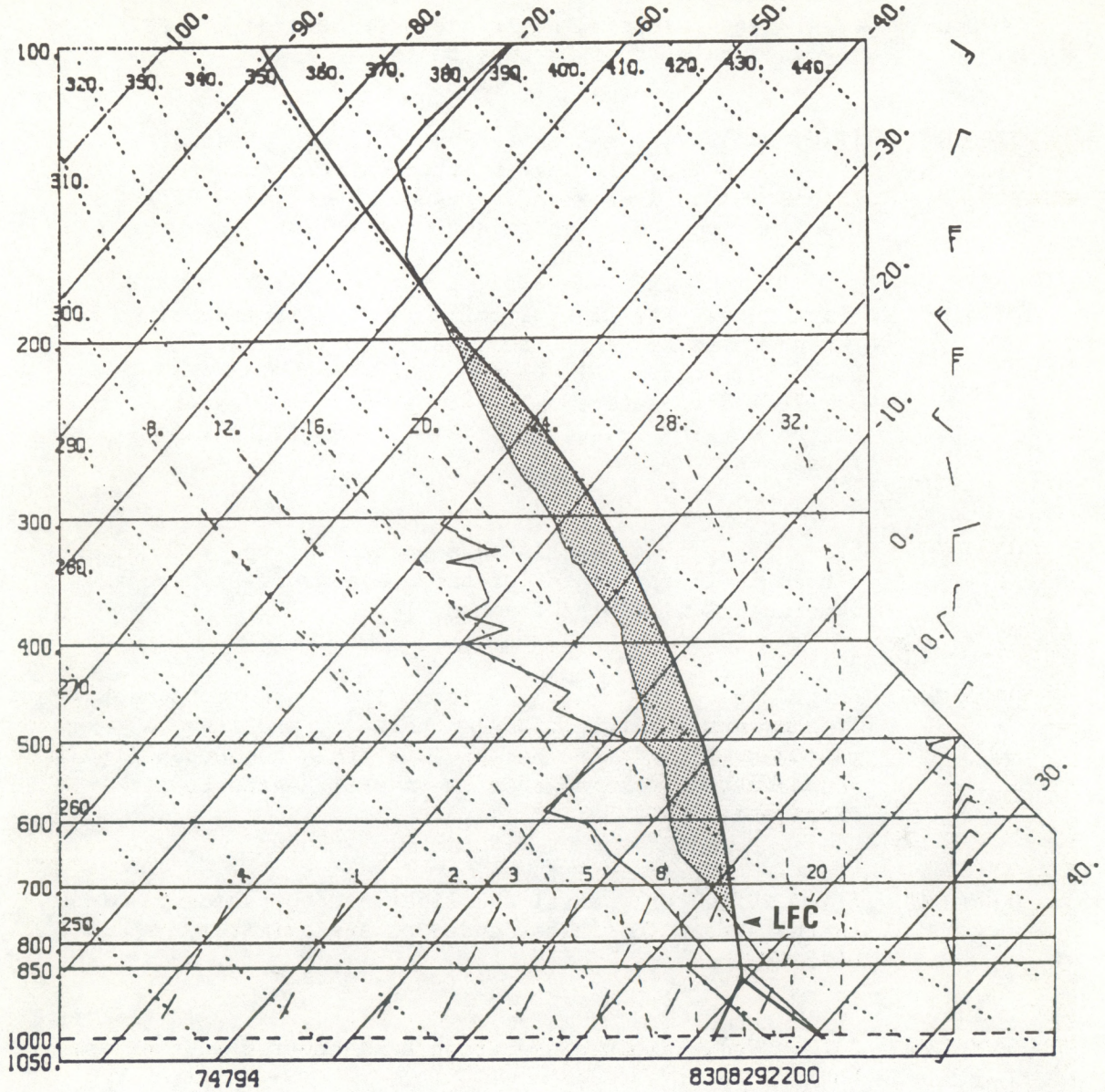

Figure 28. Cape rawinsonde sounding at 2200 GMT, 29 August 1983 plotted on a skew-T, log P diagram.

0000 GMT (Fig. 29a). Initial cells are just outside the PPI segment and east of Daytona Beach.

0100 GMT (Fig. 29b). The system is moving south. Moderate cells (level-3) are nearing the northern corner of the KSC network. Twenty-one strokes are recorded during the 5-min period offshore north of the KSC network.

0200 GMT (Fig. 29c). The line of cells is now situated along the northern border of the mesonetwork. Heavy CG lightning activity is very near the most intense reflectivity centers. The linear pattern described by the convection is quite visible in the lightning locations.

0300 GMT (Fig. 29d). The most intense portion of the line of echoes is in the center of the mesonetwork. There are numerous CG lightning flashes.

0400 GMT (Fig. 29e). The line is exiting the southern boundary of the network; precipitation north of the line is mainly anvil. The number of CG flashes has dropped considerably in an hour as the system begins to dissipate.

0500 GMT (Fig. 29f). Only anvil and light precipitation remains in the area. CG flashes ended at approximately 0425 GMT.

0600 GMT (Fig. 29g). Rapid dissipation has occurred in the last hour.

Total area divergence, radar-derived rainfall, and CG lightning time series for the KSC mesonetwork are presented in Fig. 30. As shown to be the case with most moving squall lines in Illinois (Watson and Holle, 1982), the total area divergence profile has a very sudden, steep drop to maximum convergence followed by a similarly rapid rise to maximum divergence. The steepness is a function of the speed of the system. Convergence began at approximately 0110 GMT; the sharpest drop started at 0220 GMT. Precipitation on radar began at about 0200 GMT, and first lightning in the network occurred at 0205 GMT. Convergence reached a peak at 0245 GMT. Peak lightning and maximum rain occurred at the same time, approximately 0315 GMT. Maximum divergence was recorded at 0325 GMT. Following the most intense lightning, CG flashes dropped off rapidly, the last in the network being reported at 0405 GMT.

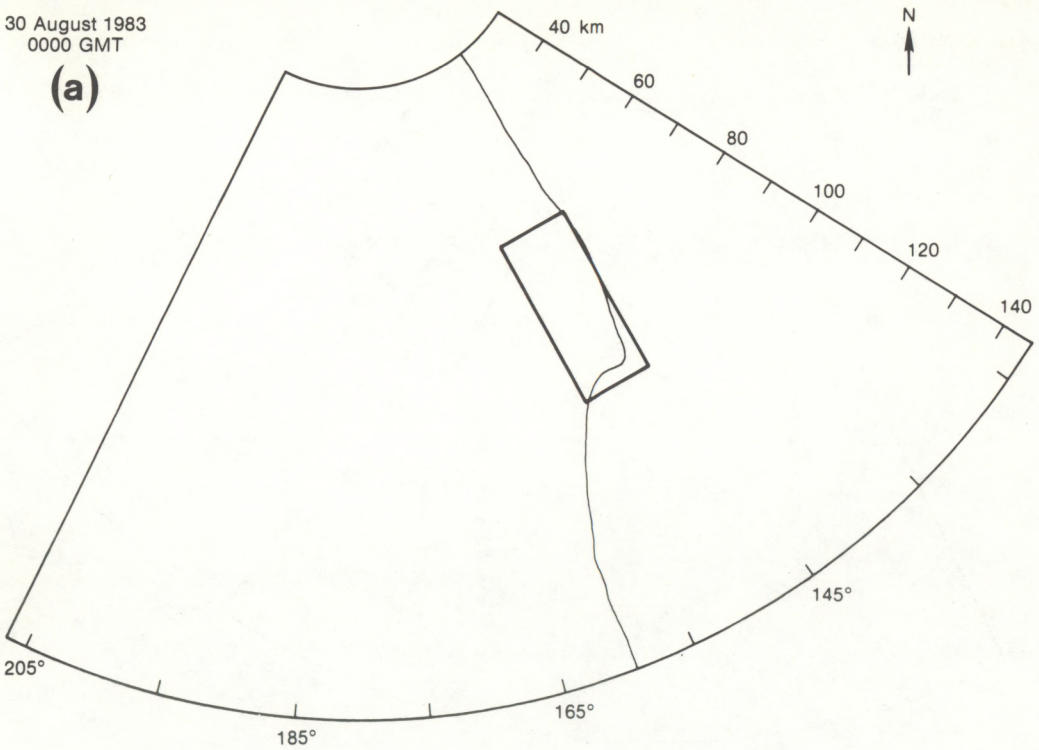

Figure 29. Regional radar and CG lightning patterns for 30 August 1983 (as in Fig. 21). DVIP levels are shown (as in Fig. 13). (a) 0000 GMT.

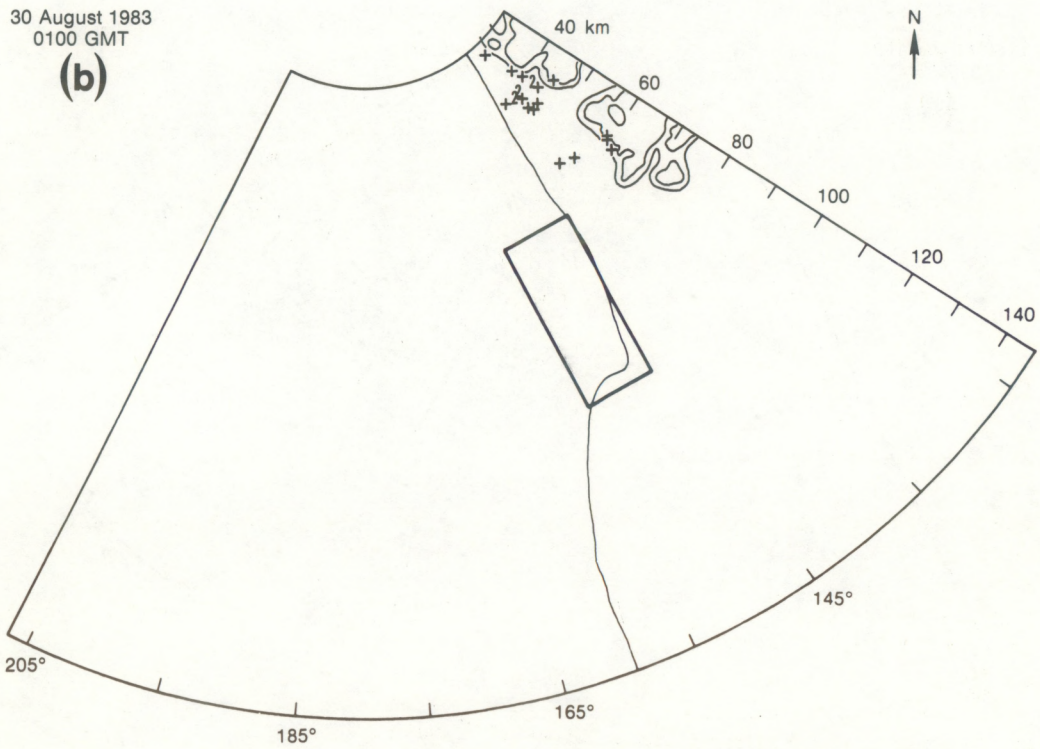

Figure 29. (Continued). (b) 0100 GMT

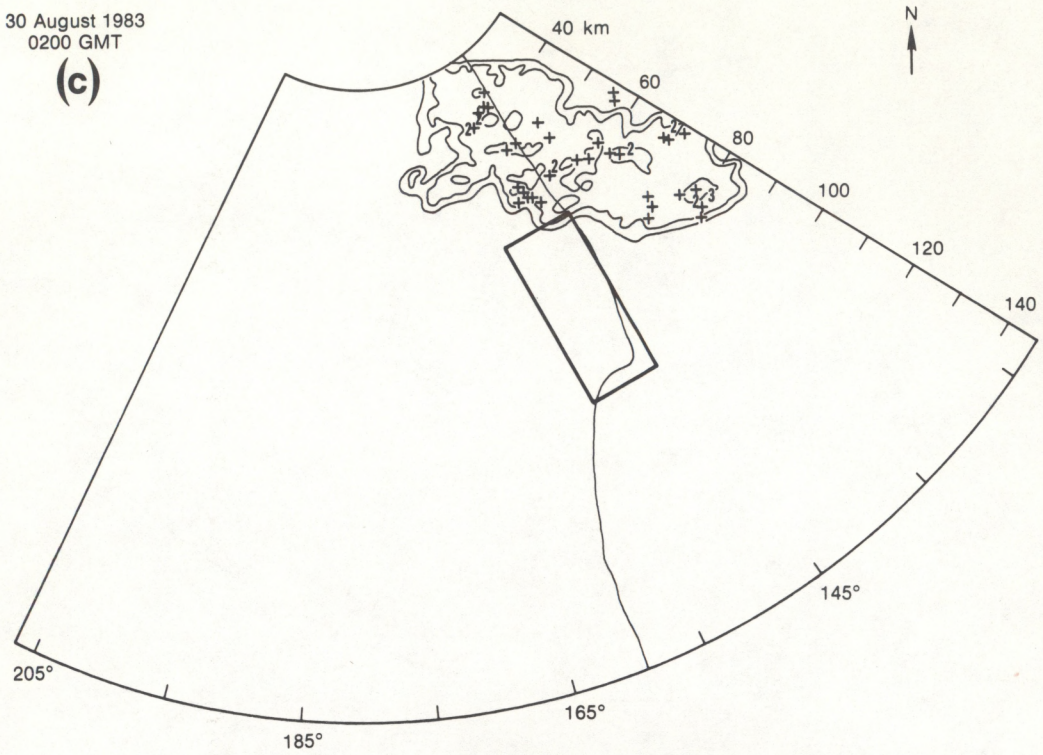

Figure 29. (Continued). (c) 0200 GMT.

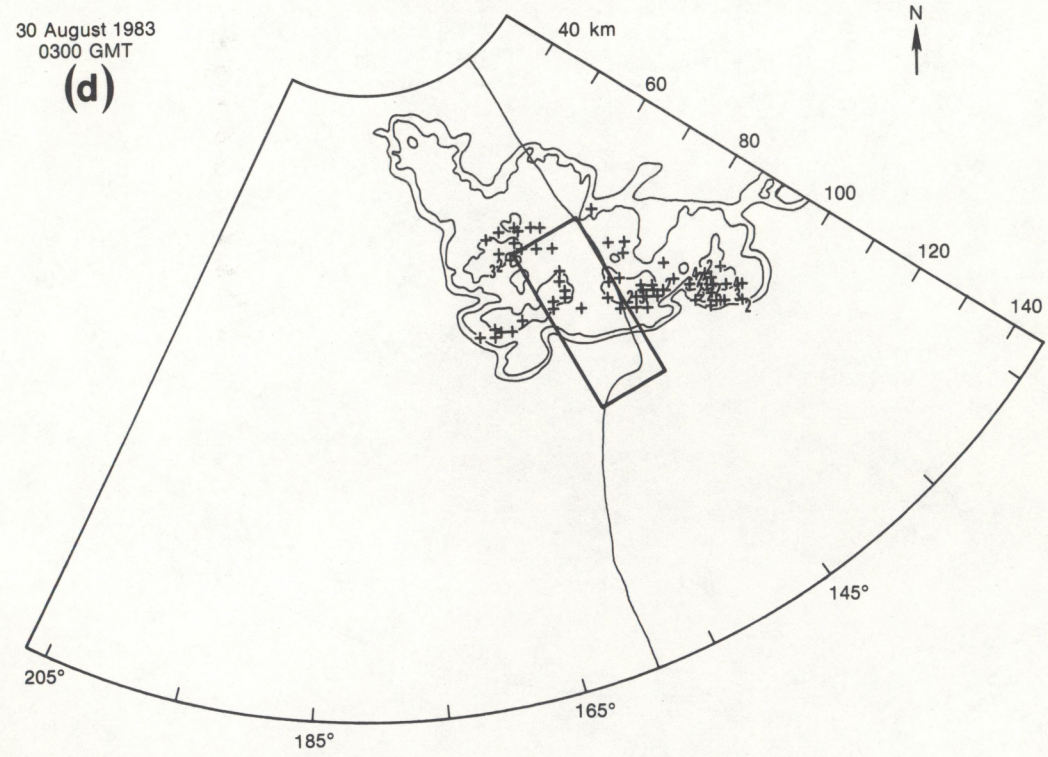

Figure 29. (Continued). (d) 0300 GMT.

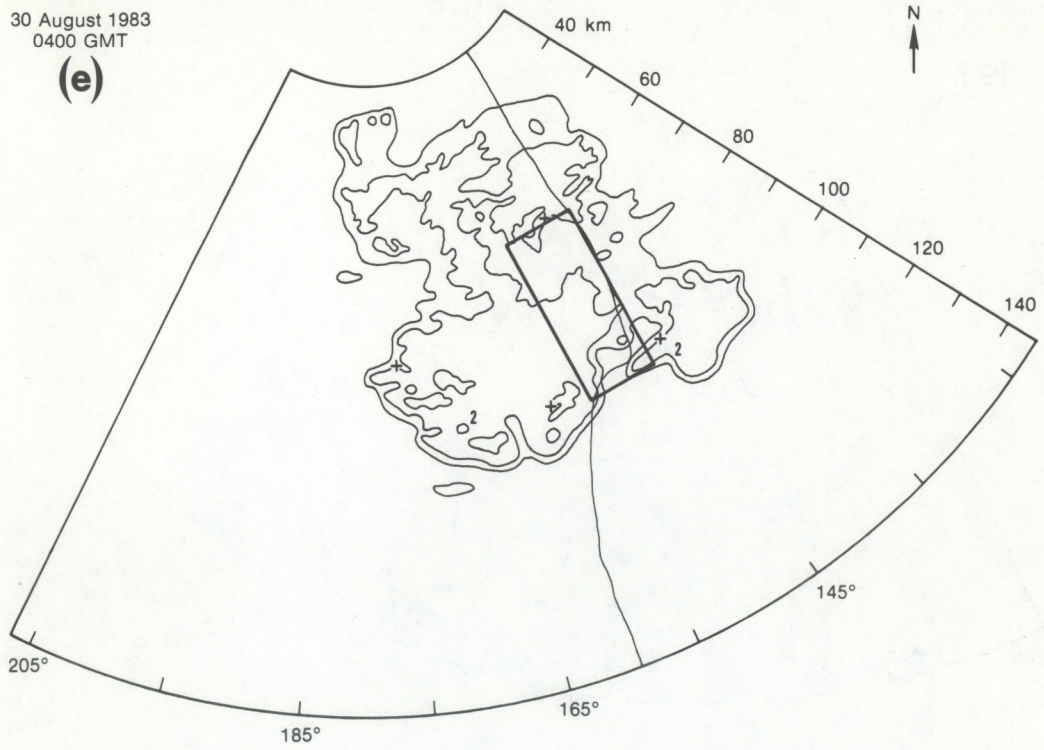

Figure 29. (Continued). (e) 0400 GMT.

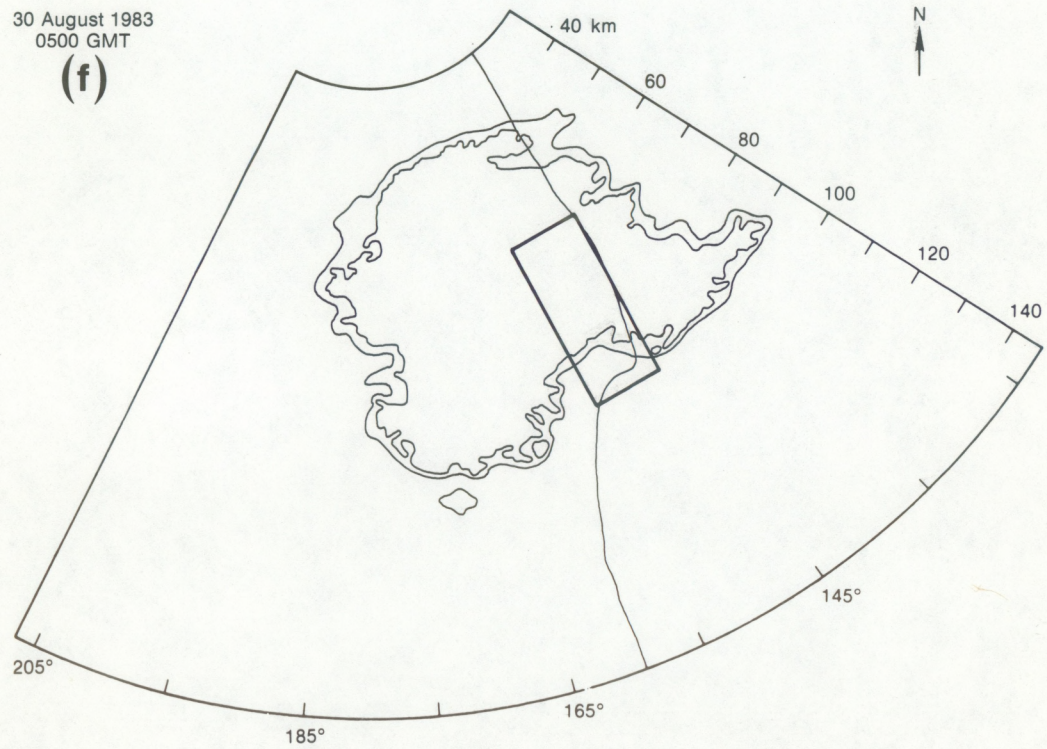

Figure 29. (Continued). (f) 0500 GMT.

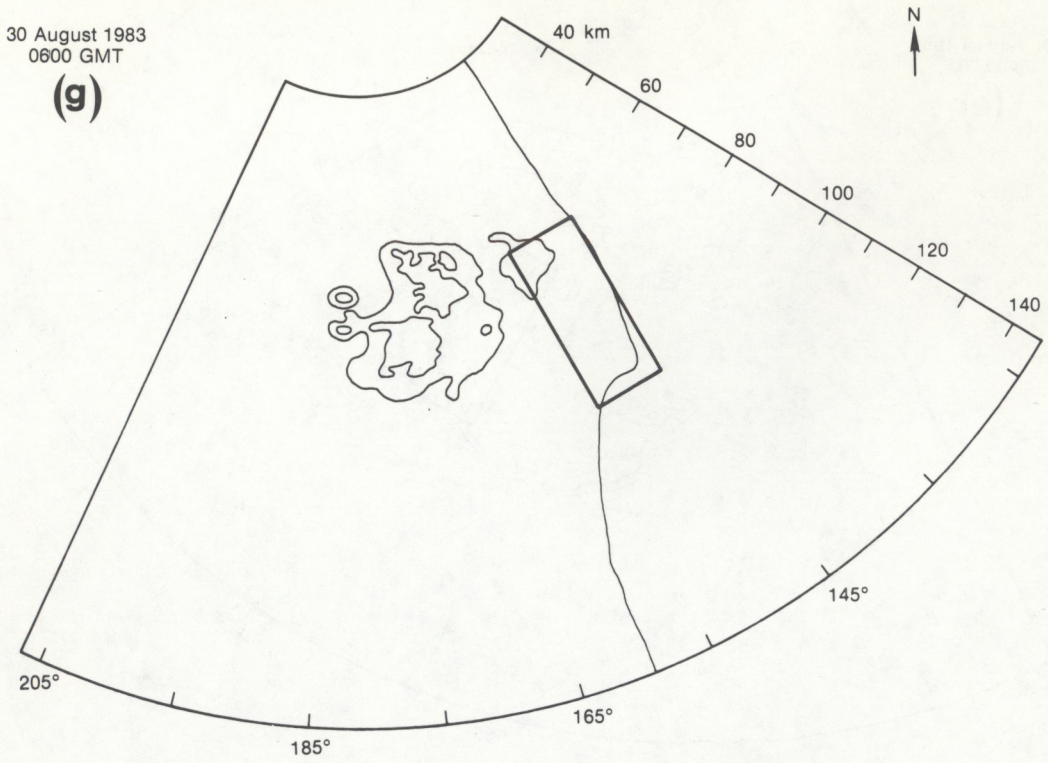

Figure 29. (Continued). (g) 0600 GMT.

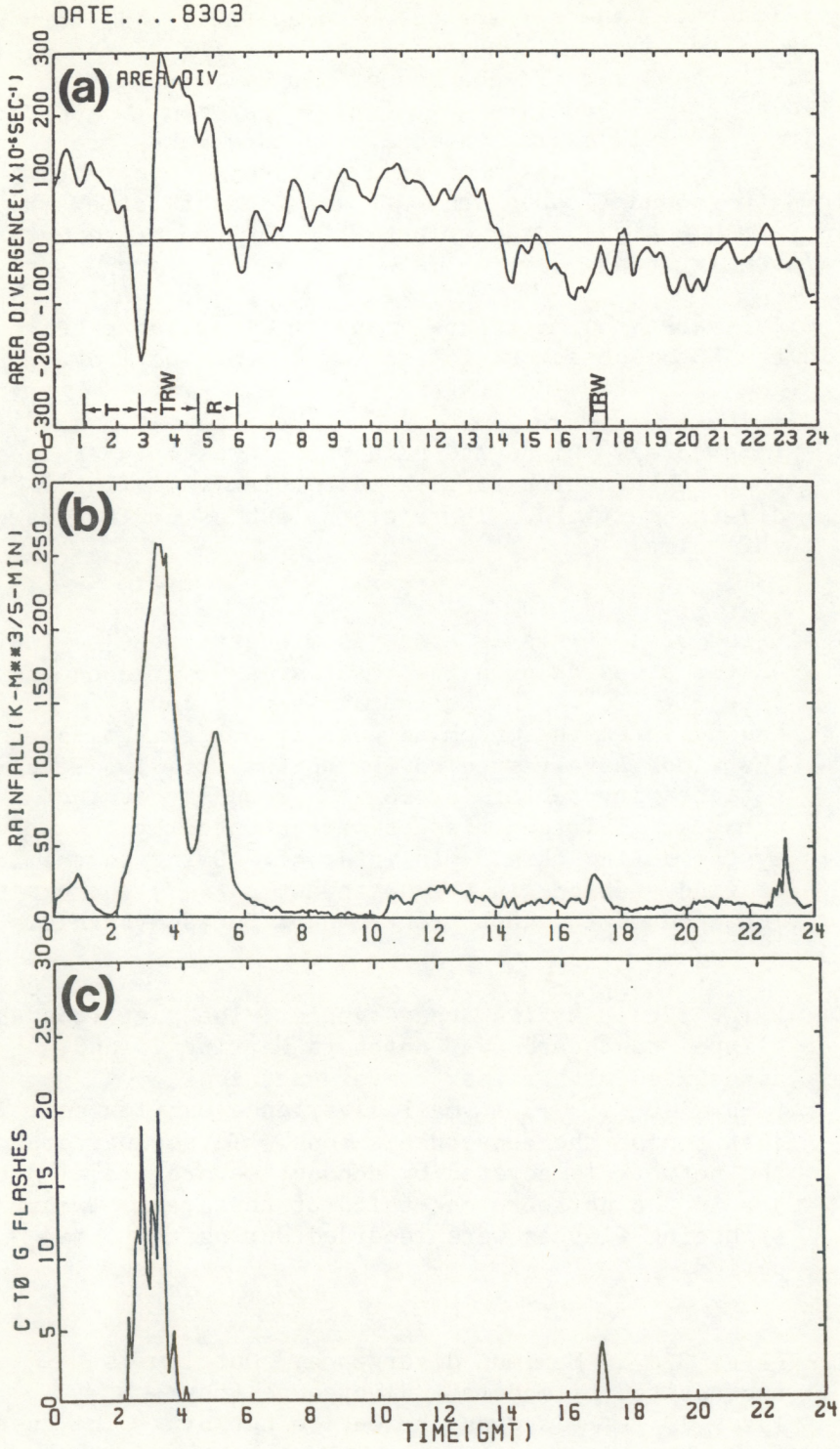

Figure 30. Time profiles (resolution = 5 min) of (a) total area divergence including present weather observed at the Shuttle airport, (b) radar-estimated rainfall from DAB, and (c) CG lightning for 30 August 1983.

Figure 31 illustrates the differences between field mill data and LLP information. The criteria normally used for determining lightning flashes from the field mill data are field changes of 850 V m^{-1} for three sites and 600 V m^{-1} for two sites. There is no distinction between CG and cloud-to-cloud flashes with the field mills, whereas only CG strokes are recorded by the LLP system. The lightning maximum for all systems appears to be about the same time. Cloud-to-ground flashes drop off considerably after that time, but the field mills retain a high degree of activity for about one more hour, indicating in-cloud lightning.

Figure 32 illustrates the horizontal maps of winds, divergence, and radar and lightning in the KSC mesonetwork for selected 5-min periods.

0100 GMT (Fig. 32a). Winds are mainly southwesterly at less than 10 kn, which results in a relatively flat divergence field. There are no echoes or CG flashes at this time.

0230 GMT (Fig. 32b). This is about 15 min after the beginning of the steep drop in the total area divergence profile (see Fig. 30). The northernmost wind tower (site 714) has detected the oncoming gust front from the north as the winds have veered to the northwest. Two level-3 reflectivity centers are on the boundary of the network. Thirteen flashes were counted by the LLP system during this 5-min interval. Owing to the lack of wind stations in the northwest corner, the exact location of the gust front cannot be ascertained.

0250 GMT (Fig. 32c). Maximum convergence. The gust front has slipped southward over northern Merritt Island, associated with a weak convergence zone ($<-6 \times 10^{-4} s^{-1}$). A small divergence outflow cell is just behind the convergence zone. Three-quarters of the network is covered by echoes; several level-3 cores are in the northern one-third of the area. Twenty CG lightning flashes were recorded during the 5-min period.

0320 GMT (Fig. 32d). Maximum divergence. Outflow is represented by moderate divergence (peak of $1.2 \times 10^{-3} s^{-1}$) across the entire network. The gust front has cleared the mesonetwork to the south. A level-4 reflectivity maximum is over the divergence maximum. Only five lightning flashes are recorded at this time.

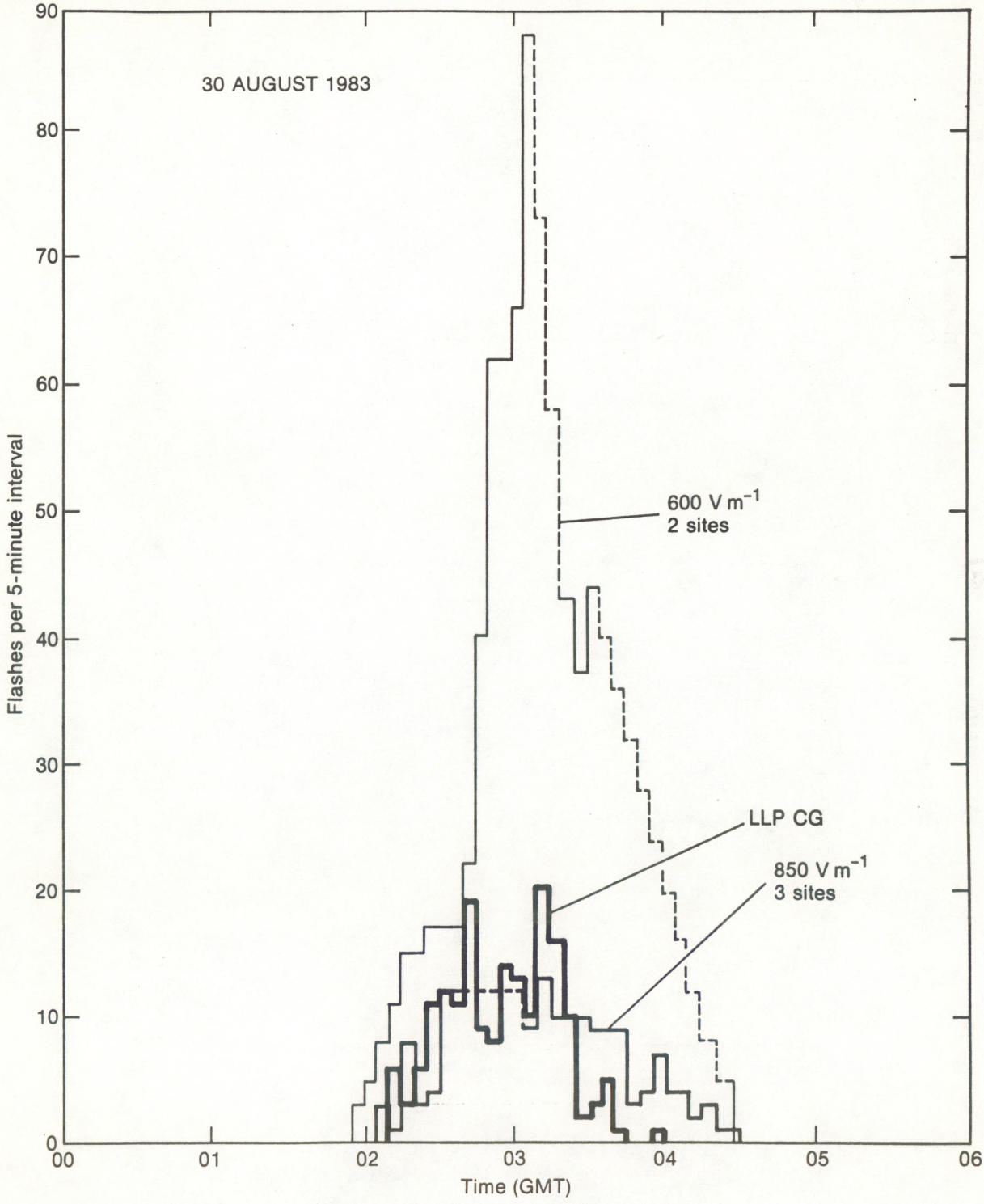

Figure 31. Five-minute lightning data for 30 August 1983 between 0000 and 0600 GMT, from the LLP system and field mills (600 V m^{-1} and 850 V m^{-1} thresholds).

30 August 1983
0100 GMT **(a)**

Streamlines

Divergence

Radar reflectivity
Cloud-to-ground lightning

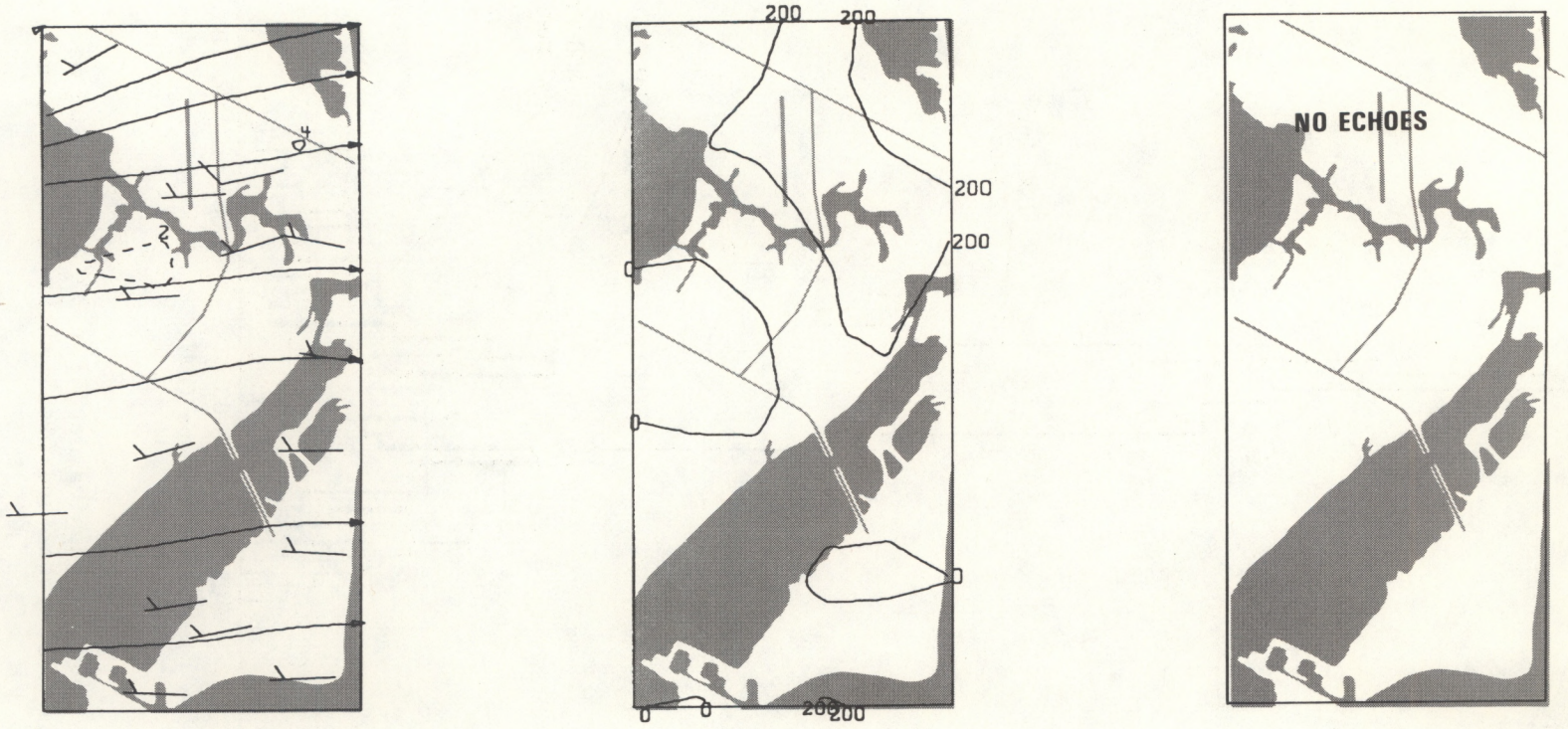

Figure 32. KSC mesonetwork analyses of winds, divergence, and radar and CG lightning locations for 30 August 1983. (a) 0100 GMT.

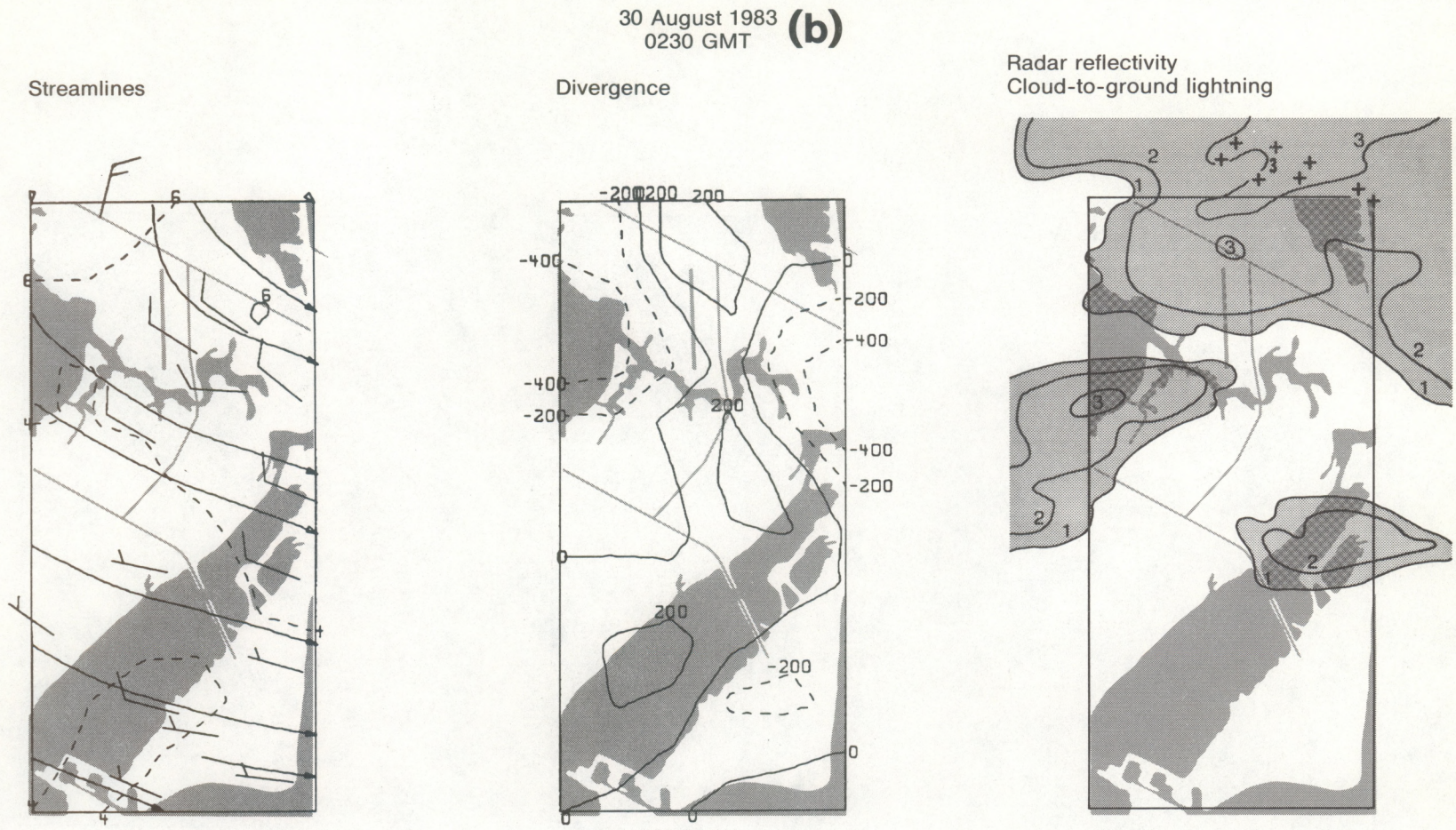

Figure 32. (Continued). (b) 0230 GMT.

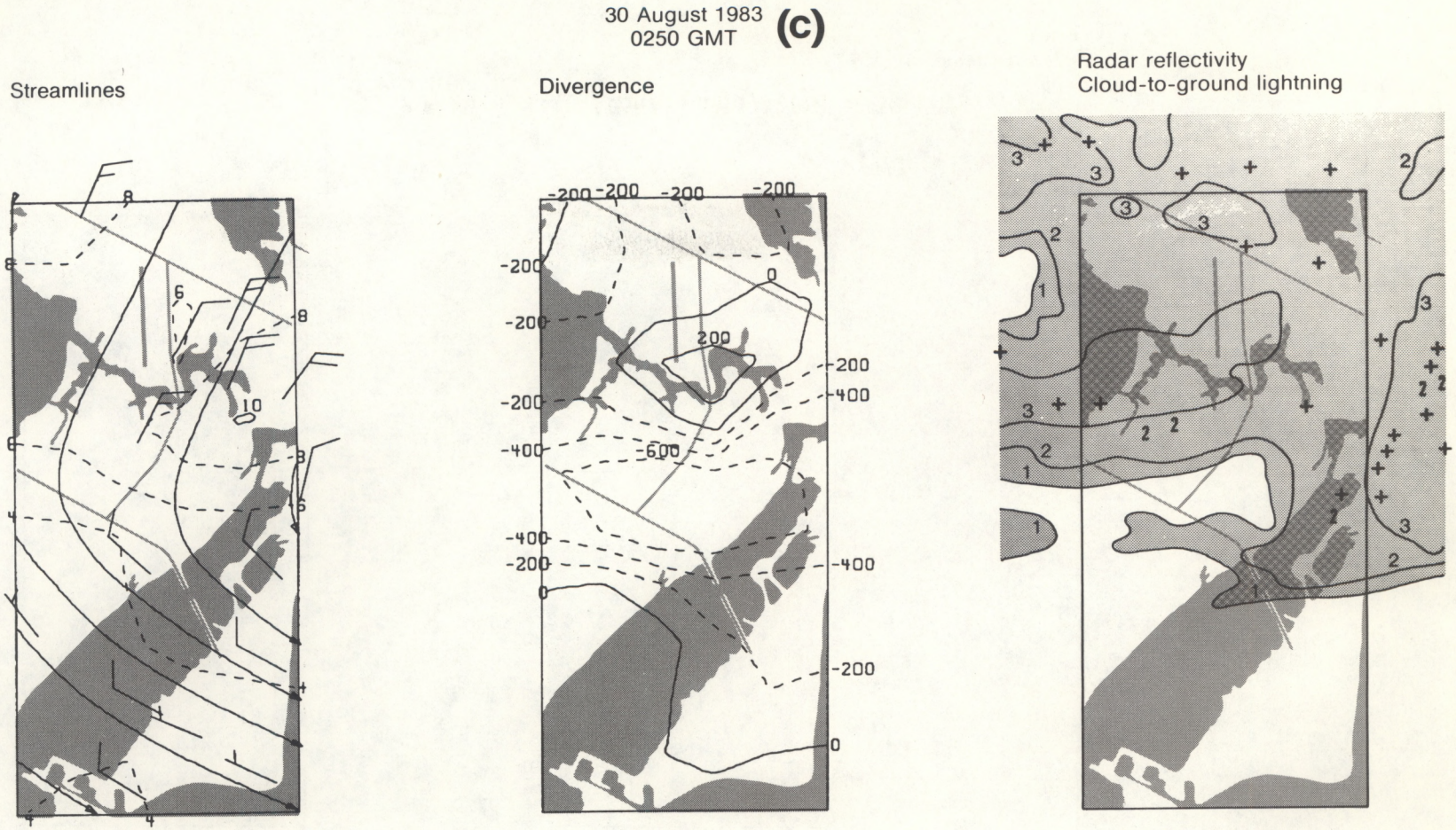

Figure 32. (Continued). (c) 0250 GMT.

30 August 1983
0320 GMT **(d)**

Streamlines

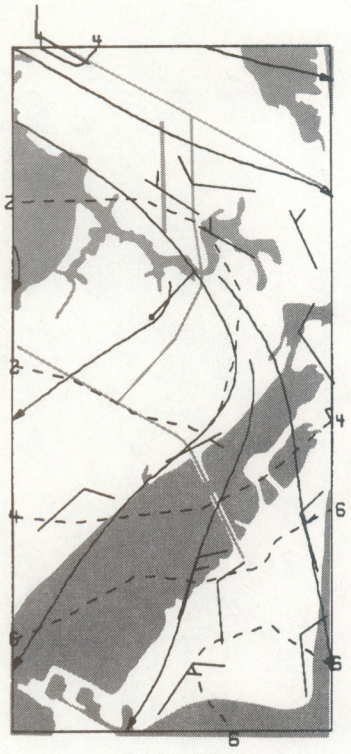

Divergence

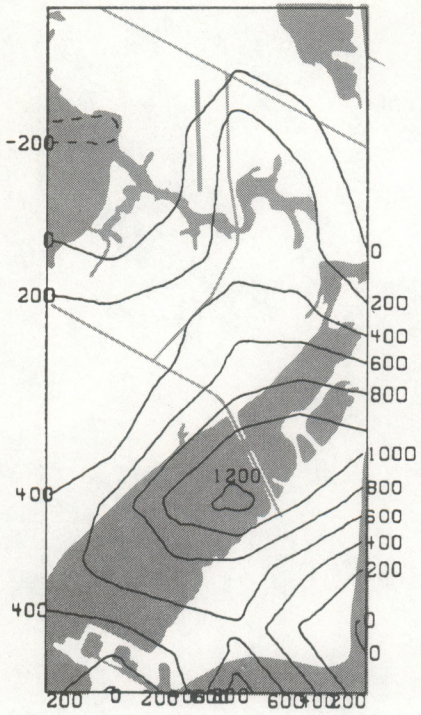

Radar reflectivity
Cloud-to-ground lightning

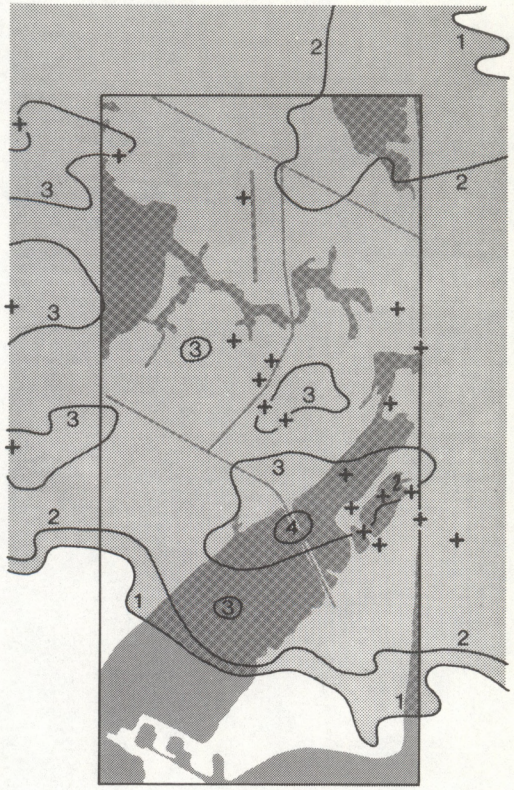

Figure 32. (Continued). (d) 0320 GMT.

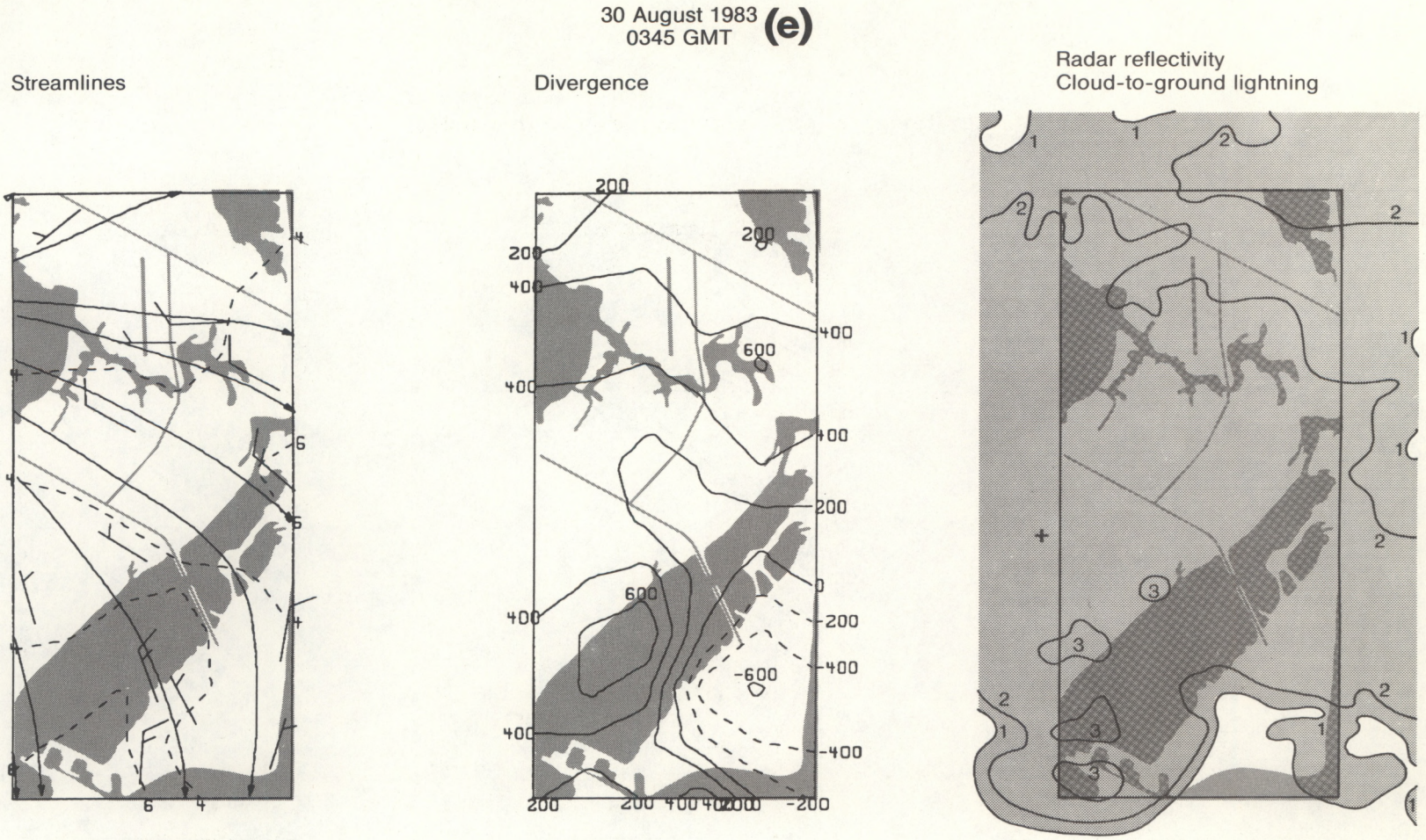

Figure 32. (Continued). (e) 0345 GMT.

0345 GMT (Fig. 32e). The winds across the northern half of the network are returning to their pre-storm direction of west-southwest. Divergence values have dropped considerably, and only a small outflow region remains in the southern corner of the mesonetwork over the Banana River. At that location, four small cores of level 3 are being detected by the radar. There are no reported CG lightning strokes at this time.

Lead times with total area divergence are minimal with the moving system. The gust front enters the network with attendant convergence, followed directly by precipitation and CG flashes. The important tools in this situation are radar and the LLP system. The development of convection could have been tracked by the lightning system and radar since its initiation at approximately 2300 GMT. The system moved true to the lower-to-mid-tropospheric flow (700 mb) at approximately 20 km h^{-1}. The strength of the convergence in the total area divergence profile signaled that a moderate convective system was in the network. The maximum in divergence was the indication that CG lightning would end shortly. On more than a dozen days examined during the summer of 1983, these same two important relationships were usually found: 1) peak lightning occurs at or slightly before peak divergence, and 2) CG lightning ends at or just after peak divergence.

E. Additional Examples

On 20 August 1983 an airmass dominated by strong subsidence covered the entire southeast portion of the United States. Figure 6 vividly displays the results of the large-scale suppression on this date. Warming occurred throughout the column, but the warming mainly above 700 mb apparently put an effective cap on any convective activity. Moisture (Fig. 7) was available, but the airmass could not support deep convection.

Figure 33 is the time series for total area divergence, radar-estimated rainfall, and CG lightning for the KSC mesonetwork on 20 August. Since there was no convective development, there was no rainfall or lightning. However, there was a strong convergence signal in the network for more than 5 hours on this day. Without the clues shown in the upper-air pattern and local sounding, the strong development of convergence beginning at 1430 GMT, associated with the passage of the sea breeze, would have indicated that moderate to strong convective activity was at hand. As discussed in Section 3B, many factors influence the evolution of total area divergence.

16 September 1983 is a somewhat easier day for thunderstorm prediction. A relatively active stationary front was situated in an east-west fashion across central Florida near or just south of the Cape. The sounding is moist, but not particularly unstable, lifted index equals -2, with a convective temperature of 86°F. Winds are west-southwest and average 5 to 10 kn through 700 mb. Therefore, convection will initially develop quite easily on the mainland and may drift east-northeastward to affect the KSC area.

Figure 34 shows the time profiles of total area divergence, radar-estimated rainfall, and field mill lightning flashes for 16 September.

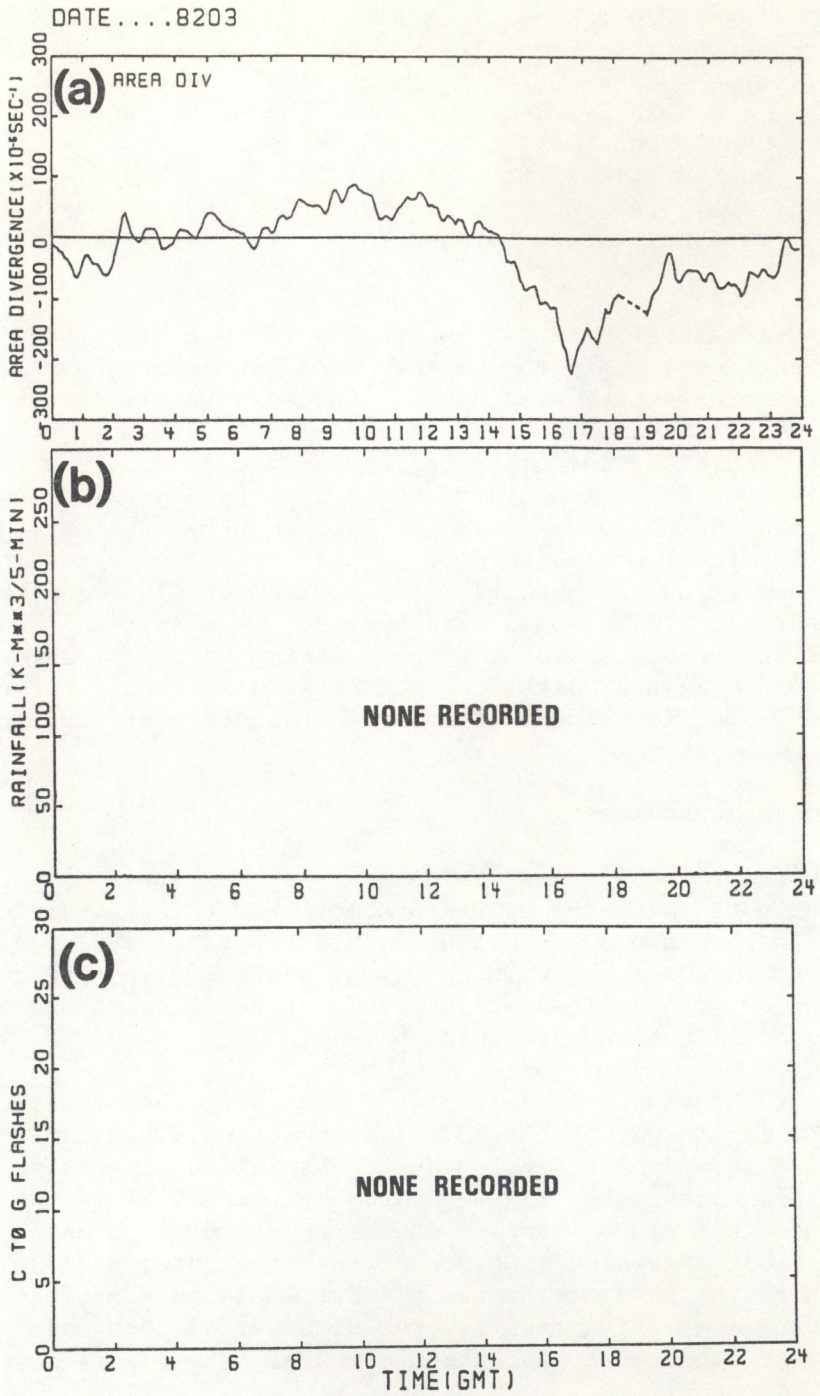

Figure 33. Time profiles (resolution = 5 min) of (a) total area divergence, (b) radar-estimated rainfall from DAB, and (c) CG lightning for 20 August 1983.

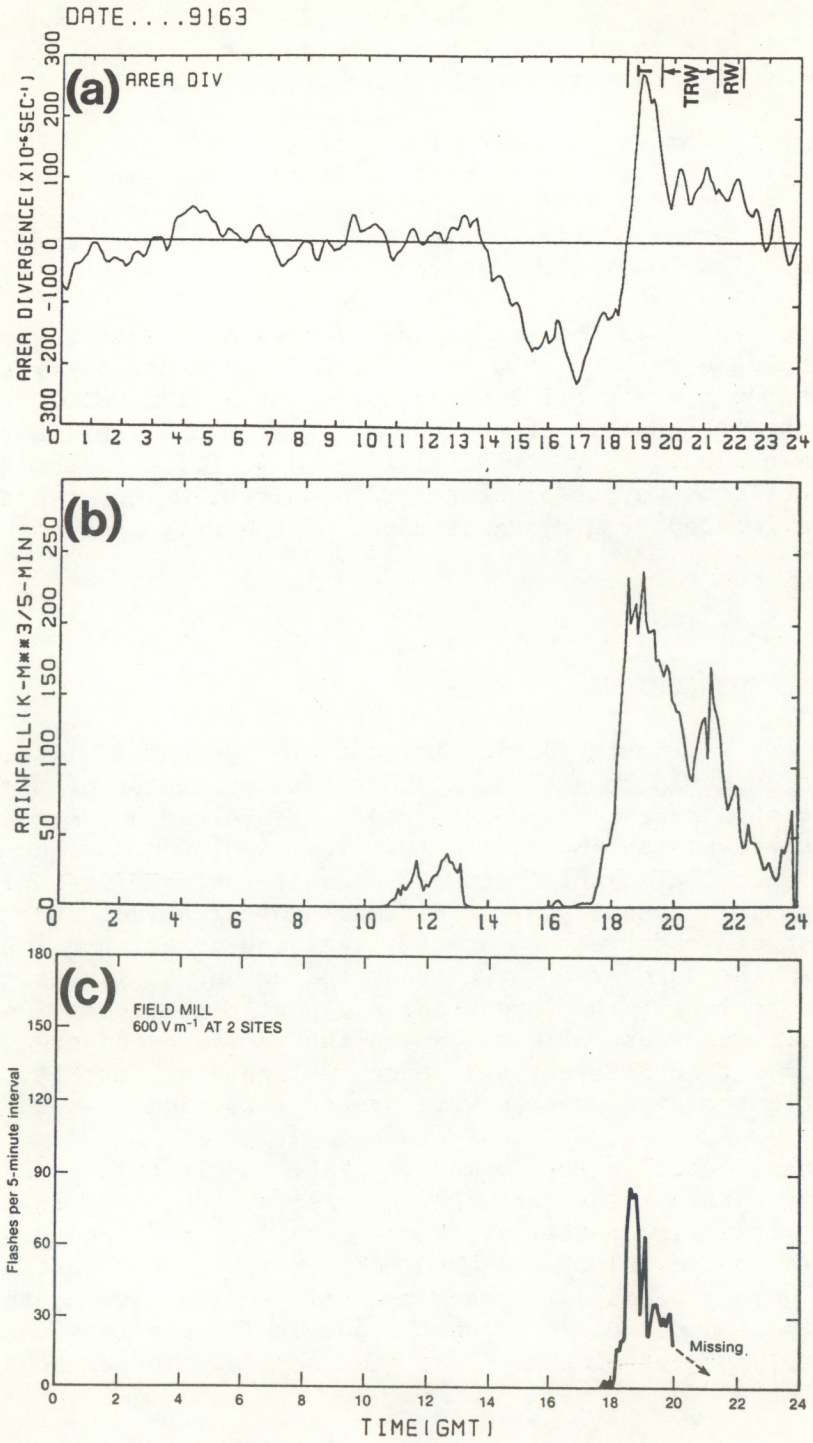

Figure 34. Time profiles (resolution = 5 min) of (a) total area divergence, (b) radar-estimated rainfall from DAB, and (c) lightning flashes using KSC field mills based upon a 600 V m^{-1} field change at two or more sites for 16 August 1983.

(Additional information is given in Section 3B, Figs. 2, 3, and 4.) This day shows a nearly classic total area divergence pattern. Precipitation begins on cue with a time series pattern exactly like that discussed in Section 3B.

Prior to beginning convergence, the surface winds over the KSC network are northwesterly but very weak (less than 5 kn). The small rainfall amount recorded (Fig. 34) between 1100 and 1300 GMT is anomalous propagation produced by a sharper than normal bending of the radar beam toward the earth's surface, probably due to a low-level temperature inversion.

Convergence begins as the sea breeze progresses inland across the Cape. Towering cumuli begin between 1600 and 1700 GMT. Thunder is first heard at 1830 GMT at the Shuttle airport and continues until 2122 GMT. Precipitation in the network begins shortly after 1800 GMT. Figure 3 shows a symmetrical outflow pattern produced in the wind field at 1845 GMT over the Banana River. The Shuttle runway observer recorded only 0.20 inches precipitation. However, he was located some distance north of the main system the entire time.

5. SUMMARY AND CONCLUSIONS

Prior research in south Florida indicated a reasonable likelihood that surface divergence could be used as a short-term predictor of lightning and activity at KSC when storms formed overhead. Convergence was found to precede rainfall, and there was an indication that the magnitude of convergence was related to the amount of precipitation. These relationships varied under different atmospheric conditions. Additional research indicated well-defined correlations between radar echoes and CG lightning occurrence. Finally, another study in the same area showed that the amount of lightning is controlled to a degree by the larger-scale synoptic controls. On the basis of these studies, it was reasonable to expect that surface convergence was related to radar reflectivities, and hence CG lightning, at KSC, especially when the synoptic scale influences were properly considered.

Data were collected in the summer of 1984, mostly during August and September. Wind data at 12 sites were analyzed at the 54-ft level for surface divergence and streamline patterns. Radar data were obtained from the Daytona Beach NWS WSR-74S between 1000 and 0200 GMT, from mid-July to the end of September, and were processed for maps and time series. Cloud-to-ground lightning data were obtained from the LLP network in the Cape Canaveral area for the same period to provide maps and time series. Three cases were analyzed in detail.

In the first case, 7 August, a line of showers and thunderstorms, supported by troughing aloft and intensified by abundant moisture and afternoon heating, moved across central Florida into the KSC vicinity. Redevelopment occurred over KSC ahead of the dissipating line of showers. A very strong inflow and intense convergence signal began, followed by heavy precipitation and lightning. Thunder was heard early (1708 GMT), 1 h after beginning convergence. Field mill data detected first lightning flashes at 1835 GMT, 1 h and 35 min after initial convergence.

The second case, 10 August, was to a certain degree, like many summer days in central Florida. Moisture was abundant and flow was weak but with a westerly component. The importance of satellite imagery as a predictive tool become apparent when two east-west cloud lines were detected marking the zones where deep convection would first develop. The time series of total area divergence showed a slow buildup of convergence as the sea breeze slowly progressed westward across the Cape. Initial convergence occurred around 1500 GMT, becoming stronger after 1700 GMT while maximum convergence was recorded at 1840 GMT. Initial lightning flashes happened at 1830 GMT, 1 h and 30 min after the initiation of moderate convergence.

The third principal case, 30 August, occurred on the evening of the STS-8 launch. The meteorological conditions were somewhat unusual as central Florida and the Gulf of Mexico were under a developing disturbance aloft. As usual, the sounding was conditionally unstable and moist. The lower tropospheric winds were northerly, indicating that initial echo movement would be toward the south. Cells developed offshore of Daytona Beach, and moved southward across KSC with moderate precipitation and intense lightning. As stated earlier, the moving system poses the most problems for total area divergence as a predictive tool. In this case, the gust front entered the northern boundary of the mesonetwork, and its attendant convergence was followed directly by precipitation and lightning. The total area divergence profile was very steep, the relative steepness being a function of the speed of the system. Convergence began at 0220 GMT, radar-estimated rain began at 0200 GMT, and first CG lightning was detected in the network at 0205 GMT. Therefore, all elements began approximately simultaneously. The important tools in this case would have been radar and the LLP system, not the local wind field. The surface winds were unaffected until the arrival of the system. However, the development of convection was traced very well by the radar and LLP lightning systems.

Two other cases, for contrast, were also briefly analyzed. On August 20, the sea breeze was stationary over the KSC network and showed continued convergence without any radar-derived precipitation or lightning for the whole day. The key was the strong suppression aloft, which was clearly identifiable on synoptic charts. On September 16, a classic convergence signal was accompanied by a well-behaved radar echo time series and the sequence of field-mill-derived lightning activity, although LLP data were not available. This case indicated how well the mechanisms originally expected to be operating in this area can be shown, and that clearly defined signals can occasionally be seen when a cloud grows directly over the small KSC network -- that is, surface divergence fields are useful in nowcasting of lightning activity.

The KSC network is quite small, compared with the size of convective systems found in the subtropics. The smaller the wind network, the greater the chance of only partially recording the stages of convective development. Therefore, changes in total area divergence would not be an accurate estimate of the strength of the convective system for the 1983 network. The location and separation of wind sensors are important, also. The current KSC station layout is marginally suited for defining convergence strength and centers. A more uniform station grid would provide a focusing of the location and strength of convergence.

No single predictive or analysis technique can stand alone. Estimates of future development can be obtained only through a continual synthesis of the current and past situations as shown by a variety of data sources and analyses. Nevertheless, applying the relationship between convergence, precipitation, and lightning within a total mesoscale system can quantify the timing, strength, and intensity of a developing convective system.

ACKNOWLEDGMENTS

The authors are indebted to a large number of individuals and agencies who made this study possible.

Mr. Michael Maier of Lightning Location and Protection, Inc. (LLP), Tucson, AZ, provided many ideas for linking flashes with surface convergence, as well as corrections produced by LLP for the cloud-to-ground lightning data.

The National Weather Service (NWS) provided critical support in the collection of the radar data. The Southern Region of the NWS provided access to the Daytona Beach NWS radar. Mr. Dow Boykin, Meteorologist in Charge of the Daytona Beach NWS office, permitted us to locate a digitizer and tape recorder there, and his staff conscientiously changed tapes and sent them to us. Mr. Darrell Covey of the NWS Training Center in Kansas City provided a portable digitizer and recorder at Daytona Beach, and details of the data.

The United States Air Force staff at Patrick Air Force Base provided data from the Shuttle runway for the case studies.

Dr. E. Philip Krider and Ms. Launa Maier of the University of Arizona, and Mr. William Jafferis of NASA-KSC provided field mill data for several of the cases.

The research was supported by NASA contract number CC-29811B.

REFERENCES

Cooper, H.J., M. Garstang, and J. Simpson, 1982: The diurnal interaction between convection and peninsula-scale forcing over south Florida. Mon. Wea. Rev., 110, 486-503.

Cressman, G.P., 1959: An operational objective analysis system. Mon. Wea. Rev., 87, 367-374.

Cunning, J.B., 1976: Comparison of the Z-R relationships for seeded and nonseeded Florida cumuli. J. Appl. Meteorol., 15, 1121-1125.

Cunning, J.B., R.L. Holle, P.T. Gannon, and A.I. Watson, 1982: Convective evolution and merger in the FACE experimental area: Mesoscale convection and boundary layer interactions. J. Appl. Meteorol., 21, 953-977.

Holle, R.L. and M.W. Maier, 1980: Tornado formation from downdraft interaction in the FACE mesonetwork. Mon. Wea. Rev., 108, 1010-1028.

Holle, R.L., R. Lopez, W.L. Hiscox, and D. Rosenfeld, 1984: Cloud-ground lightning associated with radar returns in south Florida. Postprints, 15th Conf. on Hurricanes and the Tropical Meteorology, Miami, FL, January 9-13, American Meteorological Society, Boston, Mass.

Jacobson, E.A., and E.P. Krider, 1976: Electrostatic field changes produced by Florida lightning. J. Atmos. Sci., 33, 103-117.

Krider, E.P., R.C. Noggle, A.E. Pifer, and D.L. Vance, 1980: Lightning direction-finding systems for forest fire detection. Bull. Am. Meteorol. Soc., 61, 980-986.

Krider, E.P., R.C. Noggle, and M.A. Uman, 1976: A gated, wideband magnetic direction finder for lightning return strokes. J. of Appl. Meteorol., 15, 301-306.

Lopez, R.E., R.L. Holle, C.C. Balch, and W.L. Hiscox, 1984a: The relationship between lightning activity over south Florida and different synoptic situations. Postprints, 15th Conf. on Hurricanes and Tropical Meteorology, Miami, FL, January 9-13, American Meteorological Society, Boston, Mass.

Lopez, R.E., P.T. Gannon, Sr., D.O. Blanchard, and C.C. Balch, 1984b: Synoptic and regional circulation parameters associated with the degree of convective shower activity in south Florida. Mon. Wea. Rev., 112, 686-703.

Maier, M.W., R.C. Binford, L.G. Byerley, E.P. Krider, A.E. Pifer, and M.A. Uman, 1983: Preprints, Fifth Symposium on Meteorological Observations and Instrumentation. April 11-15, 1983, Toronto, Ontario, Canada. American Meteorological Society, Boston, Mass., 497-504.

Piepgrass, M.V., and E.P. Krider, 1982: Lightning and surface rainfall during Florida thunderstorms. J. Geophys. Res., 87, 11,193-11,201.

Ulanski, S.L., and M. Garstang, 1978: The role of surface divergence and vorticity in the life cycle of convective rainfall. Part I: Observation and analysis. J. Atmos. Sci., 35, 1047-1062.

Watson, A.I., and D.O. Blanchard, 1984: The relationship between total area divergence and convective precipitation in south Florida. Mon. Wea. Rev., 112, 673-685.

Watson, A.I., and R.L. Holle, 1982: The relationship between low-level convergence and convective precipitation in Illinois and south Florida. VIN Tech. Rept. 7, Office of Weather Research and Modification, NOAA/ERL, Boulder, CO, and Illinois State Water Survey, Champaign, IL (National Tech. Info. Service, Springfield, VA, AD-A127 615/3), 67 pp.

Watson, A.I., R.L. Holle, J.B. Cunning, P.T. Gannon and D.O. Blanchard, 1981: Low-level convergence and the prediction of convective precipitation in south Florida. VIN Tech. Rept. No. 4, NOAA Environmental Research Laboratories, Office of Weather Research and Modification, Boulder, Colo., and Illinois State Water Survey, Champaign-Urban, Ill, 228 pp.